High-dimensional profiling demonstrates complexity, tissue imprinting, and lineage-specific precursors within the mononuclear phagocyte compartment of the human intestine

One sentence summary: Fenton and Wulff *et al*. use single-cell methods to explore the complexity of the mononuclear phagocyte compartment of the human intestinal lamina propria, identifying distinct dendritic cell and macrophage subsets, site-specific transcriptional signatures, and lineage-specific precursors.

Thomas M. Fenton[1,2,†*], Line Wulff[1,†], Gareth-Rhys Jones[3], Julien Vandamme[1], Peter B. Jørgensen[1], Calum C. Bain[3], Julie Lee[4], Jose MG. Izarzugaza[5], Kirstine G. Belling[6], Gwo-Tzer Ho[3], Ole H. Nielsen[7], Lene B. Riis[8], Tune H. Pers[9], Henrik L. Jakobsen[10], Allan M. Mowat[11], Søren Brunak[6], William W. Agace[1,12,*]

[1]Mucosal Immunology group, Department of Health Technology, Technical University of Denmark, Kemitorvet, 2800 Kgs. Lyngby, Denmark

[2]Institute of Immunology and Infection Research, University of Edinburgh, Ashworth buildings, Edinburgh, EH9 3FL, UK

[3]University of Edinburgh Centre for Inflammation Research, Queens Medical Research institute, Edinburgh, EH16 4TJ, UK

[4]Novo Nordisk Foundation Centre for Stem Cell Biology, DanStem, University of Copenhagen, 2200 Copenhagen N, Denmark

[5]Center for Biological Sequence Analysis, Technical University of Denmark, 2800 Lyngby, Denmark

[6]Translational Disease Systems Biology, Novo Nordisk Foundation Centre for Protein Research, Faculty of Health and Medical Sciences, University of Copenhagen, 2200 Copenhagen, Denmark

[7]Department of Gastroenterology, Medical Section, Herlev Hospital, University of Copenhagen, 2730 Herlev, Denmark.

[8]Department of Pathology, Herlev Hospital, University of Copenhagen, 2730 Herlev, Denmark

[9]Novo Nordisk Foundation Centre for Basic Metabolic Research, University of Copenhagen, 2200 Copenhagen N, Denmark

[10]Department of Gastroenterology, Surgical Section, Herlev Hospital, University of Copenhagen, 2730 Herlev, Denmark.

[11]School of Infection and Immunity, College of Medicine, Veterinary Medicine and Life Sciences, University of Glasgow, Glasgow, G12 8TA, UK

[12]Immunology Section, Lund University, BMC D14, 221-84 Lund, Sweden

[†]These authors contributed equally to this work

[*]Corresponding authors: thomas.m.fenton@gmail.com, wiag@dtu.dk

Abstract

Mononuclear phagocytes (MNP), including macrophages and classical dendritic cells (cDC), are highly heterogeneous cells with distinct functions. Understanding MNP complexity in the intestinal lamina propria (LP), particularly in humans, has proved difficult due to the expression of overlapping phenotypic markers and the inability to isolate these cells without contamination from gut-associated lymphoid tissues (GALT). Here, we exploited our novel method for isolation of human GALT-free LP to carry out single-cell (sc)RNA-seq, CITE-seq and flow cytometry analysis of human ileal and colonic LP MNPs. As well as classical monocytes, non-classical monocytes, mature macrophage subsets, cDC1s, and cDC2s, we identified a $CD1c^+$ cDC subset with features of both cDC2 and monocytes, which were transcriptionally similar to the recently described cDC3. While similar MNP subsets were present in both ileal and colonic LP, the proportions and transcriptional profiles of these populations differed between these sites and in diseased states, indicating local specialization and environmental imprinting. Using computational trajectory tools, we identified putative early committed pre-cDC subsets and developmental intermediates of mature cDC1, cDC2 and cDC3, as well as monocyte–to-macrophage trajectories. Collectively, our results provide novel insights into the heterogeneity and development of intestinal LP MNP and an important framework for studying the role of these populations in intestinal homeostasis and disease.

Introduction

The mononuclear phagocyte (MNP) family consists of conventional dendritic cells (cDC), classical monocytes, non-classical monocytes and macrophages, each of which play specific roles in immune responses, tissue homeostasis and inflammation[1–3]. Whereas cDC are the main cells involved in the induction and shaping of adaptive immune responses[4], tissue-resident macrophages are primarily involved in maintaining local tissue homeostasis, defense against infection and tissue repair[5,6]. Recent studies have highlighted considerable heterogeneity amongst MNP[7–10], and it is now evident that these cells develop unique functions depending on the tissue context and niches in which they reside[11,12]. Despite this, our understanding of MNP diversity within human tissues remains limited. A better understanding of MNP diversity is essential not only for understanding tissue specific immune processes, but also for the possibility of therapeutically targeting MNP subsets.

The intestine is continually exposed to food and microbial products that are essential for our health[13,14]. The intestinal immune system must respond appropriately to these products to maintain tissue homeostasis and at the same time retain the ability to mount effective immunity to intestinal pathogens. Furthermore, the intestine is not just a homogenous tube but consists of several anatomically and functionally distinct segments. For example, the small intestine, whose surface is characterized by finger-like projections termed villi, is the major site of food digestion and absorption. Conversely, the colonic surface consists of flattened crypts and it is home to the largest number and variety of microbes[15]. As a result, the concentration of dietary and microbial products and metabolites, many of which have direct impacts on local immune cell development

and function, varies greatly along the length of the intestine. How such variations in intestinal anatomy, function, and luminal contents impact local MNP diversity in humans remains unclear.

Given its continual exposure to foreign material, it is unsurprising that the intestine contains the largest and most diverse immune compartments in the body. MNP are found in multiple niches throughout the intestine, including the intestinal lamina propria (LP), the muscularis mucosa and the gut-associated lymphoid tissues (GALT), including the multi-follicular Peyer's Patches (PP) of the ileum and the mucosal- and submucosal- isolated lymphoid follicles (ILFs) that are distributed along the length of the intestine[16]. Much of our understanding of the roles of intestinal MNP diversity and function comes from studies in mice. These studies have not only highlighted the different roles that MNP subsets play in intestinal homeostasis, but also show that MNP composition and function is highly dependent on the intestinal niche in which they reside[1,3,12,17,18]. Consistent with this, recent single-cell transcriptomic analysis suggests considerable heterogeneity within the macrophage compartment of the human colonic mucosa and muscularis mucosa[19]. While these findings highlight the importance of assessing MNP diversity in different intestinal niches, this has not been possible in the human LP due to a lack of protocols to isolate LP tissue free from contaminating submucosa and GALT.

Here we used our recently developed techniques to isolate intestinal LP free from contaminating GALT and submucosa[20,21] to assess the phenotypic, transcriptional and developmental diversity of MNP populations in the human ileum and colon LP. Our results provide novel insights into LP MNP diversity as well as site-specific adaptations within these populations, and provide an important framework for designing target approaches for modulating intestinal immune responses.

Results

MNP populations of the human ileum and colon LP are highly diverse

To assess MNP diversity within the intestinal LP, surgical samples of uninvolved ileum and colon from colorectal cancer patients (>10 cm from the tumour) were processed to remove contaminating GALT and submucosa (SM), as we described recently[20,21]. Following LP digestion, single-cell RNA sequencing (scRNA-seq) was performed on flow cytometry-sorted $CD45^+CD3^-CD19^-$ $HLADR^{int/+}$ cells from LP cell suspensions, using the 10x Chromium system (**Fig. 1A**). Sequences were obtained from six colonic LP and four paired ileal LP samples (**Table S1**). Distinct clusters of *CD3E*$^+$ T cells, *CD79A*$^+$ B cells, *VWF*$^+$ endothelial cells, *MS4A2*$^+$ mast cells, *COL3A1*$^+$ stromal cells, and *NRXN1*$^+$ glia were identified and excluded from further analysis (**Fig. S1A**). The MHCII genes were expressed by one 'supercluster' and two peripheral clusters (**Fig. S1B**), which were computationally isolated and re-clustered. These 28,758 MHCII$^+$ cells comprised distinct clusters of *IL3RA*$^+$ plasmacytoid DC (pDC), *CLEC9A*$^+$ cDC1, and *FCGR3A*$^+$ non-classical monocytes (**Fig. 1B**), together with a supercluster that contained cells expressing either the cDC2-associated marker *CD1C,* the monocyte/macrophage (Mono/Mac)-associated marker *CD14*, or both *CD1C* and *CD14* (**Fig. 1C**). Flow cytometry analysis of colon LP $CD45^+$ HLA-DR^+ $lineage^-$ cells confirmed the presence of CD1c and CD14 single positive cells, as well as cells expressing variable levels of both CD1c and CD14 (**Fig. 1D**).

To further characterize subsets within this MNP supercluster, we re-clustered these cells at high resolution (**Fig. 1E**). These clusters were present in all four ileal samples and six colonic LP samples, albeit in slightly different proportions (**Fig S1C**). To explore the identity of these clusters

we used a supervised approach to assess individual clusters for their expression of known monocyte-, macrophage-, and cDC2-associated genes[7,22–25]. Based on this analysis, clusters were broadly separated into three main groups. The first clearly defined group (clusters 1-3) expressed the classical monocyte transcription factor *ZBTB16*[26], while the second group (clusters 15-20) expressed high levels of macrophage-associated genes *SEPP1, MERTK* and *MAF,* as well as other TFs involved in tissue-resident macrophage development such as *ID3*[27] (**Fig. 1E**). Clusters 4-14 expressed intermediate levels of these monocyte and macrophage signature genes. Thus, clusters 1-20 appeared to represent monocytes, macrophages and transitional intermediates between these cell types. Within the third group (clusters 21-39), clusters 21-35 expressed lower levels of monocyte and macrophage associated genes and high levels of the cDC2-associated genes *AP1S3*, *FLT3, SEPT6* and *IRF*[9,28] (**Fig. 1E**), while clusters 36-39 expressed both cDC2-associated genes, including *FLT3* and *IRF4,* as well as monocyte and macrophage-associated genes, including *CD14* and *C5AR1* (CD88) (**Fig. 1E**). As a novel population of cDC3 has been reported to co-express cDC2 and monocyte markers[7,25,26,28–30] (reviewed in[31]), we designated this third group as consisting of mixed cDC2 and cDC3-like cells.

To independently assess the accuracy of this grouping, we performed pseudo-bulk PCA analysis of the clusters using gene signatures taken from published cDC2, classical monocyte, and *in vitro* monocyte-derived macrophage data sets[32]. This analysis separated the clusters in a similar manner to our supervised approach, as PC1 drove separation of cDC2/DC3-like clusters from monocytes and macrophages and PC2 drove separation of monocyte from macrophage clusters (**Fig. 1F**). In summary, our analysis suggests that MHCII^{+} clusters within the human ileal and

colonic LP consist of classical and non-classical monocytes, pDC, cDC1, macrophages, and cDC2/DC3-like cells.

Identification of cDC1, cDC2 and cDC3-like subsets in the human intestine

To further explore cDC diversity within the intestinal LP, we computationally isolated and recombined the cDC1 and cDC2/DC3-like cells identified in Figure 1. Cells were clustered at high resolution to allow more accurate cluster designation, tSpace was used to perform trajectory-based clustering identification[33] and the data was visualised by 2-dimensional representation of a 3-dimensional tSpace UMAP (Flat tUMAP). All sub-clusters were present in both ileal and colonic LP datasets (**Fig. S2A**). Seven clusters, located together at the top of the tUMAP, were enriched in cells expressing high levels of mitotic G2M/S genes (**Fig. S2B)** and relatively low levels of MHCII genes (**Fig. S2C**), both of which are characteristics of cDC precursors and will be considered later. To assess the identity of the remaining clusters, we first analysed expression of canonical cDC1 signature genes *CLEC9A, CADM1, XCR1, BATF3,* and *IRF8* and identified 7 clusters with a clear cDC1 signature score (**Fig. S2D**). We then ranked the remaining clusters based on their average module expression of cDC2- or cDC3-associated signature genes published by Bourdeley et al[30] and generated with the AddModuleScore from Seurat (**Fig. S2E**). This allowed us to tentatively identify cDC2-like and cDC3-like clusters, as well as clusters that exhibited no particular bias in their cDC2/DC3 signature score, which we termed ambiguous clusters (**Fig. S2E**). We also identified a population of *LAMP3*$^{+}$ cDC, which expressed high levels of the maturation markers *CCR7* and *CD40* (**Fig. S2F**), suggested to represent mature cDC with a migratory capacity towards lymph nodes[34,35] .

cDC1, cDC2-like and cDC3-like clusters grouped together into 3 super-clusters located in largely distinct areas of the tUMAP projection, with the ambiguous clusters positioned between the cDC2- and cDC3-like cells (**Fig. 2A**). Analysis of genes differentially expressed (DEG) between these subsets further supported their designation as cDC1, cDC2 and cDC3-like cells (**Fig. 2B** and **Table S2**). Specifically, the top DEG for the cDC1 cluster included *CLEC9A, CADM1* and *ID2,* the cDC2 cluster expressed high levels of *IRF4, PLAC8* and *CCL22*, the cDC3-like cluster expressed high levels of *C1QA, S100A9* and *CD163,* while the ambiguous cluster expressed genes associated with both cDC2 and cDC3-like cells (**Fig. 2B**). *CD1C, CLEC10A* and *FCER1A* were expressed at comparable levels by the ambiguous as well as the cDC2 and cDC3-like clusters in both ileal and colonic LP, as observed previously in blood cDC2 and cDC3[26,30] (**Fig. 2B**). Gene Ontology (GO) terms differentially expressed between the cDC subsets included 'Antigen processing and presentation of peptide antigen via MHC class I' for cDC1, 'positive regulation of T-helper cell differentiation' for cDC2 and cDC3-like cells, and 'cellular response to molecule of bacterial origin' and 'inflammatory response' for cDC3-like cells (**Figure S2G**).

To gain further insights into potential functional differences between cDC subsets, we manually curated a list of DEG between cDC subsets based on GO terms associated with transcription factors and cytokines/chemokines[36] (**Fig. 2C** and **D)**. In addition to classical cDC1-associated TFs such as *IRF8*, *ID2* and *BATF3,* ileal and colonic cDC1 specifically expressed other TFs such as *ZEB1* (**Fig. 2C**), which was recently implicated in cDC1-mediated Th1 responses[37]. A number of TFs associated with development, including *ARID3A*, *FOXC1*, *HES4*, and *MSX1,* were enriched in cDC2-like cells, as well as *NR4A3,* which has been implicated in DC activation[38]. As expected, cDC3-like cells expressed the highest levels of macrophage-associated genes including

MAF, MAFB, MAF and *ZBTB16*, as well as the inhibitory TFs *NFKBIA* and *NFKBIZ*, while cells within the ambiguous cluster expressed high levels of several TFs associated with activation, including *ATF3* and *JUNB* (**Fig. 2C**). The cDC also expressed various cytokines and chemokines in subset-specific patterns. Thus, both ileal and colonic LP cDC1 expressed high levels of the TNF family members *TNF* and *TNFSF11* (RANK-L), cDC2-like cells expressed high levels of *CCL19, CCL22* and *EBI3* and cDC3-like cells expressed a wide range of cytokines and chemokines, including *IL10*, *IL1B* and *IL6* and the interferon-inducible chemokines *CXCL9, CXCL10, and CXCL11* (**Fig 2D**); the latter, primarily expressed by a subset of cDC3-like cells (**Fig S2F**).

To assess potential transcriptional differences between ileal and colonic LP cDC, we performed DEG analysis between these sites for each of the cDC1, cDC2 and cDC3-like subsets. The transcriptional profile of each cDC subset differed between the ileum and colon LP (**Fig. 2E, Table S3**). While many DEG were cDC subset-specific, 64 genes were upregulated by all three cDC subsets in the colonic compared with the ileal LP and 12 genes were upregulated by all three cDC subsets in the ileal compared with the colonic LP (**Fig 2F**). To broadly assess differences between ileal and colon cDC subsets we performed GO analysis using enrichR (GO biological processes 2021). Pathways upregulated in all colonic cDC subsets included 'regulation of cellular response to stress' and 'positive regulation of cytokine production' (**Fig S2H**). Ileal cDC showed more subset-specific responses, with upregulation of genes involved in 'protein targeting to ER' (cDC1 and cDC2), ´intestinal cholesterol absorption´ (cDC2 and cDC3-like cells), and 'regulation of complement activation' (cDC1 and cDC3-like cells) (**Fig. S2H**).

To assess potential differences in TF and signalling pathway activity between ileal and colonic LP cDC subsets, we used the Discriminant Regulon Expression Analysis package

(DoRothEA), which infers transcription factor activity from expression of downstream target genes[39] (**Fig. 2G**), and the Pathway RespOnsive GENes package (PROGENy), which infers pathway activity in cells based on expression levels of pathway response genes[40] (**Fig. 2H**). DoRothEA analysis suggested selective SOX2, FLI1, LEF1, and FOXA1 activity in cDC1 (**Fig 2G**), while the cDC3-like cells showed enhanced activity of a broad range of TF associated with cell activation including JUN, JUND, NFKB1, REL, RELA, STAT1 and STAT3 (**Fig. 2G**), consistent with their TF and cytokine/chemokine gene expression profiles (**Fig 2C** and **D**). DoRothEA analysis also suggested tissue-specific differences in cDC TF activity. For example, all ileal LP cDC subsets showed increased SREBF1 and SREBF2 activity, both of which are involved in sterol/cholesterol metabolism), as well as HNFA1 and CDX2 activity, both of which have been implicated in driving intestine-specific cell fate transcriptional programs[41,42] (**Fig 2G**). Conversely, colonic cDC subsets showed highly specific activity of FOXA1 (**Fig 2G**), which has been implicated in intestinal epithelial cell fate decisions[43]. PROGENy analysis suggested that the PI3K pathway was particularly active in cDC1, while cDC3-like cells displayed a broad activation of the Estrogen, Androgen, WNT, TRAIL, VEGF, p53, JAK-STAT, hypoxia, NFκB, and TNFα pathways relative to the other cDC subsets (**Fig 2H**), consistent with gene expression and DoRothEA analysis (**Fig. 2C**, **D** and **G**). Again, differences were found between ileum and colon LP cDC, with, for example, TGFβ, EGFR and MAPK signalling appearing more active in colonic cDC compared with ileal cDC and TRAIL signalling appearing more active in ileal compared with colonic LP cDC1 and DC3-like cells (**Fig 2H**). Collectively, these results highlight the distinct transcriptional activities of human intestinal cDC subsets and the importance of the environment in regulating the transcriptional profile of these cells.

Intestinal cDC subset composition differs along the length of the intestine and changes during inflammation.

CITE-seq analysis demonstrated that cDC2-like, cDC3-like and ambiguous cDC populations could be distinguished from monocytes and macrophages based on their high expression of CD1c and low expression of CD14 (**Fig. 3A**). We next used LEGENDScreen^{TM} to identify surface markers that could subdivide intestinal CD1c^{+}CD14^{-} MNP and thus potentially distinguish intestinal cDC2 from cDC3-like cells by flow cytometry. We observed that CD11a and CD207 separated both colonic and ileal LP CD1c^{+}CD14^{-} MNP into 4 populations (**Fig. 3B**, for pre-gating see **Fig. S3A**). To determine the usefulness of these markers in enriching for cDC2 and cDC3-like cells, we stained colonic LP MNP with CITE-seq antibodies to CD11a and CD207, again identifying cells within the cDC super cluster that were CD207^{-}CD11a^{-}, CD207^{+}CD11a^{-}, CD207^{+}CD11a^{+} or CD207^{-} CD11a^{+} (**Fig. 3C**). While the ambiguous cDC population distributed evenly between all 4 quadrants (**Fig. 3D**), cDC2-like cells were enriched in the CD207^{+} CD11a^{-} (Q1) gate, while the cDC3-like cells were enriched in the CD207^{-}CD11a^{+} (Q4) gate (**Fig. 3C** and **D**). CITE-seq analysis of paired ileal and colonic LP samples from one patient showed similar enrichment of cDC2-like cells amongst Q1 cells and cDC3-like cells amongst Q4 cells in the ileum (**Fig. S3B** and **C**).

To assess whether ileal and colon LP contained different proportions of these populations, flow cytometry analysis was performed on CD1c^{+}CD14^{-} MNP from paired ileal and colonic resection samples (**Fig. 3E**). Ileal LP CD1c^{+}CD14^{-} MNP were significantly enriched in CD207^{+}CD11a^{-} (Q1) cDC2-like cells compared with the colonic LP, while colonic LP CD11c^{+}CD14^{-}MNP were enriched in CD207^{-}CD11a^{+} (Q4) cDC3-like cells (**Fig. 3E**). To

investigate whether the proportions of these populations may change during intestinal inflammation, we analysed biopsies from treatment-naïve patients undergoing endoscopic screening for inflammatory bowel disease (IBD) diagnosis who were subsequently diagnosed with Crohn's disease (CD). This analysis suggested a trend towards reduced proportions of $CD207^{+}CD11a^{-}$ (Q1) cDC2-like cells and enhanced proportions of $CD207^{-}CD11a^{+}$ (Q4) cDC3-like cells in areas of active inflammation, although the differences were not significant (**Fig. 3F**).

The human intestinal LP contains putative cDC1, cDC2 and cDC3 precursors

Recent studies have identified putative committed precursors of cDC1 (pre-cDC1), cDC2 (pre-cDC2), and more recently, cDC3 (pre-cDC3), as well as uncommitted pre-cDC precursors, in human bone marrow, blood and tonsils[25,26,29,30,44,45]. To explore whether cDC precursors might also be present in human intestine, we focused on the HLA-DR^{low} cDC (**Fig. S2C**), which, using high-resolution tSpace based clustering, consisted of 8 clusters (**Fig. 4A**). These cells were highly proliferative compared with the mature cDC (**Fig. 4B**) and expressed low levels of *ITGAX* (encoding CD11c) (**Fig. 4C**); features consistent with previous studies of pre-cDCs in mice[46,47] and in humans[29,45]. Given that these proliferating clusters formed three distinct branches that aligned with cDC1, cDC2 and cDC3-like cells, we hypothesized that each branch potentially represented cDC subset-specific precursors.

To assess this possibility, we generated signatures composed of the top 50 DEGs which distinguished the mature cDC subsets from each other and examined how these were expressed by the various clusters of HLA^{low} cDC. This analysis showed that cluster 4 and 5 shared a gene expression profile with cDC1, while cluster 7 expressed cDC2-like DEGs and cluster 3 and 8 had

a similar gene expression pattern to DC3-like cells (**Fig. 4D**), suggesting the possibility that these clusters represented distinct cDC lineage specific precursors. RNA velocity analysis of mRNA splicing patterns[48] further supported this idea, with cluster 4 appearing to be at the beginning of a trajectory with directionality into cluster 5, and thereafter into the mature cDC1 clusters (**Fig. 4E**). Similarly, cluster 7 showed a trajectory into the mature cDC2 clusters, while cluster 3 showed a trajectory towards cluster 8 and then into mature cDC3 (**Fig 4E**); similar patterns were observed in the ileum and colon LP (**Fig. S4A**). Collectively, these gene expression and splicing patterns suggest that clusters 4 and 5 represent pre-cDC1, while cluster 7 represents pre-cDC2 and clusters 3 and 8 represent pre-cDC3.

Three adjacent clusters (clusters 1, 2, and 6) did not express DEG specific to the mature cDC subsets (**Fig. 4D**) and we hypothesized that they may be earlier, less-committed precursors. To determine whether clusters 1, 2, and 6 showed evidence of commitment to any of the cDC lineages, we used the top 50 DEGs from each of the committed precursor clusters 5 (putative pre-cDC1), 7 (putative pre-cDC2), and 8 (putative pre-cDC3) as input for a PCA of all the HLA^{low} clusters. Of these total 150 DEGs between putative precursor clusters, 79 were also DEGs in the mature cDC populations. Committed precursor clusters 4, 5, 7 and 8 split into 3 distinct areas in PC1-2 (**Fig. 4F**). Using this approach, cluster 6 aligned clearly with pre-cDC2, while most of cluster 3 aligned, as expected, with pre-cDC3 (3B) and there were a few cells in the pre-cDC1 area (3A); one subset of cluster 2 (2A) aligned with pre-cDC1 and another subset of cluster 2 (2B) aligned with pre-cDC3 (2B) (**Fig. 4G** and **Fig. S4B)**). In contrast, cluster 1 did not overlap clearly with any of the pre-cDC groups (**Fig. 4G**).

To investigate the identity of the cells in cluster 1, we compared their gene expression profile with that of a recently published human bone marrow hematopoietic single-cell dataset[49]. Cluster 1 showed greatest correlation with hematopoietic stem cells (HSC), multipotent progenitors (MPP), lympho-myeloid precursors and early promyelocytes, together with some overlap with mature BM cDC. However they showed no overlap with late promyelocytes, myelocytes and classical monocytes (**Fig. S4C**). Thus cluster 1 appears to represent early lympho-myeloid progenitors with a potential bias towards the cDC lineage.

To further assess the relationship between mature cDC and their putative precursors we aligned clusters along the three putative cDC1, cDC2 and cDC3 developmental trajectories (**Fig. 4H**), and examined the expression of DC precursor and cDC subset associated genes across these trajectories (**Fig. 4I)**. Compared with other clusters, cluster 1 expressed the highest levels of *KIT*, similar levels of *ITGAX* and the lowest levels of MHCII gene (**Fig. 4I**), consistent with the suggestion that cells within this cluster represent early progenitors[25,26,29,44]. In agreement with the proposed trajectories, pre-cDC1 clusters progressively increased their expression of cDC1 related genes *BATF3*, *IRF8, CLEC9A* and *CADM1* as they transitioned through clusters 2A, 3A, 4 and 5 to mature cDC1. *XCR1* expression increased during the final transition from cluster 5 to mature cDC1 (**Fig. 4I**), consistent with recent studies in mice suggesting this is a late pre-cDC1 marker[50]. Expression of these genes remained low along the putative cDC2 and cDC3 trajectories. Conversely, expression of the cDC2 associated genes *IRF4* and *LTB* remained high across the cDC2 trajectory but was down-regulated along the cDC1 and cDC3 trajectories (**Fig. 4I**). *CD207* expression selectively increased along the cDC2 trajectory while *CD1C* expression increased along both cDC2 and cDC3 trajectories and decreased along the cDC1 trajectory (**Fig. 4I**). Finally, the

putative pre-cDC3 clusters displayed a progressive increase in expression of the cDC3 associated genes *CD163, CD14, S100A9, C1QA* and *MERTK* as they transitioned through clusters 2B, 3B and 8 to mature cDC3-like cells (**Fig 4I**).

Diversity of intestinal LP monocytes and macrophages

Studies of tissue macrophages in both humans and mice have highlighted significant niche-specific phenotypic, functional and ontogenic diversity[11,12,27,51,52]. Whether the human ileum and colon LP contains transcriptionally similar or distinct populations of intestinal macrophages remains unclear. Further, while most murine intestinal LP macrophages derive from monocytes along a 'waterfall' of phenotypic intermediates[53–56], whether a similar monocyte 'waterfall' exists in the human intestine LP and the characteristics of such intermediates remains to be determined. To address these questions, ileal and colonic LP clusters that were identified as monocytes and macrophages (**Fig. 1E** and **F**) were analysed in isolation. tSpace principal components were used for trajectory-based clustering and UMAP embedding, resulting in the identification of 11 clusters (M1-M11) (**Fig. 5A**). DEG analysis of these trajectory-based clusters demonstrated that cluster M1 expressed high levels of the monocyte-associated genes, *S100A9*, *FCN1* and *VCAN*[25,57]*;* clusters M2 and M3 expressed intermediate levels of *S100A9*, *VCAN*, and *ITGAX* and low levels of *C1QC;* clusters M4-6 lacked expression of *S100A9* and *FCN1* and expressed intermediate levels of *ITGAX* and *C1QC;* and clusters M7 and M8 expressed high levels of *CD209* and *C1QC*, consistent with mature macrophages[57,58] (**Fig. 5B** and **C**). The minor clusters M9 and M10 shared some features with mature macrophages, including high expression of *MHCII* and *C1Q* genes, but expressed low levels of *CD209* and *CD163* (**Fig. 5B** and **C**). Finally, the smallest cluster, M11, expressed high

levels of cell-cycle associated genes including *MKI67* and *KIAA0101* (**Fig. 5B**), indicating that these represented a population of proliferating cells. Given the transcriptional identification of cluster M1 as monocytes, we used M1 as the starting point for pseudo-time analysis. Consistent with the transcriptional data (**Fig. 5B** and **C**), pseudo-time analysis suggested that clusters M2-M3 represented early, and clusters M4-M6, late transitional states, moving towards clusters M7-M10 (**Fig. 5D**). Using PROGENy analysis, the mature macrophage clusters M7-M9 showed evidence of responding to TGFβ (**Fig. S5A**), consistent with previous work in mice[58]. They also showed activation of the p53 pathway involved in multiple aspects of cell function, including cell-cycle arrest (**Fig. S5A**). Thus, we defined M2-M3 clusters and M4-M6 clusters as early and late intermediates, respectively, and clusters M7-M10 as mature macrophages (**Fig. 5B**). Analysis of single-cell data from paired ileal and colonic LP samples from four CRC patients showed that all clusters were present in both sites (**Fig. 5E**). There was also a trend towards increased proportions of intermediate clusters in the colon compared with the ileum LP, and increased proportions of more mature M7 and M8 macrophages in the ileal compared to the colonic LP (**Fig. 5E**).

Analysis of clusters in both the ileal and colonic LP demonstrated that the early intermediate cluster M3, the late intermediate cluster M5 and the mature macrophage cluster M7 shared features of activation, including expression of the proinflammatory genes *IL1B, CXCL8*, *CCL3*, *CCL4,* and *NFKBIA* (**Fig. 5F**). Consistent with this, PROGENy analysis indicated enhanced TNFα and NFκB signalling (**Fig. S5A**), while DoRothEA analysis suggested enhanced canonical NFκB activation (NFKB1, RELA, REL, SP1 signalling), in particular in cluster M3, but extending to clusters M5 and M7, compared with other clusters (**Fig. S5B**). These clusters also showed evidence of enhanced EGFR and MAPK signalling (**Fig. S5A**), with M5 and M7 additionally showing activity of ELK1,

a stimulus response transcription factor[59], and activating transcription factor (ATF) 2 and ATF4[60] (**Fig. S5B**). In contrast, clusters M2, M4 and M6 shared few common DEG distinct from clusters M3, M5 and M7, but these clusters did show evidence of enhanced WNT and JAK-STAT signalling (**Fig. S5A**), and activity of the transcriptional repressor RE1-Silencing Transcription factor (REST), and the MHCII promoter-associated regulatory factor X5 (RFX5) (**Fig. S5B**). Collectively, these results suggest that monocytes undergo a functional dichotomy in the intestine as they mature into tissue resident macrophages.

To gain further insights into the identity of the mature macrophage clusters M7-M10 we isolated these subsets and performed DEG analysis between them (**Fig. 5G, Table S4)**. The major mature macrophage cluster M7 expressed high levels of proinflammatory genes (**Fig. 5F** and **G, Table S4**), and genes associated with inhibition of NF-κB and PRR signaling including *NR4A2*[61], *EGR1*[62], and *KLF2/KLF4*[63] (**Fig. 5G**). Consistent with their inflammatory profile, GO analysis demonstrated that M7 macrophages were enriched in several inflammatory pathways compared with other mature macrophage clusters, including 'cellular response to molecule of bacterial origin', 'cellular response to cytokine stimulus' and 'regulation of inflammatory response' **(Fig. S5C**). Amongst the mature macrophage clusters, M7 also expressed the highest levels of *LYVE1, SIGLEC1* (CD169)*, FOLR2,* and *MAF* (**Fig. S5D**), markers previously associated with perivascular macrophages[64,65]. While these genes have been associated with self-renewing embryonically derived MHCII^{lo} macrophages in other tissues[66], the M7 cluster expressed high levels of *MHCII*, but not high levels of *ADAMDEC1* or *C2* (**Fig. 5C**) that have previously been associated with intestinal self-renewing macrophages[67]. Furthermore, while high levels of LYVE1 have been associated with intestinal submucosal macrophages[19,68], the submucosa was removed during our

LP isolation protocol, and cluster M7 did not express the submucosal macrophage associated genes *COLEC12*[19] or *MARCO*[68] (**Fig. S5D**). Thus, cluster M7 likely represents the recently identified *FOLR2* expressing macrophages present in the middle and base of intestinal crypts[68].

The second major macrophage cluster M8, and the minor macrophage cluster M10, both expressed high levels of the metallothionein genes *MT1G*, *MT1X*, and *MT2A* (**Fig. 5G**), which have been implicated in metal sequestration in GM-CSF-dependent anti-microbial responses[69]. These clusters also expressed high levels of *LIPA, PLD3, LGALS3* and *CD68* (**Fig. 5G** and **Fig. S5D**), all of which have been associated with lipid metabolism and phagocytosis, and are signatures of lipid-associated macrophages[70,71]. Cluster M10 additionally expressed high levels of *APOE*, *PLA2G7*, and *FUCA1* (**Fig. 5G**), involved in lipid transport/metabolism, as well *FTL* involved in iron transport (**Fig. 5G***),* both of which represent important functions of adipose tissue macrophages (ATMs)[72,73]. Consistent with this, cluster M10 showed evidence of TRAIL pathway activity (**Fig. S5A**), that has been associated with ATMs[74], as well as activity of NR5A1, a transcription factor involved in steroidogenesis and lipid metabolism[75] (**Fig. S5B**). Both clusters M8 and M10 were enriched in GO terms associated with responses to metal ions and 'chylomicron remnant clearance'. Thus, macrophage clusters M8 and M10 showed transcriptional signatures indicative of lipid signaling, and cluster M10 in particular shared a transcriptional profile previously associated with ATMs.

Cells within the minor macrophage cluster M9 expressed high levels of the anti-inflammatory genes *ATOX1* and *IL1RN,* as well *IL22RA2,* the gene encoding IL22 binding protein (**Fig. 5G)**. They also expressed high levels of the metalloproteases *MMP9* and *MMP12* and the pro-angiogenic genes *ENPP2* and *PTGDS*, **(Fig. 5G**), all of which have been implicated in vascular

homeostasis, and they showed the highest vascular endothelial growth factor (VEGF) pathway activity (**Fig S5A**), collectively indicating potential interactions with endothelium. M9 also expressed the highest levels of *CD4, C2*, and *ADAMDEC1* (**Fig. S5D**), genes associated with self-renewing macrophages in the mouse intestine[67] and of *IL4I1* (**Fig. S5D**), recently identified as a marker of LP macrophages located at the top of colonic crypts and small intestinal villi[68].

To determine whether the transcriptional profile of macrophage clusters M7-M10 differed between intestinal sites, we performed DEG analysis between the ileum and colon for each of these subsets. The major macrophage clusters M7 and M8 showed many DEG between the ileum and colon, while M10 and, even more so, M9, showed fewer differences (**Fig. 5H, Table S5**). GO analysis demonstrated that the M7 cluster within the ileum was enriched in genes associated with 'antigen processing and presentation of exogenous peptide antigen', 'positive regulation of immune response', 'regulation of tumor necrosis factor production', 'positive regulation of reactive oxygen species metabolic process', and 'interferon-gamma-mediated signaling pathway' compared with the colonic M7 cluster, and these pathways were similarly enriched in the ileal M8 compared to colonic M8 cluster **(Fig. S5E**). In contrast, the M7 cluster within the colon was enriched for genes associated with 'receptor-mediated endocytosis', 'protein targeting to the ER', 'response to unfolded protein', 'regulation of cellular response to stress', and 'Fc-gamma receptor signaling pathway involved in phagocytosis' and these pathways were also enriched in the colonic M8 compared with ileal M8 cluster **(Fig. S5E**). Collectively, these data suggest that the transcriptional profiles and functions of mature LP macrophages are influenced by the intestinal site in which they reside in a highly subset-specific manner.

Flow cytometry-based identification of intestinal monocytes, intermediates and mature macrophage subsets.

To identify surface antigens that may help identify the stages of intestinal monocyte development by flow cytometry, LEGENDScreen™ was used to screen for surface marker expression on colonic $CD14^{+}CD1c^{lo}$ MNP (**Fig. S6A** and **B**). CD11c, CD11a, CD206, and CD55 showed heterogenous expression levels on $CD14^{+}CD1c^{lo}$ cells (**Fig. S6B**) and we thus used antibodies recognising these surface markers, together with CD14 and CD1c, in CITE-seq analysis of MNP from three colonic LP (**Fig. 6A**) and one ileal LP (**Fig. S6C**). CD55 was expressed at high levels by the monocyte cluster M1, at intermediate levels by the early intermediate clusters M2 and M3, but not by more mature clusters (**Fig. 6A**). CD11a was highly expressed by M1, M2 and M3 clusters, and at intermediate levels by the late intermediate clusters M4 and M5, but not by other clusters (**Fig. 6A**). CD206 was expressed by late intermediate clusters and by mature clusters M7 and M8, but not by the small M9 and M10 clusters. CD11c was expressed at high levels by cluster M1, all intermediate clusters and cluster M9, while mature M7 and M8 clusters showed heterogenous levels of expression and M10 little expression (**Fig. 6A**). CD14 was expressed at highest levels by cluster M1 and the early intermediate clusters M2 and M3 (**Fig. 6A**), while CD1c was poorly expressed by monocytes and macrophages, but a proportion of each of the intermediate clusters (M2-M6) expressed some CD1c (**Fig. 6A**). This analysis further suggested that the mature macrophage clusters could be broadly distinguished from monocytes and intermediates by their lack of expression of CD55 and CD11a and subsequently distinguished from one another based on their expression of CD14, CD206 and CD11c, with cluster M7 being $CD14^{+}CD206^{+}$, cluster M8

CD14^{lo}CD206^{int}, cluster M9 CD14^{lo}CD206^{-}CD11c^{hi} and cluster M10 CD14^{lo}CD206^{-}CD11c^{-} (**Fig. 6A**). The smallest M11 cluster contained too few cells for accurate CITE-seq analysis.

Based on these results and the transcriptional analysis depicted in **Fig. 5C**, we designed an antibody panel for putative identification of M1 and early intermediates, late intermediates, and mature macrophages by flow cytometry (**Fig. 6B**). Gating on mature macrophages, we identified three populations based on differential expression of CD14 and CD206 (**Fig. 6C**). These included CD14^{hi}CD206^{hi} cells, which based on our CITE-seq analysis are likely enriched in M7 macrophages, while the CD14^{lo}CD206^{int} cells are likely enriched in M8 macrophages, and the minor population of CD14^{lo}CD206^{lo} cells is likely enriched in M9-M10 macrophages (**Fig. 6C**). To assess whether the proportions of these populations differed between the ileum and colon LP, we performed flow cytometry analysis on CD1c^{-}CD14^{+}MNP from 10 matched ileal and colonic resection samples (**Fig. 6D**). The proportion of intermediate cells among total mono/mac appeared higher in the colon compared with the ileal LP (**Fig. 6D**) and the colonic LP contained a higher proportion of CD14^{hi} CD206^{hi} macrophages and lower proportion of CD14^{lo}CD206^{lo} macrophages compared within the ileal LP (**Fig. 6D** and **E**). To assess whether the proportions of these populations changed during inflammation, we performed similar analysis of colonic biopsies from healthy, CD and ulcerative colitis patients (**Fig. 6F**). This revealed a clear correlation between the presence of inflammation and increased proportions of early and late intermediates and decreased proportions of both mature CD14^{hi}CD206^{hi} and CD14^{lo}CD206^{lo} macrophage populations (**Fig. 6F**). Thus, multiple stages of monocyte-macrophage differentiation can be identified in the human intestine by flow cytometry, and these differ between the between the ileum and colon as well as in the setting of IBD.

Discussion

MNPs play critical roles in tolerance, immunity and inflammation, but MNP are functionally heterogeneous and their subsets acquire distinct functions depending on the niche in which they reside. Characterizing MNP diversity in distinct human tissues is thus essential for our understanding of their various roles in tissue homeostasis and disease. Here, we used scRNA-seq, CITE-seq and flow cytometry analysis to characterize MNP diversity within the human intestinal mucosa, the largest barrier surface of the body. We provide evidence that the human ileum and colon contain numerous mature, transcriptionally distinct MNP subsets, as well as putative lineage-specific precursors. We further show that the proportion and transcriptional profile of MNP subsets changes along the length of the intestine and in the setting of intestinal inflammation. Our results provide an important roadmap of the human intestinal MNP compartment and a framework for future studies aimed at modulating this compartment therapeutically.

Consistent with previous findings[76,77], pDC and non-classical monocytes represented only a minor fraction of cells within our intestinal LP MNP scRNA-seq datasets. As non-classical monocytes patrol the vasculature[78,79], it may be that these represent contamination from the bloodstream, although there is also evidence that murine non-classical monocytes may migrate into tissues in response to tissue damage[78], potentially including into the gut wall[80]. Consistent with previous immunohistochemical and flow cytometric analysis[81], cDC1 were clearly identified as a distinct population in our LP MNP scRNA-seq datasets, but high-resolution clustering and a mixture of supervised and unsupervised approaches were required to distinguish the remaining MNP subsets

from one another. This led to the identification of monocytes, monocyte-macrophage intermediates, mature macrophages and cDC2 subsets. In addition, there was a population of MNP that expressed both cDC2 and monocyte-associated genes, that were transcriptionally similar to the recently described population of cDC3 identified in several human tissues[7,25,26,30]. Compared with cDC2 and cDC1, these cDC3-like cells expressed a broad range of TFs associated with cell activation, together with a unique range of cytokines and chemokines, suggesting they play distinct roles in intestinal immune homeostasis.

Interestingly, our trajectory analysis suggested a degree of transcriptional convergence between cDC2 and cDC3-like cells within the intestinal LP, and we were unable to distinguish some of these cells at the transcriptional level. Consistent with this, we were also unsuccessful in identifying surface markers that could distinguish cDC2 from cDC3-like cells definitively. However, our CITE-seq analysis demonstrated that $CD207^{+}CD11a^{-}CD1c^{+}$ cells were highly enriched in cDC2, while $CD207^{-}CD11a^{+}CD1c^{+}$ cells were enriched in cDC3-like cells. Using these markers, we found that cDC3-like cells were present in higher proportions in the colon compared with the ileal LP, while cDC2 showed the opposite pattern. Furthermore, and consistent with previous studies in mice[82–84], related cDC subsets displayed distinct transcriptional profiles and evidence of different signalling pathways when originating from the ileal or colonic LP. Thus, local environmental signals along the length of the human intestine may fine-tune cDC function.

Lineage-restricted cDC precursors have been identified in human blood, bone marrow and lymphoid tissues[25,29,44,45,85,86], but it has been unclear whether such precursors exist in human non-

lymphoid peripheral tissues, such as the intestine. Here, our combined bioinformatic analyses provide evidence that both the human ileal and colonic LP contain cDC precursors that appear committed to either the cDC1, cDC2 or cDC3 lineage. Thus, we found that each mature cDC subset was directly connected in trajectory space to a distinct population of proliferating *HLA*^{low}*ITGAX*^{low} cells. Secondly, these distinct proliferating populations displayed a unidirectional velocity-based developmental trajectory into either mature cDC1, cDC2 or cDC3-like cells. Finally, these putative lineage-restricted precursors displayed a progressive acquisition or loss of cDC lineage-associated marker genes and TFs as they transitioned towards each mature cDC subset. As expected, the number of these putative lineage-restricted cDC precursors was low and our ability to capture such cells was only made possible by our sorting strategy and use of surgical resections as opposed to biopsies. Our evidence of lineage-restricted cDC precursors in the human intestinal LP is consistent with recent studies indicating the presence of cDC1 and cDC2 restricted cDC precursors in the murine small intestine[46], and that human cDC3 derive from distinct precursors to those of cDC1 and cDC2[26,30].

In addition to putative lineage-restricted cDC precursors, we also identified a minor population of proliferating *ITGAX* expressing *HLA*^{low} cells that did not show transcriptional bias towards any particular cDC lineage. The transcriptional profile of these cells instead correlated best with early bone marrow precursors, indicating that these cells may lie upstream of lineage-committed cDC precursors. While such findings are consistent with the observation that haematopoietic stem cells and/or downstream myeloid precursors are present in the human intestine[87], the lineage potential and role these cells play in maintaining the intestinal MNP compartment awaits further study.

Prior scRNA-seq analyses of human intestinal macrophages have focused primarily on the colon and demonstrated macrophage diversity within both the mucosa and underlying mucosa muscularis[19,68]. Here, we confirm and extend these findings by demonstrating that, although the ileal and colonic LP contain similar mature macrophage populations, these are present in different proportions in the two tissues. Furthermore, similar to recent findings in mice[88], we found that the transcriptional profile of the two major mature LP macrophage subsets, M7 and M8, differed between the ileal and colonic LP. Specifically, both populations in the ileum were enriched in pathways associated with immune activation and antigen presentation, while those in the colon were enriched in genes associated with response to unfolded protein and stress. Thus, similar to our observations with cDC subsets, the function of analogous macrophage subsets appears to be fine-tuned depending on their location along the length of the intestine.

Our trajectory-based bioinformatics analysis suggested that both major macrophage subsets, M7 and M8, derived from infiltrating monocytes, via transitional intermediates, a process reminiscent of the 'monocyte waterfall' described in mouse intestine[53,54,58,89]. Interestingly, a transcriptional dichotomy was observed within these transitional intermediates, whereby some clusters of early and late intermediates expressed high levels of pro-inflammatory cytokine and chemokine genes, as well as inferred activity of NFκB/TNFα/EGFR signalling pathways and NFκB/ATF/AP-1 transcription factors; these were characteristics also of mature M7 macrophages. In contrast, other early and late intermediate clusters showed inferred activity of JAK-STAT and WNT pathways, and of the transcriptional repressor REST, which were also characteristics of mature M8

macrophages. Collectively, these results suggest that monocytes transition along two transcriptionally distinct trajectories after their entry into the intestinal LP, resulting in the generation of the two major mature M7 and M8 macrophage subsets. Given the distinct location of mature macrophage subsets within the LP[68], we speculate that these trajectories are driven by distinct signals transitioning cells receive within their local environmental niche.

We established a flow cytometry panel capable of identifying intestinal seeding monocytes, early and late intermediates as well as mature LP macrophage populations and found that the colon LP was enriched in late intermediate cells and $CD206^{hi}CD14^{hi}$ macrophages (M7 cluster), while the ileum LP was enriched in $CD206^{lo}CD14^{lo}$ macrophages (M8 cluster). Thus, in addition to exhibiting site-specific transcriptional profiles, the proportions of mature macrophages and monocyte intermediates differs between the ileum and colon LP. While the mechanisms driving these site-specific differences remain unclear, we speculate that the presence of high proportions of intermediate monocytes in the colon LP may reflect higher turnover of this compartment under steady-state conditions. Our flow cytometry analysis also confirmed and extended prior studies[76,90,91], by showing that the proportions of both early and late intermediate cells increased in active IBD colon, while the proportions of both major mature macrophage populations decreased. Furthermore, these alterations correlated with disease severity. Whether intermediate cells accumulating in IBD are transcriptionally similar to those present in the healthy intestine, or acquire a distinct transcriptional profile as a result of local inflammatory cues, as recently suggested in mice[56], requires further study.

In summary, our single-cell data highlight marked heterogeneity in the MNP compartment of the human intestinal LP, varying along the length of the human intestine and in the setting of disease. Additionally, by identifying novel transcriptomic and phenotypic markers, our work provides a road map for the study of MNP subsets, and their contribution to intestinal immune responses in health and disease.

Materials and Methods

Study Design

The main objectives of this study were to determine (a) MNP heterogeneity within the human intestinal lamina propria, (b) whether precursors to mature MNP subsets were present in the intestine and, (c) whether the proportions and transcriptional profiles of mature MNP subsets differed between human ileum and colon. Our hypothesis was that multi-modal single-cell methods (scRNA-seq, CITE-seq, flow cytometry) combined with bioinformatic analysis would allow for the unambiguous identification of MNP subsets within the intestine. Patient material included (a) surgical material from colorectal cancer patients (>10 cm from tumour site) and (b) biopsies from treatment-naïve patients undergoing endoscopy for suspected IBD. Patients below 18 and above 85 years of age were excluded from the study. Surgical samples were only used when it was possible to readily dissect mucosa from submucosa. Each experiment was replicated in at least three patients unless otherwise specified. No sampling replication was performed within an individual patient due to limited tissue availability.

Methods

HUMAN SUBJECTS

Resection samples were obtained from patients undergoing surgery for colorectal cancer after informed consent with ethical approval from the Videnskabsetiske Komité for Region Hovedstaden, Denmark (H-3-2013-118). Biopsy samples were obtained from adult patients attending routine colonoscopy for initial IBD disease surveillance (both CD and UC) or for ongoing

disease assessment (see **Table S6** for anonymized patient information) at the Western General Hospital, Edinburgh, UK, after informed consent under existing approvals (REC:19/ES/0087). All patients were part of the Lothian IBD registry[92] and a diagnosis of IBD was made using the Lennard-Jones criteria[93]. Endoscopic assessment of disease severity at the biopsy site was made at the time of endoscopy and biopsy sites were classified as quiescent, mild, moderate or severe. Three to five biopsies were taken per site and pooled for analysis.

METHOD DETAILS

Tissue processing

Surgical samples were processed as described previously[21]. Briefly, resection samples were taken at least 10 cm distant from the tumor site. Muscularis externa was removed using curved surgical scissors and the remaining tissue was incubated in RPMI-5 (RPMI/5% FCS/1% penicillin and streptomycin) containing 4 mM DTT for 2 x 10 min at 37ºC on a shaking incubator (370 rpm) to remove mucus. Macroscopically visible submucosa (SM) was trimmed away using scissors and mucosa separated from SM under a stereo microscope using forceps. Epithelial cells were removed by incubating the mucosa in $Ca2^{+}$ and $Mg2^{+}$ - free HBSS containing 1% penicillin and streptomycin and 5 mM EDTA at 37ºC for 10 min in a shaking incubator, and this procedure repeated four times. Isolated lymphoid follicles were dissected from the mucosa using a scalpel under a stereo microscope with a transmitted light source, and remaining GALT-free LP was cut into 2-4 mm^2 pieces in preparation for digestion. LP was incubated in RPMI-5 containing DNase (30 µg/ml) and collagenase D (5 mg/ml or Liberase TM (2.5 mg/ml) for 45 min at 37ºC under gentle shaking (370

rpm). The resulting LP cell suspension was passed through a 100 μm filter and washed twice in fresh RPMI for downstream analysis. Biopsy samples were processed using the same protocol.

Flow cytometry, MNP enrichment and cell sorting

Cell suspensions were stained with indicated antibodies in Brilliant stain buffer (BD Biosciences) containing 4% normal mouse serum, according to standard procedures, with dead cells identified by 7-AAD staining and excluded from analysis. Samples were analyzed on an LSR Fortessa 2 (BD Biosciences) using Flowjo software (Treestar). The Legendscreen assay (Biolegend) was performed as per the manufacturer's instructions. For scRNA-seq experiments, LP cell suspensions were enriched for HLA-DR$^+$ cells using anti-HLA-DR microbeads (Miltenyi Biotec) and LS MACS columns according to manufacturer's instructions. Resulting cells were stained with the indicated antibodies (**Table S7)** and 7-AAD was added before sorting to exclude dead cells. Cells were sorted on a FACSMelody (BD) into MACS buffer and re-suspended in PBS containing BSA (0.4%) for subsequent 10x analysis. For some samples, cells were first stained with barcode-labelled antibodies prior to sorting for CITE-seq analysis (**Table S7**).

10x Chromium and sequencing

Sorted single cells were subjected to droplet-based massively parallel scRNA-seq using the *Chromium Single Cell 3' Reagent Kit v3.1 with Feature Barcoding technology for Cell Surface Protein* (10x Genomics) following the manufacturer's instructions. In short, the 10x Chromium Controller generated nanoliter-scale Gel Bead-In Emulsions (GEMs) droplets, where each cell was labeled with a specific barcode and each transcript labeled with a unique molecular identifier

(UMI). After reverse transcription, GEMs were broken down and the barcoded cDNA purified with Dynabeads MyOne Silane beads (Thermofisher). cDNA was amplified by PCR using the supplied 10x genomics primers and protocols (12 amplification cycles). Products were size separated with SPRIselect beads (Beckman Coulter) to obtain larger purified transcribed mRNA products for gene expression libraries as well as smaller cell surface protein products for CITE-seq library generation. To prepare gene expression libraries for sequencing, purified large size cDNA products were processed and ligated to an index for sample pooling before the sequencing process following the manufacturer's instructions. For CITE-seq analysis, 5 µl of the purified smaller cDNA product was used as template for antibody-derived tag (ADT) sequencing and ADT sequencing libraries were constructed and indexed following the manufacturer's instructions. Quality and quantity of the final libraries were measured using the Agilent 2100 Bioanalyzer equipped with High Sensitivity DNA chip (Agilent). Illumina sequencing was carried out at the Genomics Core Unit, Center of Excellence for Fluorescent Bioanalytics (University of Regensburg, Germany) or at the SNP&SEQ Technology Platform, Sweden. Libraries were sequenced using HiSeq, NextSeq and NovaSeq systems (300 cycles), aiming for a minimum of 30,000 read pairs/cell for sc-RNA and 3000 read pairs/cell for ADTs.

Bioinformatic analysis

Data processing

Sequencing data was pre-processed and aligned with CellRanger (version 2.2.0 for the first patient samples and version 3.1.0 for all other samples)[94,95]. Sequencing data from the samples stained

with TotalSeq antibodies was processed with CITE-seq count[96]. Each sample was read into a Seurat (version 3.1.5)[97] object in R (versions 3.5.1/4.0.1)[98] and processed by removing cells with exceptionally low or high UMI, gene counts (< 500-1000 and > 3000-6000 genes/cell) and mitochondrial gene content (>10%) according to current best practice[99] and likely representing debris and doublets. To normalize CITE-seq data by denoising and scaling protein levels against background (DSB-normalization), the debris removed from each sample was used as empty droplet information (free floating CITE-seq antibody), while isotype controls were used to normalize for non-specific binding[100]. The normalized protein data were incorporated with the RNA data for the individual samples by adding to it to the corresponding Seurat objects.

After log-normalization of RNA levels for individual samples, cell cycle gene modules were calculated using the Seurat CellCycleScoring function and a gene module representing cell cycle genes from the tool ccRemover by summing the raw counts of these genes/cell divided by the total number of reads per cell[101]. Then the top 3000 most variable genes were identified per sample with the selection method vst.

After initial data processing, all the samples were integrated with Seurat anchor integration and gene expression was scaled while regressing out the effect of cell cycle, UMI counts, and mitochondrial gene content based on their scoring on the individual samples. The merged data were dimensionality reduced with PCA and the 15 first PCs were chosen for downstream analysis. A shared nearest neighbor graph was constructed and used to cluster the data with Louvain clustering. The PCs were also used to dimensionally reduce the data further with UMAP for visualization purposes.

Differential gene expression and gene ontology

Differential gene expression was calculated with Seurat FindMarkers for comparisons between specific groups or FindAllMarkers for DEGs for all clusters, both using the standard non-parametric Wilcoxon rank sum test and base=exp(1).

Gene ontology analysis was performed based DEG lists of above and run on EnrichR's web interface. The output tables based on GO Biological Processes 2021 were downloaded and plotted in R using the package ggradar.

Pseudo-bulk analysis and comparison with populations in public databases

Pseudo-bulk analysis for heatmaps and PCA was performed with the Seurat AverageExpression function. Module scores were calculated with Seurat's AddModuleScore function on indicated selected gene sets or gene sets from literature. DoRothEA was run using confidence levels A+B and referring to the human DoRothEA transcription factor interaction database[39]. Progeny was run using organism = human and top = 500 genes[40].

The processed Seurat object from Triana *et al*[49]. was downloaded and subsetted on the clusters labelled "HSCs & MPPs", "Lymphomyeloid prog", "Early promyelocytes", "Conventional dendritic cell 1", "Conventional dendritic cell 2", "Late promyelocytes", "Myelocytes", "Classical Monocytes". The gene expression data was averaged, and Pearson correlations calculated based on variable genes from our data also present in the bone marrow data set.

Trajectory inference

Trajectory inference was performed with tSPACE on PC spaces of indicated populations[33]. The outputs were dimensionality reduced with UMAP[102,103] from tPCs 1-15 (for both cDCs and macrophages), to 2 and 3 dimensional tUMAPs with distance metric set to Pearson. 3D tUMAP for the cDC trajectory was angled and embedded into 2D using the Dufy package[104]. Clustering was performed with Louvain clustering for Seurat on the tPCs as input. Pseudotime (arbitrary time scale unit) was calculated by taking all trajectories from the tSPACE output from M1 and averaging these per cell. Splicing patterns were first determined on individual samples with the advanced run setting for velocyto[48] with a repeated annotation file[105]. Genes were filtered by 0.2 for spliced data and 0.05 for unspliced data. RNA velocity estimates were then calculated for T=1 and only included genes with splicing information also present in the variable genes and only on cells of interest (e.g. precursors). The information was embedded on top of 2D tUMAP using n=400, scale=sqrt, grid.n=50 and arrow.scale=2.

QUANTIFICATION AND STATISTICAL ANALYSIS

Statistical analysis of flow cytometry data was performed using Prism software (GraphPad). Statistical analysis of sequencing data was performed in R. Statistical tests used for experimental data are outlined in the figure legends.

DATA AND CODE AVAILABILITY

scRNA-seq count data is available through CZ CELLxGENE: https://cellxgene.cziscience.com/e/bcdec5fa-a7fa-4806-92bc-0cd02f40242f.cxg/ .

Code is available: https://github.com/LineWulff/FentonWulff_LP_MNP

References

1. Joeris T, Müller-Luda K, Agace WW, Mowat AMI. Diversity and functions of intestinal mononuclear phagocytes. *Mucosal Immunol*. 2017;10. doi:10.1038/mi.2017.22
2. Caër C, Wick MJ. Human Intestinal Mononuclear Phagocytes in Health and Inflammatory Bowel Disease. *Front Immunol*. 2020;11(March):410. doi:10.3389/fimmu.2020.00410
3. Arroyo Portilla C, Tomas J, Gorvel JP, Lelouard H. From Species to Regional and Local Specialization of Intestinal Macrophages. *Front Cell Dev Biol*. 2021;8(February). doi:10.3389/fcell.2020.624213
4. Cabeza-Cabrerizo M, Cardoso A, Minutti CM, Pereira da Costa M, Reis E Sousa C. Dendritic Cells Revisited. *Annu Rev Immunol*. Published online January 2021:131-166. doi:10.1146/annurev-immunol-061020-053707
5. Na YR, Stakenborg M, Seok SH, Matteoli G. Macrophages in intestinal inflammation and resolution: a potential therapeutic target in IBD. *Nat Rev Gastroenterol Hepatol*. 2019;16(9):531-543. doi:10.1038/s41575-019-0172-4
6. Bain CC, Schridde A. Origin, differentiation, and function of intestinal macrophages. *Front Immunol*. 2018;9(NOV):1-15. doi:10.3389/fimmu.2018.02733
7. Dutertre CA, Becht E, Irac SE, et al. Single-Cell Analysis of Human Mononuclear Phagocytes Reveals Subset-Defining Markers and Identifies Circulating Inflammatory Dendritic Cells. *Immunity*. 2019;51(3):573-589.e8. doi:10.1016/j.immuni.2019.08.008
8. Brown CC, Gudjonson H, Pritykin Y, et al. Transcriptional Basis of Mouse and Human Dendritic Cell Heterogeneity. *Cell*. 2019;179(4):846-863.e24.

doi:10.1016/j.cell.2019.09.035

9. Guilliams M, Dutertre C-A, Scott CL, et al. Unsupervised High-Dimensional Analysis Aligns Dendritic Cells across Tissues and Species. *Immunity*. 2016;45(3):669-684. doi:10.1016/j.immuni.2016.08.015

10. Villar J, Segura E. Decoding the Heterogeneity of Human Dendritic Cell Subsets. *Trends Immunol*. 2020;41(12):1062-1071. doi:10.1016/j.it.2020.10.002

11. Blériot C, Chakarov S, Ginhoux F. Determinants of Resident Tissue Macrophage Identity and Function. *Immunity*. 2020;52(6):957-970. doi:10.1016/j.immuni.2020.05.014

12. Viola MF, Boeckxstaens G. Niche-specific functional heterogeneity of intestinal resident macrophages. *Gut*. 2021;70(7):1383-1395. doi:10.1136/gutjnl-2020-323121

13. Tilg H, Moschen AR. Food, immunity, and the microbiome. *Gastroenterology*. 2015;148(6):1107-1119. doi:10.1053/j.gastro.2014.12.036

14. Suriano F, Nyström EEL, Sergi D, Gustafsson JK. Diet, microbiota, and the mucus layer: The guardians of our health. *Front Immunol*. 2022;13(September):1-14. doi:10.3389/fimmu.2022.953196

15. Mowat AM, Agace WW. Regional specialization within the intestinal immune system. *Nat Rev Immunol*. 2014;14(10):667-685. doi:10.1038/nri3738

16. Mörbe UM, Jørgensen PB, Fenton TM, et al. Human gut-associated lymphoid tissues (GALT); diversity, structure, and function. *Mucosal Immunol*. 2021;14(4):793-802. doi:10.1038/s41385-021-00389-4

17. Luciani C, Hager FT, Cerovic V, Lelouard H. Dendritic cell functions in the inductive and effector sites of intestinal immunity. *Mucosal Immunol*. 2022;15(1):40-50.

doi:10.1038/s41385-021-00448-w

18. Guendel F, Kofoed-Branzk M, Gronke K, et al. Group 3 Innate Lymphoid Cells Program a Distinct Subset of IL-22BP-Producing Dendritic Cells Demarcating Solitary Intestinal Lymphoid Tissues. *Immunity*. 2020;53(5):1015-1032.e8. doi:10.1016/j.immuni.2020.10.012

19. Domanska D, Majid U, Karlsen VT, et al. Single-cell transcriptomic analysis of human colonic macrophages reveals niche-specific subsets. *J Exp Med*. 2022;219(3):e20211846. doi:10.1084/jem.20211846

20. Fenton TM, Jørgensen PB, Niss K, et al. Immune Profiling of Human Gut-Associated Lymphoid Tissue Identifies a Role for Isolated Lymphoid Follicles in Priming of Region-Specific Immunity. *Immunity*. 2020;52(3):557-570.e6. doi:10.1016/j.immuni.2020.02.001

21. Jørgensen PB, Fenton TM, Mörbe UM, et al. Identification, isolation and analysis of human gut-associated lymphoid tissues. *Nat Protoc*. 2021;16(4):2051-2067. doi:10.1038/s41596-020-00482-1

22. Miller JC, Brown BD, Shay T, et al. Deciphering the transcriptional network of the dendritic cell lineage. *Nat Immunol*. 2012;13(9):888-899. doi:10.1038/ni.2370

23. Waskow C, Liu K, Darrasse-Jèze G, et al. The receptor tyrosine kinase Flt3 is required for dendritic cell development in peripheral lymphoid tissues. *Nat Immunol*. 2008;9(6):676-683. doi:10.1038/ni.1615

24. McKenna HJ, Stocking KL, Miller RE, et al. Mice lacking flt3 ligand have deficient hematopoiesis affecting hematopoietic progenitor cells, dendritic cells, and natural killer cells. *Blood*. Published online 2000. doi:10.1182/blood.v95.11.3489.011k45_3489_3497

25. Villani A-C, Satija R, Reynolds G, et al. Single-cell RNA-seq reveals new types of human blood dendritic cells, monocytes, and progenitors. *Science (80-)*. 2017;356(6335):eaah4573. doi:10.1126/science.aah4573

26. Cytlak U, Resteu A, Pagan S, et al. Differential IRF8 Transcription Factor Requirement Defines Two Pathways of Dendritic Cell Development in Humans. *Immunity*. 2020;53(2):353-370.e8. doi:10.1016/j.immuni.2020.07.003

27. T'Jonck W, Guilliams M, Bonnardel J. Niche signals and transcription factors involved in tissue-resident macrophage development. *Cell Immunol*. 2018;330(November 2017):43-53. doi:10.1016/j.cellimm.2018.02.005

28. Yin X, Yu H, Jin X, et al. Human Blood CD1c + Dendritic Cells Encompass CD5 high and CD5 low Subsets That Differ Significantly in Phenotype, Gene Expression, and Functions. *J Immunol*. 2017;198(4):1553-1564. doi:10.4049/jimmunol.1600193

29. See P, Dutertre C-AA, Chen J, et al. Mapping the human DC lineage through the integration of high-dimensional techniques. *Science (80-)*. 2017;356(6342):eaag3009. doi:10.1126/science.aag3009

30. Bourdely P, Anselmi G, Vaivode K, et al. Transcriptional and Functional Analysis of CD1c+ Human Dendritic Cells Identifies a CD163+ Subset Priming CD8+CD103+ T Cells. *Immunity*. 2020;53(2):335-352.e8. doi:10.1016/j.immuni.2020.06.002

31. Chen B, Zhu L, Yang S, Su W. Unraveling the Heterogeneity and Ontogeny of Dendritic Cells Using Single-Cell RNA Sequencing. *Front Immunol*. 2021;12(September):1-13. doi:10.3389/fimmu.2021.711329

32. Tang-Huau T-L, Gueguen P, Goudot C, et al. Human in vivo-generated monocyte-derived

dendritic cells and macrophages cross-present antigens through a vacuolar pathway. *Nat Commun*. 2018;9(1):2570. doi:10.1038/s41467-018-04985-0

33. Dermadi D, Bscheider M, Bjegovic K, et al. Exploration of Cell Development Pathways through High-Dimensional Single Cell Analysis in Trajectory Space. *iScience*. 2020;23(2):100842. doi:10.1016/j.isci.2020.100842

34. Zhang Q, He Y, Luo N, et al. Landscape and Dynamics of Single Immune Cells in Hepatocellular Carcinoma. *Cell*. 2019;179(4):829-845.e20. doi:10.1016/j.cell.2019.10.003

35. Maier B, Leader AM, Chen ST, et al. A conserved dendritic-cell regulatory program limits antitumour immunity. *Nature*. 2020;580(7802):257-262. doi:10.1038/s41586-020-2134-y

36. Blake JA, Baldarelli R, Kadin JA, Richardson JE, Smith CL, Bult CJ. Mouse Genome Database (MGD): Knowledgebase for mouse-human comparative biology. *Nucleic Acids Res*. Published online 2021. doi:10.1093/nar/gkaa1083

37. Smita S, Ahad A, Ghosh A, et al. Importance of EMT factor ZEB1 in cDC1 "mutuDC line" mediated induction of Th1 immune response. *Front Immunol*. 2018;9(NOV):9-12. doi:10.3389/fimmu.2018.02604

38. Nagaoka M, Yashiro T, Uchida Y, et al. The Orphan Nuclear Receptor NR4A3 Is Involved in the Function of Dendritic Cells. *J Immunol*. 2017;199(8):2958-2967. doi:10.4049/jimmunol.1601911

39. Garcia-Alonso L, Holland CH, Ibrahim MM, Turei D, Saez-Rodriguez J. Benchmark and integration of resources for the estimation of human transcription factor activities. *Genome Res*. 2019;29(8):1363-1375. doi:10.1101/gr.240663.118

40. Schubert M, Klinger B, Klünemann M, et al. Perturbation-response genes reveal signaling

footprints in cancer gene expression. *Nat Commun*. 2018;9(1):20. doi:10.1038/s41467-017-02391-6

41. Chewchuk S, Jahan S, Lohnes D. Cdx2 regulates immune cell infiltration in the intestine. *Sci Rep*. 2021;11(1):15841. doi:10.1038/s41598-021-95412-w

42. D'Angelo A, Bluteau O, Garcia-Gonzalez MA, et al. Hepatocyte nuclear factor 1α and β control terminal differentiation and cell fate commitment in the gut epithelium. *Development*. 2010;137(9):1573-1582. doi:10.1242/dev.044420

43. Ye DZ, Kaestner KH. Foxa1 and Foxa2 Control the Differentiation of Goblet and Enteroendocrine L- and D-Cells in Mice. *Gastroenterology*. 2009;137(6):2052-2062. doi:10.1053/j.gastro.2009.08.059

44. Breton G, Lee J, Zhou YJ, et al. Circulating precursors of human CD1c+ and CD141+ dendritic cells. *J Exp Med*. 2015;212(3):401-413. doi:10.1084/jem.20141441

45. Ma W, Lee J, Backenroth D, et al. Single cell RNA-Seq reveals pre-cDCs fate determined by transcription factor combinatorial dose. *BMC Mol Cell Biol*. 2019;20(1):1-14. doi:10.1186/s12860-019-0199-y

46. Cabeza-Cabrerizo M, van Blijswijk J, Wienert S, et al. Tissue clonality of dendritic cell subsets and emergency DCpoiesis revealed by multicolor fate mapping of DC progenitors. *Sci Immunol*. 2019;4(33):1-14. doi:10.1126/sciimmunol.aaw1941

47. Chen J, Schlitzer A, Chakarov S, Ginhoux F, Poidinger M. Mpath maps multi-branching single-cell trajectories revealing progenitor cell progression during development. *Nat Commun*. 2016;7(May):11988. doi:10.1038/ncomms11988

48. La Manno G, Soldatov R, Zeisel A, et al. RNA velocity of single cells. *Nature*.

2018;560(7719):494-498. doi:10.1038/s41586-018-0414-6

49. Triana S, Vonficht D, Jopp-saile L, Raffel S, Lutz R. Single-cell proteo-genomic reference maps of the hematopoietic system enable the purification and massive profiling of precisely defined cell states. *Nat Immunol*. 2021;22:1577–1589. doi:10.1038/s41590-021-01059-0

50. Lança T, Ungerbäck J, Da Silva C, et al. IRF8 deficiency induces the transcriptional, functional, and epigenetic reprogramming of cDC1 into the cDC2 lineage. *Immunity*. 2022;55(8):1431-1447.e11. doi:10.1016/j.immuni.2022.06.006

51. De Schepper S, Verheijden S, Aguilera-Lizarraga J, et al. Self-Maintaining Gut Macrophages Are Essential for Intestinal Homeostasis. *Cell*. 2018;175(2):400-415.e13. doi:10.1016/j.cell.2018.07.048

52. Mowat AMI, Scott CL, Bain CC. Barrier-tissue macrophages: Functional adaptation to environmental challenges. *Nat Med*. 2017;23(11):1258-1270. doi:10.1038/nm.4430

53. Bain CC, Scott CL, Uronen-Hansson H, et al. Resident and pro-inflammatory macrophages in the colon represent alternative context-dependent fates of the same Ly6Chi monocyte precursors. *Mucosal Immunol*. 2013;6(3):498-510. doi:10.1038/mi.2012.89

54. Rivollier A, He J, Kole A, Valatas V, Kelsall BL. Inflammation switches the differentiation program of Ly6Chi monocytes from antiinflammatory macrophages to inflammatory dendritic cells in the colon. *J Exp Med*. 2012;209(1):139-155. doi:10.1084/jem.20101387

55. Bain CC, Bravo-Blas A, Scott CL, et al. Constant replenishment from circulating

monocytes maintains the macrophage pool in the intestine of adult mice. *Nat Immunol*. 2014;15(10):929-937. doi:10.1038/ni.2967

56. Desalegn G, Pabst O. Inflammation triggers immediate rather than progressive changes in monocyte differentiation in the small intestine. *Nat Commun*. 2019;10(1):3229. doi:10.1038/s41467-019-11148-2

57. Bujko A, Atlasy N, Landsverk OJB, et al. Transcriptional and functional profiling defines human small intestinal macrophage subsets. *J Exp Med*. 2018;215(2):441-458. doi:10.1084/jem.20170057

58. Schridde A, Bain CC, Mayer JU, et al. Tissue-specific differentiation of colonic macrophages requires TGFβ receptor-mediated signaling. *Mucosal Immunol*. 2017;10(6):1387-1399. doi:10.1038/mi.2016.142

59. Thiel G, Backes TM, Guethlein LA, Rössler OG. Critical Protein–Protein Interactions Determine the Biological Activity of Elk-1, a Master Regulator of Stimulus-Induced Gene Transcription. *Molecules*. 2021;26(20):6125. doi:10.3390/molecules26206125

60. Chen M, Liu Y, Yang Y, et al. Emerging roles of activating transcription factor (ATF) family members in tumourigenesis and immunity: Implications in cancer immunotherapy. *Genes Dis*. 2022;9(4):981-999. doi:10.1016/j.gendis.2021.04.008

61. Mahajan S, Saini A, Chandra V, et al. Nuclear receptor Nr4a2 promotes alternative polarization of macrophages and confers protection in sepsis. *J Biol Chem*. 2015;290(30):18304-18314. doi:10.1074/jbc.M115.638064

62. Trizzino M, Zucco A, Deliard S, et al. EGR1 is a gatekeeper of inflammatory enhancers in human macrophages. *Sci Adv*. 2021;7(3):1-11. doi:10.1126/sciadv.aaz8836

63. Roberts AW, Lee BL, Deguine J, John S, Shlomchik MJ, Barton GM. Tissue-Resident Macrophages Are Locally Programmed for Silent Clearance of Apoptotic Cells. *Immunity*. 2017;47(5):913-927.e6. doi:10.1016/j.immuni.2017.10.006

64. Moura Silva H, Kitoko JZ, Queiroz CP, et al. c-MAF–dependent perivascular macrophages regulate diet-induced metabolic syndrome. *Sci Immunol*. 2021;6(64). doi:10.1126/sciimmunol.abg7506

65. Lim HY, Lim SY, Tan CK, et al. Hyaluronan Receptor LYVE-1-Expressing Macrophages Maintain Arterial Tone through Hyaluronan-Mediated Regulation of Smooth Muscle Cell Collagen. *Immunity*. 2018;49(2):326-341.e7. doi:10.1016/j.immuni.2018.06.008

66. Dick SA, Wong A, Hamidzada H, et al. Three tissue resident macrophage subsets coexist across organs with conserved origins and life cycles. *Sci Immunol*. 2022;7(67):1-19. doi:10.1126/sciimmunol.abf7777

67. Shaw TN, Houston SA, Wemyss K, et al. Tissue-resident macrophages in the intestine are long lived and defined by Tim-4 and CD4 expression. *J Exp Med*. 2018;215(6):1507-1518. doi:10.1084/jem.20180019

68. Matusiak M, Hickey JW, Luca B, et al. A spatial map of human macrophage niches links tissue location with function. *bioRxiv*. Published online 2022. doi:10.1101/2022.08.18.504434

69. Subramanian Vignesh K, Landero Figueroa JA, Porollo A, Caruso JA, Deepe GS. Granulocyte Macrophage-Colony Stimulating Factor Induced Zn Sequestration Enhances Macrophage Superoxide and Limits Intracellular Pathogen Survival. *Immunity*. 2013;39(4):697-710. doi:10.1016/j.immuni.2013.09.006

70. Hill DA, Lim H-W, Kim YH, et al. Distinct macrophage populations direct inflammatory versus physiological changes in adipose tissue. *Proc Natl Acad Sci*. 2018;115(22). doi:10.1073/pnas.1802611115

71. Jaitin DA, Adlung L, Thaiss CA, et al. Lipid-Associated Macrophages Control Metabolic Homeostasis in a Trem2-Dependent Manner. *Cell*. 2019;178(3):686-698.e14. doi:10.1016/j.cell.2019.05.054

72. Hubler MJ, Peterson KR, Hasty AH. Iron homeostasis: a new job for macrophages in adipose tissue? *Trends Endocrinol Metab*. 2015;26(2):101-109. doi:10.1016/j.tem.2014.12.005

73. Li Y, Yun K, Mu R. A review on the biology and properties of adipose tissue macrophages involved in adipose tissue physiological and pathophysiological processes. *Lipids Health Dis*. 2020;19(1):1-9. doi:10.1186/s12944-020-01342-3

74. Maixner N, Pecht T, Haim Y, et al. A trail-tl1a paracrine network involving adipocytes, macrophages, and lymphocytes induces adipose tissue dysfunction downstream of e2f1 in human obesity. *Diabetes*. 2020;69(11):2310-2323. doi:10.2337/db19-1231

75. Schimmer BP, White PC. Minireview: Steroidogenic Factor 1: Its Roles in Differentiation, Development, and Disease. *Mol Endocrinol*. 2010;24(7):1322-1337. doi:10.1210/me.2009-0519

76. Thiesen S, Janciauskiene S, Uronen-Hansson H, et al. CD14hiHLA-DRdim macrophages, with a resemblance to classical blood monocytes, dominate inflamed mucosa in Crohn's disease. *J Leukoc Biol*. 2013;95(3):531-541. doi:10.1189/jlb.0113021

77. Ráki M, Beitnes ACR, Lundin KEA, Jahnsen J, Jahnsen FL, Sollid LM. Plasmacytoid

dendritic cells are scarcely represented in the human gut mucosa and are not recruited to the celiac lesion. *Mucosal Immunol*. 2013;6(5):985-992. doi:10.1038/mi.2012.136

78. Auffray C, Fogg D, Garfa M, et al. Monitoring of Blood Vessels and Tissues by a Population of Monocytes with Patrolling Behavior. *Science (80-)*. 2007;317(5838):666-670. doi:10.1126/science.1142883

79. Carlin LM, Stamatiades EG, Auffray C, et al. Nr4a1-dependent Ly6C(low) monocytes monitor endothelial cells and orchestrate their disposal. *Cell*. 2013;153(2):362-375. doi:10.1016/j.cell.2013.03.010

80. Schleier L, Wiendl M, Heidbreder K, et al. Non-classical monocyte homing to the gut via α4β7 integrin mediates macrophage-dependent intestinal wound healing. *Gut*. 2020;69(2):252-263. doi:10.1136/gutjnl-2018-316772

81. Poulin LF, Reyal Y, Uronen-Hansson H, et al. DNGR-1 is a specific and universal marker of mouse and human Batf3-dependent dendritic cells in lymphoid and nonlymphoid tissues. *Blood*. 2012;119(25):6052-6062. doi:10.1182/blood-2012-01-406967

82. Luda KM, Da Silva C, Ahmadi F, et al. Identification and characterization of murine glycoprotein 2-expressing intestinal dendritic cells. *Scand J Immunol*. 2022;96(5):1-12. doi:10.1111/sji.13219

83. Jaensson E, Uronen-Hansson H, Pabst O, et al. Small intestinal CD103+ dendritic cells display unique functional properties that are conserved between mice and humans. *J Exp Med*. 2008;205(9):2139-2149. doi:10.1084/jem.20080414

84. Houston SA, Cerovic V, Thomson C, Brewer J, Mowat AM, Milling S. The lymph nodes draining the small intestine and colon are anatomically separate and immunologically

distinct. *Mucosal Immunol*. 2016;9(2):468-478. doi:10.1038/mi.2015.77

85. Bourdely P, Anselmi G, Vaivode K, et al. Transcriptional and Functional Analysis of CD1c+ Human Dendritic Cells Identifies a CD163+ Subset Priming CD8+CD103+ T Cells. *Immunity*. 2020;53(2):335-352.e8. doi:10.1016/j.immuni.2020.06.002

86. Cytlak U, Resteu A, Pagan S, et al. Differential IRF8 Transcription Factor Requirement Defines Two Pathways of Dendritic Cell Development in Humans. *Immunity*. 2020;53(2):353-370.e8. doi:10.1016/j.immuni.2020.07.003

87. Fu J, Zuber J, Martinez M, et al. Human Intestinal Allografts Contain Functional Hematopoietic Stem and Progenitor Cells that Are Maintained by a Circulating Pool. *Cell Stem Cell*. 2019;24(2):227-239.e8. doi:10.1016/j.stem.2018.11.007

88. Gross-Vered M, Trzebanski S, Shemer A, et al. Defining murine monocyte differentiation into colonic and ileal macrophages. *Elife*. 2020;9:1-19. doi:10.7554/eLife.49998

89. Tamoutounour S, Henri S, Lelouard H, et al. CD64 distinguishes macrophages from dendritic cells in the gut and reveals the Th1-inducing role of mesenteric lymph node macrophages during colitis. *Eur J Immunol*. 2012;42(12):3150-3166. doi:10.1002/eji.201242847

90. Jones G-R, Bain CC, Fenton TM, et al. Dynamics of Colon Monocyte and Macrophage Activation During Colitis. *Front Immunol*. 2018;9(NOV). doi:10.3389/fimmu.2018.02764

91. Martin JC, Chang C, Boschetti G, et al. Single-Cell Analysis of Crohn's Disease Lesions Identifies a Pathogenic Cellular Module Associated with Resistance to Anti-TNF Therapy. *Cell*. 2019;178(6):1493-1508.e20. doi:10.1016/j.cell.2019.08.008

92. Jones G-R, Lyons M, Plevris N, et al. IBD prevalence in Lothian, Scotland, derived by

capture–recapture methodology. *Gut*. 2019;68(11):1953-1960. doi:10.1136/gutjnl-2019-318936

93. Reinisch S, Schweiger K, Pablik E, et al. An index with improved diagnostic accuracy for the diagnosis of Crohn's disease derived from the Lennard-Jones criteria. *Aliment Pharmacol Ther*. 2016;44(6):601-611. doi:10.1111/apt.13727

94. Zheng GXY, Terry JM, Belgrader P, et al. Massively parallel digital transcriptional profiling of single cells. *Nat Commun*. 2017;8(1):14049. doi:10.1038/ncomms14049

95. Dobin A, Davis CA, Schlesinger F, et al. STAR: ultrafast universal RNA-seq aligner. *Bioinformatics*. 2013;29(1):15-21. doi:10.1093/bioinformatics/bts635

96. Stoeckius M, Hafemeister C, Stephenson W, et al. Simultaneous epitope and transcriptome measurement in single cells. *Nat Methods*. 2017;14(9):865-868. doi:10.1038/nmeth.4380

97. Stuart T, Butler A, Hoffman P, et al. Comprehensive Integration of Single-Cell Data. *Cell*. 2019;177(7):1888-1902.e21. doi:10.1016/j.cell.2019.05.031

98. R Core Team. R: A Language and Environment for Statistical Computing. Vienna, Austria.

99. Luecken MD, Theis FJ. Current best practices in single-cell RNA-seq analysis: a tutorial. *Mol Syst Biol*. 2019;15(6). doi:10.15252/msb.20188746

100. Mulè MP, Martins AJ, Tsang JS. Normalizing and denoising protein expression data from droplet-based single cell profiling. *Nat Commun*. 2022;13(1):2099. doi:10.1038/s41467-022-29356-8

101. Barron M, Li J. Identifying and removing the cell-cycle effect from single-cell RNA-Sequencing data. *Sci Rep*. 2016;6(1):33892. doi:10.1038/srep33892

102. McInnes L, Healy J, Saul N, Großberger L. UMAP: Uniform Manifold Approximation and Projection. *J Open Source Softw*. 2018;3(29):861. doi:10.21105/joss.00861

103. Becht E, McInnes L, Healy J, et al. Dimensionality reduction for visualizing single-cell data using UMAP. *Nat Biotechnol*. 2019;37(1):38-44. doi:10.1038/nbt.4314

104. Brulois K. Dufy: Density-based Reduction of single-cell data. R package version 1.0.1. github. Published online 2022.

105. Karolchik D. The UCSC Table Browser data retrieval tool. *Nucleic Acids Res*. 2004;32(90001):493D - 496. doi:10.1093/nar/gkh103

106. Tang-Huau TL, Segura E. Human in vivo-differentiated monocyte-derived dendritic cells. *Semin Cell Dev Biol*. 2019;86:44-49. doi:10.1016/j.semcdb.2018.02.018

Acknowledgments

We thank all patients and staff at Herlev hospital, in particular the Gastroenterology Team (Department of Pathology) for help in providing tissue samples. Sequencing was performed at the National Genomics Infrastructure (NGI) and Science for Life Laboratory SNP&SEQ Technology Platform in Uppsala (supported by the Swedish Research Council and the Knut and Alice Wallenberg Foundation). We thank Dr J Rizk (Copenhagen University) for valuable discussions regarding signaling pathways. This work was supported by grants awarded to W.W.A from the Danish Research Council (Sapere Aude III 1331-00136B), the Swedish Medical Research Council (2017-02072), the Swedish Cancerfonden (18 0598), the Gut Cell Atlas, an initiative funded by the Leona M. and Harry B. Helmsley Charitable Trust, US and a grant from the Lundbeck foundation (R155-2014-4184), Denmark, to W.W.A and S.B

Author contributions:

The study was designed by T.M.F., L.W., A.M.M., and W.W.A. Tissue samples were provided by H.L.J., L.B.R., T.H.P., O.H.N., G-R.J., and G-T.H. Experiments were performed by T.M.F., L.W., G-R.J., P.B.J., J.L., and J.V. Bioinformatic analysis was performed by L.W., K.G.B., and T.M.F. and supervised by S.B., K.G.B., and W.W.A. The manuscript was written by T.M.F., L.W., and W.W.A and reviewed and edited by A.M.M. and C.C.B. after input from all authors.

Data and materials availability:

scRNA-seq count data is available through CZ CELLxGENE: https://cellxgene.cziscience.com/e/bcdec5fa-a7fa-4806-92bc-0cd02f40242f.cxg/ .

Code is available: https://github.com/LineWulff/FentonWulff_LP_MNP

Accession numbers:

Figures

Fig. 1. Using high-resolution clustering to disentangle MNP subsets of the human ileal and colonic LP

(**A**) Experimental pipeline for the generation of single-cell transcriptional data of intestinal LP MNP. (**B**) UMAP clustering of pooled ileal (n=4) and colonic LP (n=6) MNPs (28,758 cells), showing normalized gene expression of signature genes for pDC1 (*IL3RA*), cDC1 (*CLEC9A*) and non-classical monocytes (*FCGR3A*) signature gene. (**C**) UMAP of *CD1C* and *CD14* gene expression by intestinal LP MNP. Dashed line encompasses MNP which are not identified as pDC, cDC1, or non-classical monocytes. (**D**) Flow cytometry gating strategy showing CD1c and CD14 expression on colonic LP $CD123^{-}CD123^{-}$ MNP, representative of 10 non-IBD resection patients. (**E**) Curated pseudo-bulk heatmap (using averaged gene expression per cluster) of clusters within the dashed line of the UMAP in (**C**), showing expression of known monocyte, macrophage and cDC2/3 signature genes for clusters 1-39. ISG= interferon-stimulated genes, CCG= cell cycle genes. (**F**) Pseudo-bulk principal component analysis of clusters from **E** using signature gene lists from blood-derived cDC2, classical monocytes, and in-vitro generated monocyte-derived macrophages[106] .

Fig. 2. Transcriptional characterization of cDC subsets from ileal and colonic LP. (**A**) Flattened 3D tspace UMAP (tUMAP) plot of ileal and colonic LP cDC clusters grouped into indicated populations based on high-definition clustering and analysis in Fig. S2. (**B**) Pseudo-bulk heatmap of top 25 DEG expressed by mature cDC1, cDC2-like, cDC3-like and ambiguous cDC

subsets of ileal (red) and colonic (blue) LP. (**C** and **D**) Manually curated pseudo-bulk heatmaps of differentially expressed (**C**) transcription factors and (**D**) cytokines and chemokines, between indicated cDC subsets. (**E**) Volcano plots of DEGs of indicated cDC subsets between pooled ileum and colon LP samples. Dashed lines indicate significance cut-offs. Adjusted P-values < 0.05 and |avg. logFC| > 0.2. (**F**) Venn diagrams depicting number of genes upregulated in indicated cDC subset in the ileum (upper) and colon (lower) LP, as well as genes commonly upregulated within these subsets. (**G**) DoRothEA based inferred transcription factor activity and (**H**) PROGENy based inferred signaling pathway activity in indicated cDC subsets and tissue.

Fig. 3. cDC2- and cDC3-like cells are found in different proportions in the ileal and colonic LP. (A) Violin plots of CD14 and CD1c surface expression by colonic MNP subsets after denoising and scaling to background (DSB)-normalization of CITE-seq. Results are pooled from three colonic and one ileal LP samples. (**B**) CD207 and CD11a surface expression on $CD1c^{+}CD14^{-}$ MNP from indicated tissues using flow cytometry. Results are representative of 10 ileal and colonic LP samples. (**C** and **D**) Pooled colonic LP samples from three CRC resection patients showing (**C**) CD207 and CD11a expression on colonic cDC2-like, cDC3-like and ambiguous cDC clusters using DSB-normalized CITE-seq, and (**D**) Proportion of each cDC cluster within each of the 4 quadrants (Q1-4) depicted in (**C**). (**E** and **F**) Proportion of $CD207^{+}CD11a^{-}$ (Q1), $CD207^{-}CD11a^{-}$ (Q2), $CD207^{+}CD11a^{+}$ (Q3) and $CD207^{-}CD11a^{+}$ (Q4) cells amongst $CD1c^{+}CD14^{-}$ MNP. Samples from **(E)** paired ileal and colonic LP from CRC resection patients (n=10), and (**F**) paired colonic biopsies taken from areas of quiescent or active inflammation from CD patients (n=4) as assessed by flow cytometry. Three to five biopsies were taken per site, and the inflammatory activity of each site

was scored as quiescent or active by the endoscopist at time of removal. Statistical significance was determined using 2-way ANOVA with Sidak's multiple comparisons, *p<0.05, **p<0.01.

Fig. 4. Identification of cDC committed precursors in the human intestine. (**A-C**) tUMAP as in Fig. 2A of ileum and colonic LP cDC clusters. (**A**) HLA-DR^{low} cDC clusters (cluster 1-8) overlaid onto cDC tUMAP, (**B**) proliferation score of indicated cell-cycle-associated genes and (**C**) *ITGAX* expression levels overlaid onto cDC tUMAP. (**D**) Heat map of top 20 DEG (calculated using p.adj. < 0.05) between cDC1, cDC2 and cDC3-like cells, showing expression levels in HLA-DR^{low} cDC clusters. (**E**) RNA velocities (arrows) of HLA-DR^{low} cDC clusters 3-5 and 7-8 calculated with Velocyto package embedded on (A). (**F**) PCA plot of cell from clusters identified by shared DEG (from **D**) as either pre-cDC1 (clusters 4 and 5), pre-cDC2 (cluster 7) or pre-cDC3 (cluster 8) and (**G**) location of clusters not identifiable in (D) (clusters 1-3 and 6) overlaid on the PCA plot in (**F**). (**H**) Model of precursor cluster trajectories towards mature cDC subsets based on tSPACE, velocity and transcriptional analysis. (**I**) Expression of indicated genes across proposed cDC1-, cDC2-, and cDC3- trajectories.

Fig. 5. Characterization of intestinal LP macrophage populations. (**A**) tSpace UMAP (tUMAP) and Louvain clustering of ileal and colonic LP MNP identified as belonging to the monocyte-macrophage lineage. (**B**) Pseudo-bulk heatmap of scaled gene expression of top 10 DEG (ordered by avg. logFC) between M1-M11 clusters. (**C**) Violin plots of normalized gene expression of indicated maturation-associated genes in M1-M11 clusters. (**D**) Pseudotime of cells calculated by

averaging all tSpace trajectories starting from M1. (**E**) Proportions of indicated clusters in paired ileal and colonic LP samples. (**F**) Pseudo-bulk heatmap of scaled gene expression of selected proinflammatory genes for clusters M1-M10 in the ileal and colonic LP. (**G**) Pseudo-bulk heatmap of scaled gene expression of top 13 DEG (ordered by avg. logFC) between mature macrophage clusters M7-M10 in ileal and colonic LP. (**H**) Volcano plots demonstrating DEGs between ileal and colonic LP in mature macrophage clusters M7-M10. Dashed lines indicating significance cut-offs. Adjusted P-values < 0.05 and |avg. logFC| > 0.2. (**I**) Venn diagrams showing overlap of ileum- and colon-specific DEGs for mature macrophage subsets M7, M8, and M10.

Fig. 6. Flow cytometry analysis of mono/mac subsets. (**A**) DSB-normalized CITE-seq expression of indicated surface markers on pooled colonic LP macrophage clusters after exclusion of the minor proliferating M11 cluster, as well as total cDC2/3 clusters as control. Data are integrated from 3 independent colon samples. (**B-E**) Flow cytometry analysis of LP $CD14^+$ mono/mac subsets obtained from digested CRC patient resection samples. (**B**) Colonic LP $CD14^+$ MNP, showing gating strategy to identify putative mono/mac subsets, and surface expression of CD11a, HLA-DR and CD1c on each identified subset. $CD14^+$ MNP were pre-gated as viable $CD3^-$ $CD19^-$ $CD38^-$ $CD123^-$ $HLADR^+$ $CD14^+$ singlets and data are representative of 10 patients. (**C**) Surface expression of CD14 vs. CD206 on ileal and colonic LP $CD14^+CD55^-CD11a^{int/low}$ mature macrophages, showing 10 patients concatenated together. (**D**) Proportion of each mono/mac subset in paired ileal and colonic LP. Each symbol represents a paired ileal/colonic sample. Statistical significance was determined using 2-way ANOVA with Sidak's multiple comparisons, *p<0.05, **p<0.01, ***p<0.001 (**E**) Ratio of $CD14^{hi}CD206^{hi}$ to $CD14^{lo}CD206^{lo}$ mature macrophage subsets

within the ileal and colonic LP. Each symbol represents a paired ileal or colonic sample. Statistical significance was determined using Wilcoxon matched-pairs signed rank test, **p<0.01. (**F**) Proportion of monocyte/macrophage subsets based on flow cytometry analysis of digested colonic biopsies. Extent of IBD inflammation was scored at the time of biopsy by the clinician as quiescent, mild, or moderate. Each symbol represents a CD (filled circle) or UC (open circle) sample. Statistical significance was determined using 2-way ANOVA with Dunnett's multiple comparisons comparing each IBD set to healthy controls, *p<0.05, **p<0.01, ***p<0.001

List of Supplementary Materials

Supplementary materials includes 6 supplementary figures and 7 supplementary tables

Figure S1. Identification of intestinal LP cell types.

Figure S2. Transcriptional characterization of intestinal LP cDC subsets.

Figure S3. Identification of surface markers that help differentiate intestinal cDC2 and cDC3-like cells.

Figure S4. Identification and trajectories of ileum and colon cDC precursor clusters.

Figure S5. Bioinformatic analysis of intestinal LP macrophage populations.

Figure S6. Surface expression of monocyte/macrophage markers

Table S1. Characteristics of anonymized resection patient samples used for single-cell RNA-seq.

Table S2. Complete list of DEG comparing clusters defined as cDC1, cDC2, and cDC3 for combined ileal and colonic LP.

Table S3. Complete list of DEG comparing ileal and colonic LP subsets for cDC1, cDC2 and cDC3.

Table S4. Complete list of DEG comparing mature macrophage clusters M7-M10, with data combined from ileal and colonic LP for each.

Table S5. Complete list of DEG comparing ileal and colonic LP mature macrophages for clusters M7-M10.

Table S6. Characteristics of anonymized biopsy patient samples used for flow cytometry analysis.

Table S7. List of antibodies used for flow cytometry, FACS, and CITEseq analysis of mononuclear phagocyte subsets.

Supplementary Materials

Figure S1. Identification of intestinal LP cell types. (**A** and **B**) UMAP depicting scRNA-seq data of enriched ileal and colonic LP HLA-DR$^+$ cells (42,506 cells) isolated using the pipeline depicted in Fig. 1A. (**A**) Examples of signature gene expression used to identify contaminating T cells, B cells, endothelia, mast cells, stromal cells, and glial cells and (**B**) HLA score based on indicated HLA genes. (**C**) Relative abundance of high resolution MNP clusters in ileal and colonic LP samples. Related to Figure 1.

Figure S2. Transcriptional characterization of intestinal LP cDC subsets. (A) Flattened 3D tSPACE UMAP (tUMAP) of bioinformatically isolated and re-clustered cDC with high resolution Louvain clustering (52 clusters) and split into ileum and colon LP. (**B**) Cell cycle profile (**C**) HLA score based on indicated HLA genes. (**B** and **C**) Dashed line represents clusters enriched in cells in G2M/S phase and with low HLA score. (**D**) cDC1 score based on cDC1 signature genes (*CLEC9A, CADM1, XCR1, BATF3,* and *IRF8*) by pseudo-bulk cDC clusters (44 clusters) after removal of the proliferating and HLA^{low} clusters in **B** and **C**. Dashed line indicating cDC1 identity, threshold cDC1 score > 0.4 for cDC1 identity. (**E**) Ranked expression of cDC2 and cDC3 scores by remaining cDC clusters (37 clusters) using signature genes identified by Bourdeley et al[30]. Dashed lines indicating cDC2, cDC3 and ambiguous identities.

Clusters were classified as cDC2 when cDC2 score > 0.4 & cDC3 score < 0.3 and as cDC3 when cDC3 score > 0.4. (**F**) tUMAP plots colored by expression of indicated genes (upper panel) associated with cDC maturation and migration migratory marker and (lower panel) interferon inducible genes. (**G** and **H**) Selected biologically relevant terms from GO analysis with EnrichR (Biological Processes 2021). Y-axis = sqrt(-log(adjusted P-value)). Dashed line indicates significance threshold of adjusted P-value = 0.05. (**G**) Based on DEGs from each cDC subset (supplementary table 2) (**H)** Based on DEGs Fig. 2E (supplementary table 4). Related to Figure 2.

Figure S3. Identification of surface markers that help differentiate intestinal cDC2 and cDC3-like cells. (A) Pre-gating strategy to identify colonic-LP $CD1c^{+}CD14^{-}$ cDC2, ambiguous and cDC3-like cells. (**B)** CD207 and CD11a expression as assessed by DSB-normalized CITE-seq, Q, quadrant and (**C**) relative proportions of cDC2-like, cDC3-like and ambiguous cDCs within the four CD207 and CD11a CITE-seq quadrants (**B** and **C**) in indicated tissue from a single CRC resection patient. Related to Figure 3.

Figure S4. Identification and trajectories of ileum and colon cDC precursor clusters. (**A**) RNA velocities (arrows) of $HLA\text{-}DR^{low}$ cDC clusters 3-5 and 7-8 split into ileum and colon derived cDC clusters and calculated with Velocyto package and embedded on Fig. 4A. (**B**) Location of indicated clusters not identifiable using DEG for mature cDC split into ileum and colon (Fig. 4D) on a PCA plot of clusters identified by shared DEG as either pre-cDC1, pre-cDC2 or pre-cDC3 (see Fig. 4F). (**C**) Heat map depicting Pearson correlation of each intestinal putative pre-cDC cluster and $CD14^{+}$

monocytes with indicated progenitor populations from BM described in Triana et al. [49]. Related to Figure 4.

Figure S5. Bioinformatic analysis of intestinal LP macrophage populations. (**A)** PROGENy and (**B**) DoRothEA analysis of indicated clusters from the ileum and colon LP. (**C**) Selected biologically relevant terms from GO analysis with EnrichR (Biological Processes 2021). Y-axis = sqrt(-log(adjusted P-value)). Dashed line indicates significance threshold of adjusted P-value = 0.05. Data are based on DEGs from each mature macrophage subset (supplementary Table 6). (**D**) Violin plots of indicated genes for colonic and ileal LP mature macrophage clusters. (**E**) Significance levels of selected biologically relevant terms from GO analysis with EnrichR (Biological Processes 2021). Y-axis = sqrt(-log(adjusted P-value)). Dark grey dashed line indicates significance threshold of adjusted P-value = 0.05. Data are based on DEGs in Fig. 5H and supplementary Table 8). Related to Figure 5.

Figure S6. (**A**) Representative flow cytometry analysis showing pre-gating for $CD14^+$ MNP. (**B**) Flow cytometry-based expression of indicated markers on $CD14^+$ MNP using Legendscreen. Grey fill, FMO. Red line, specific antibody stain. (**C**) DSB-normalized CITE-seq expression of indicated surface markers on ileal LP macrophage clusters after exclusion of the minor proliferating M11 cluster based on n=1. Related to Figure 6.

Figure 1

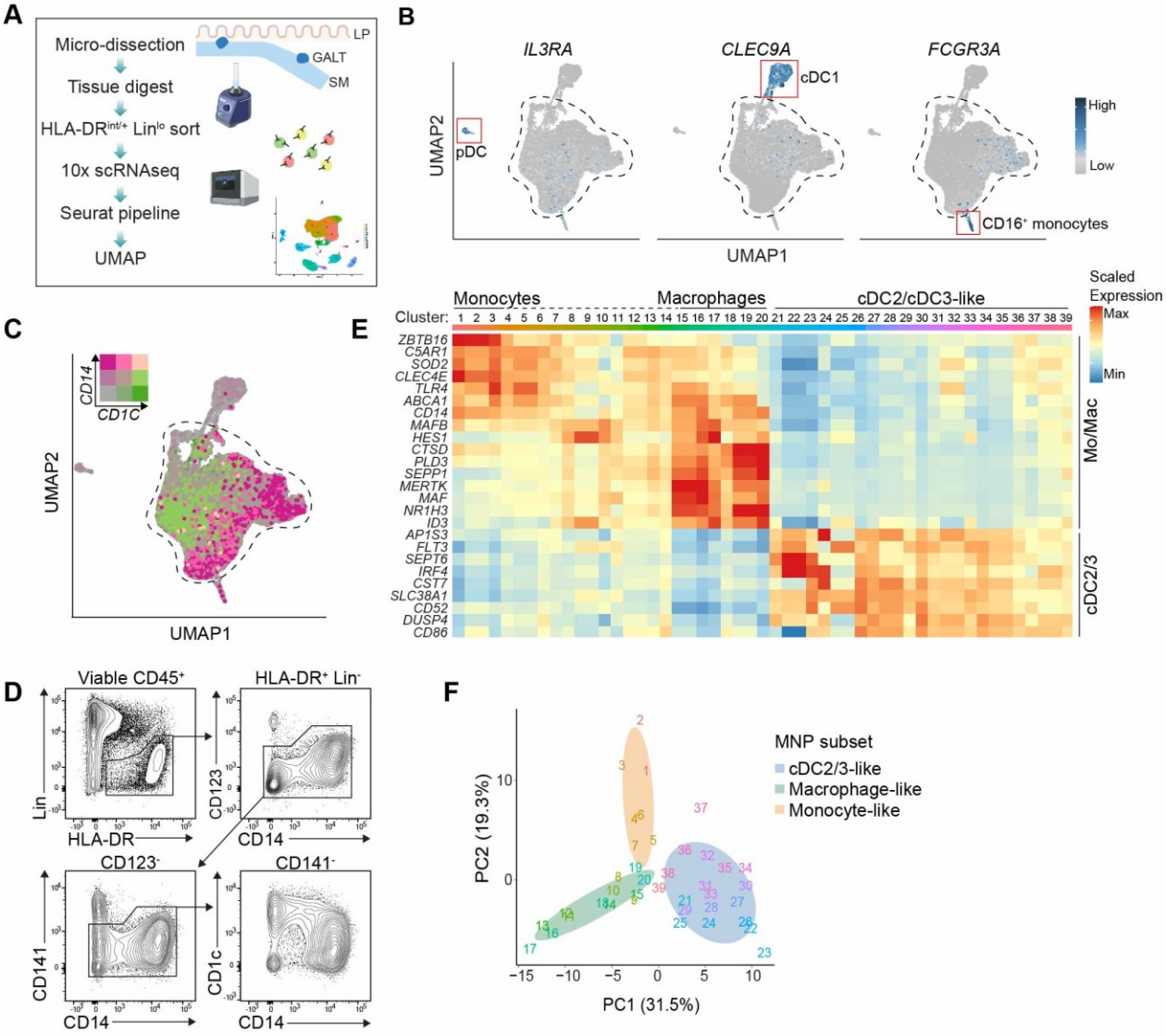

Figure 2

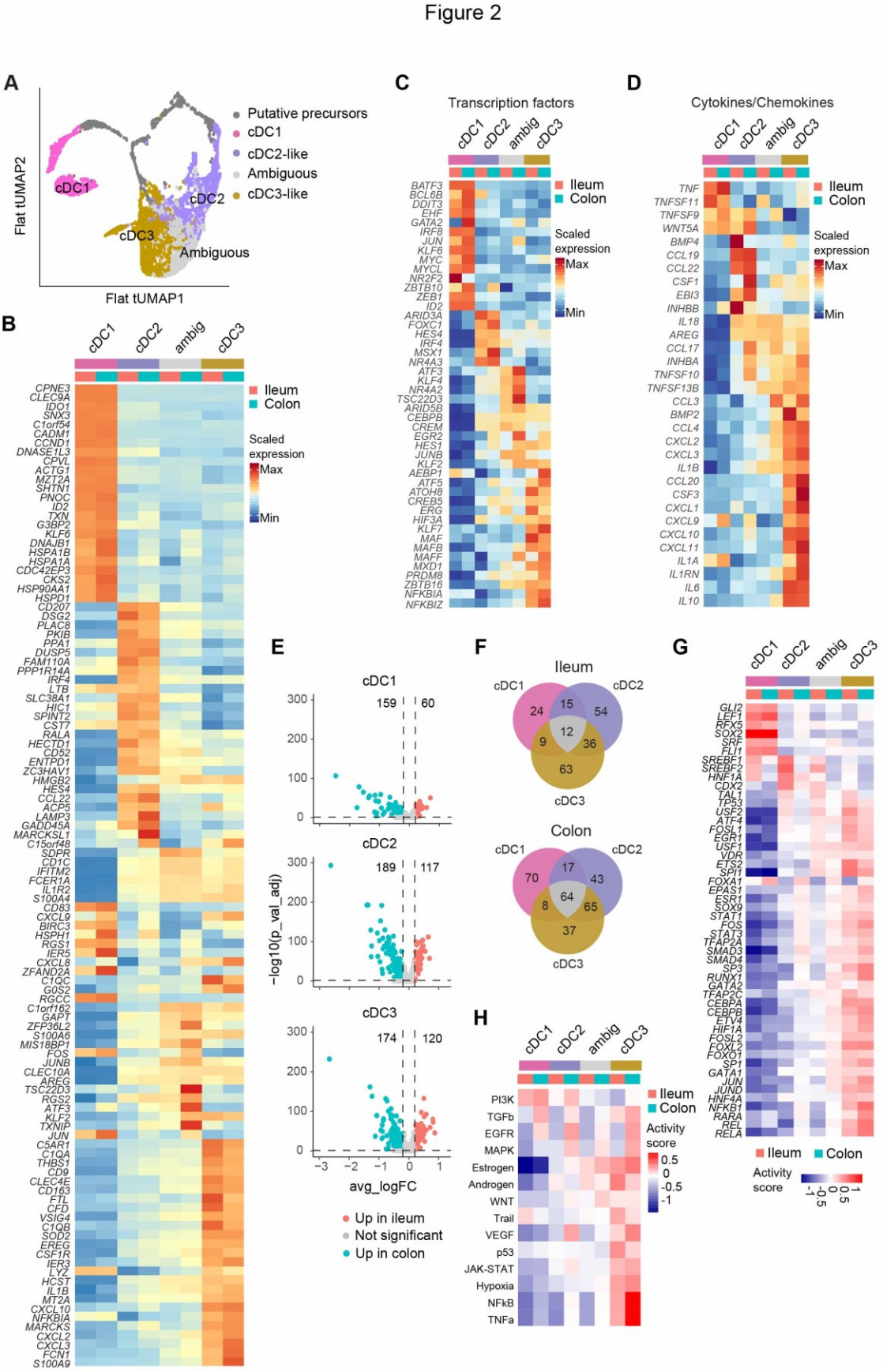

Figure 3

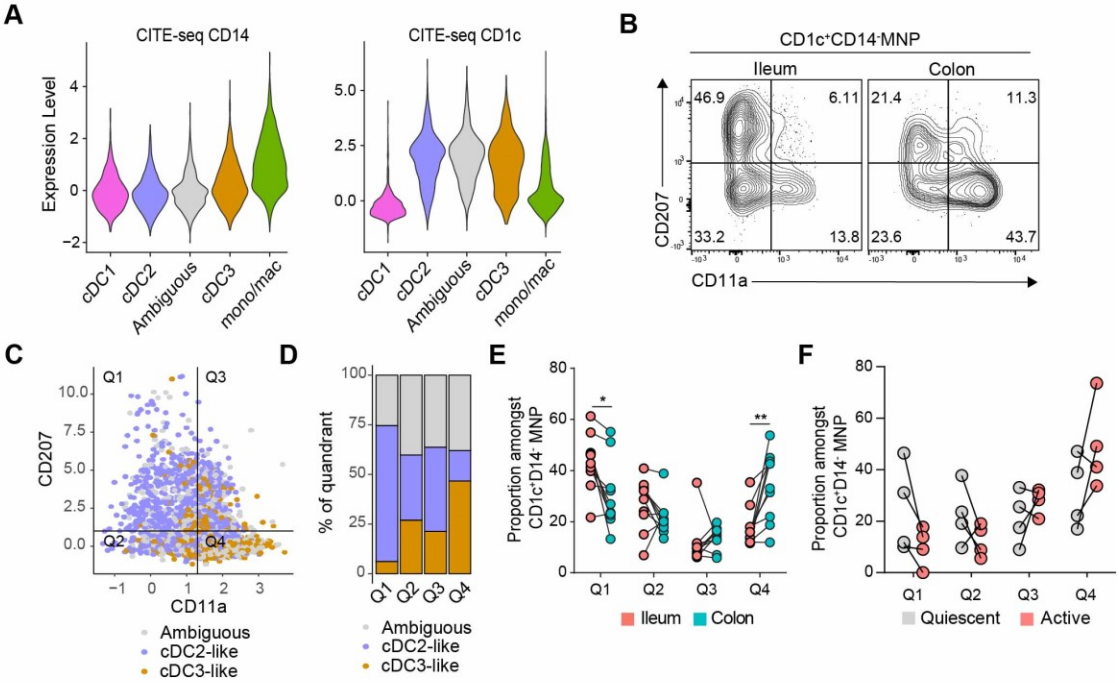

Figure 4

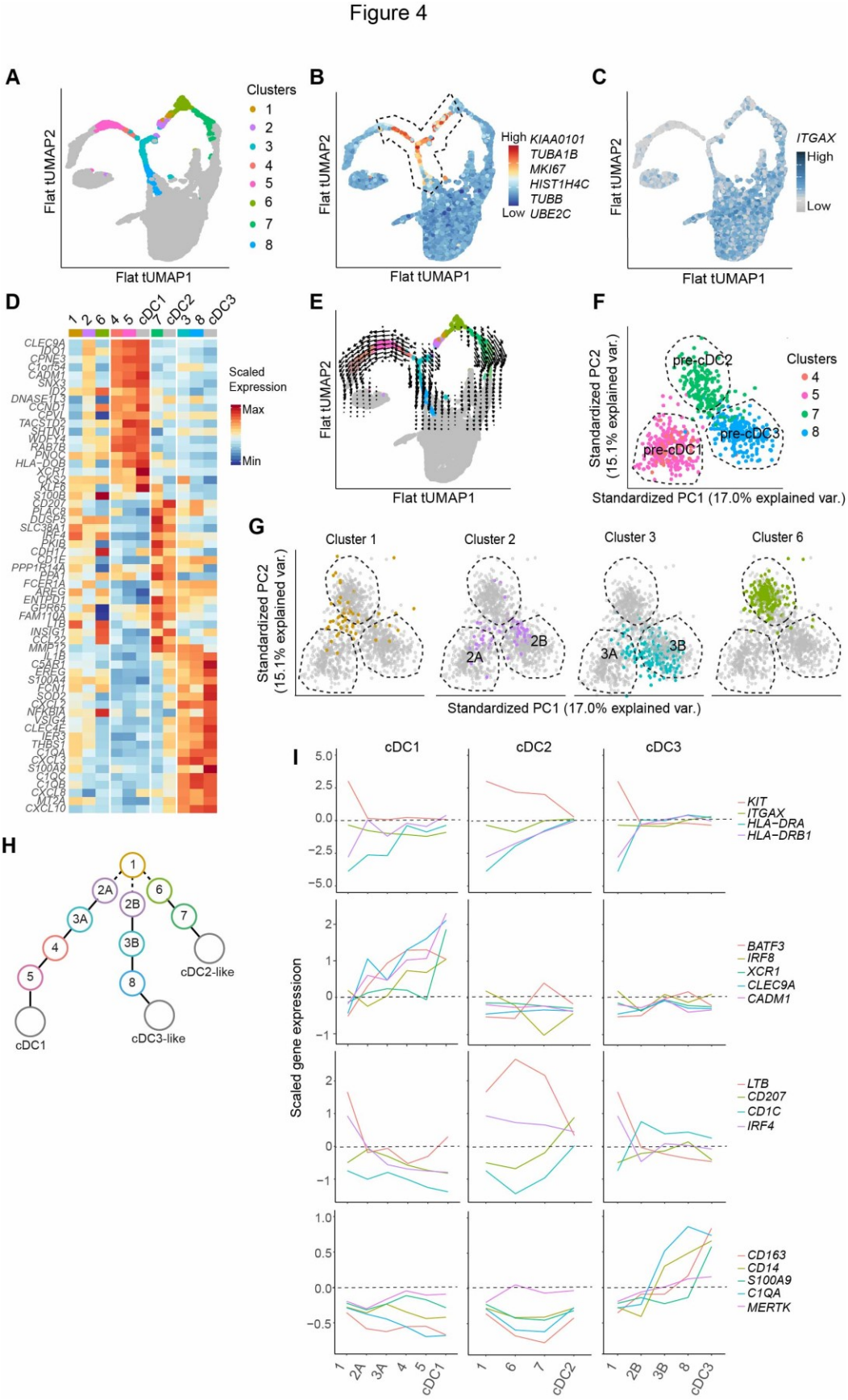

Figure 5

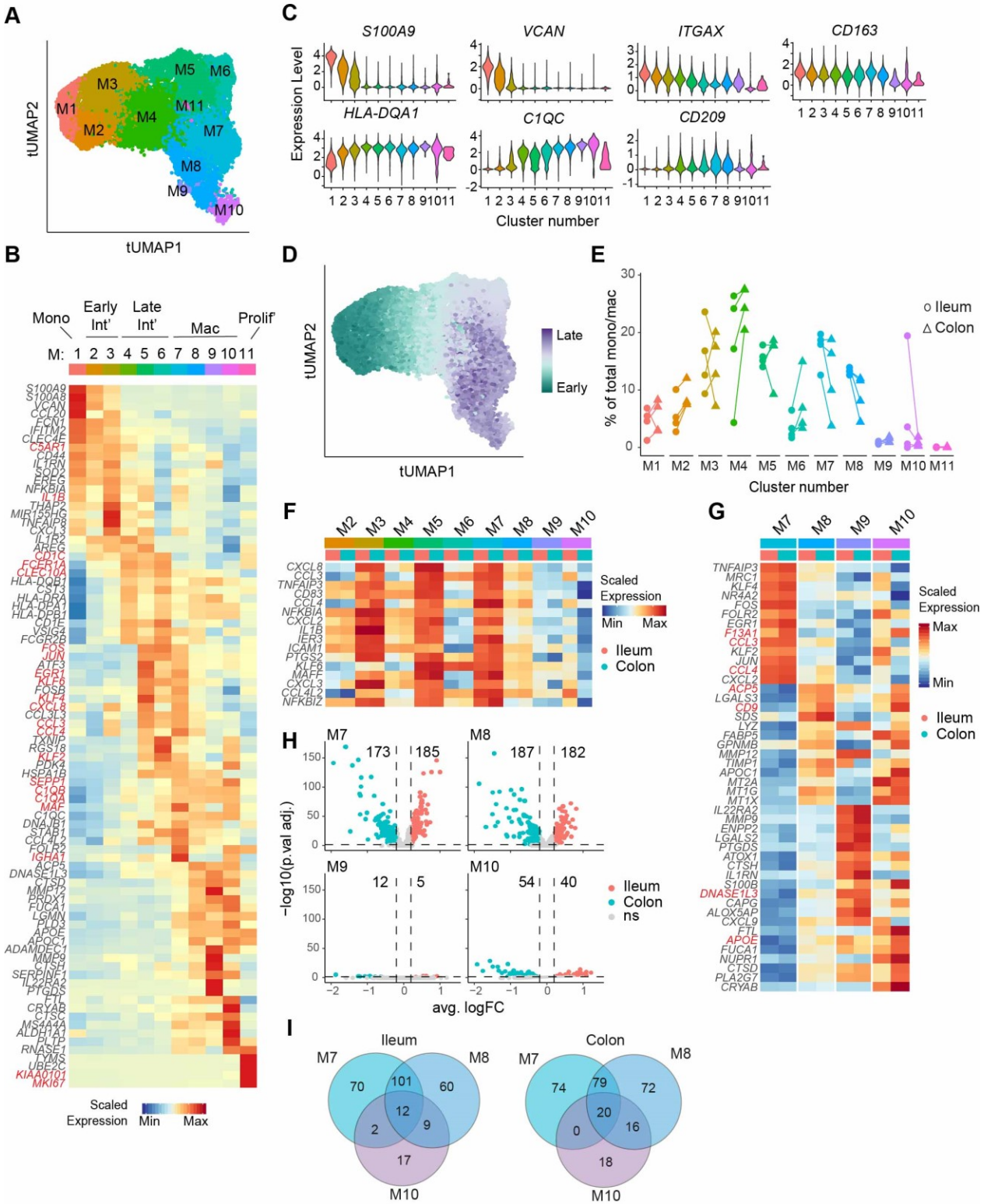

Figure 6

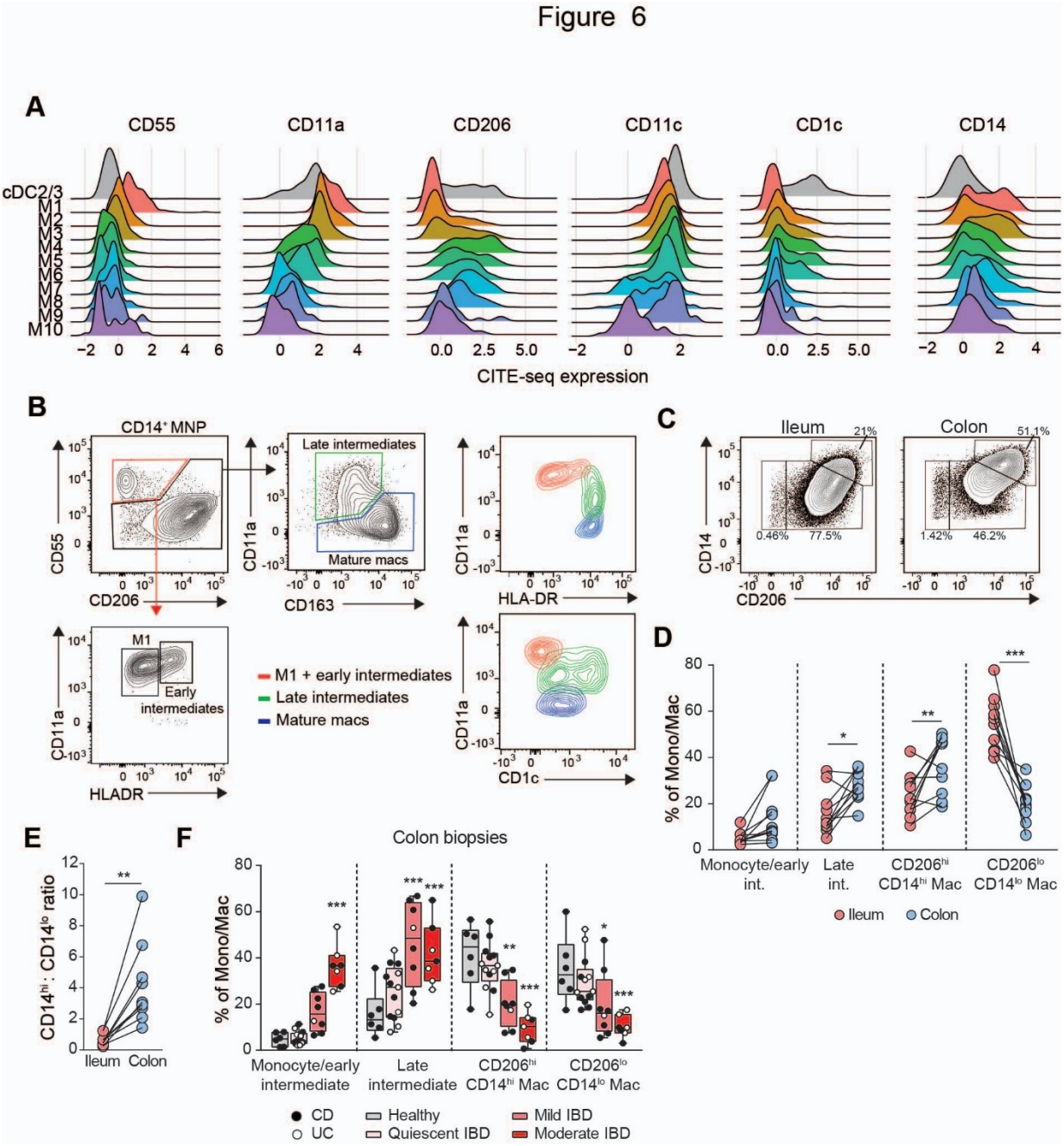

Supplementary Figure 1

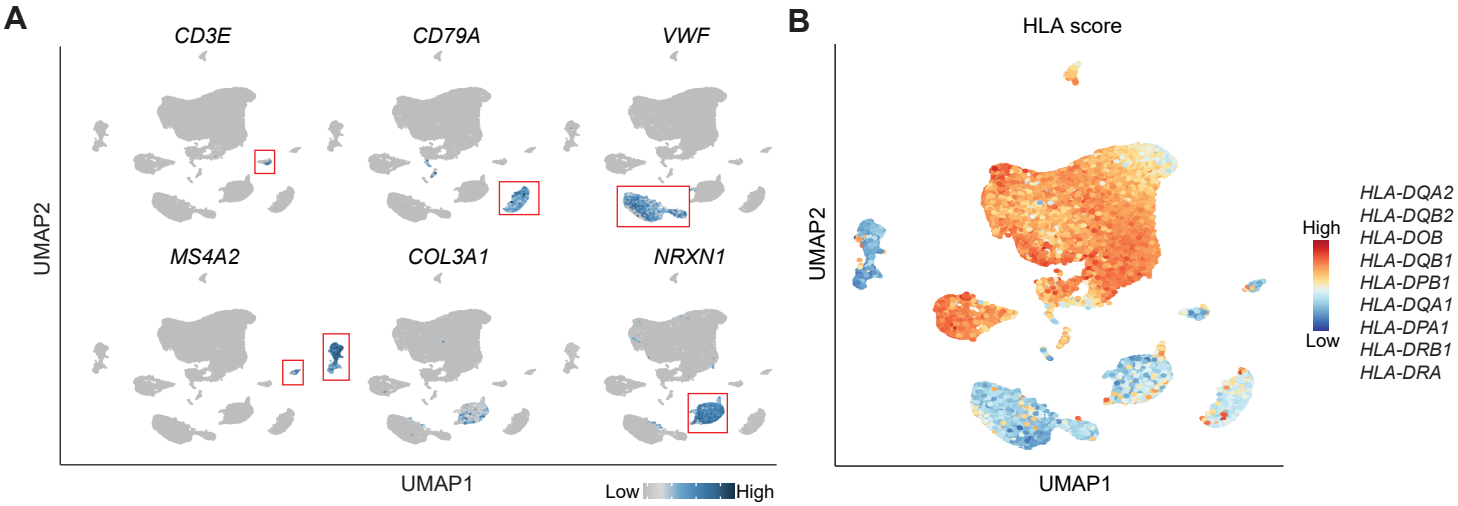

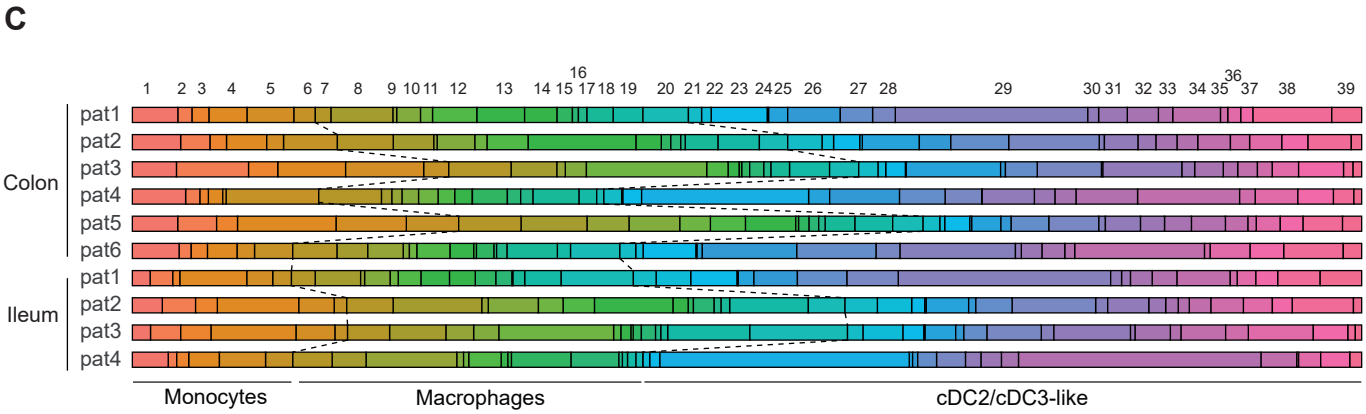

Supplementary Figure 2

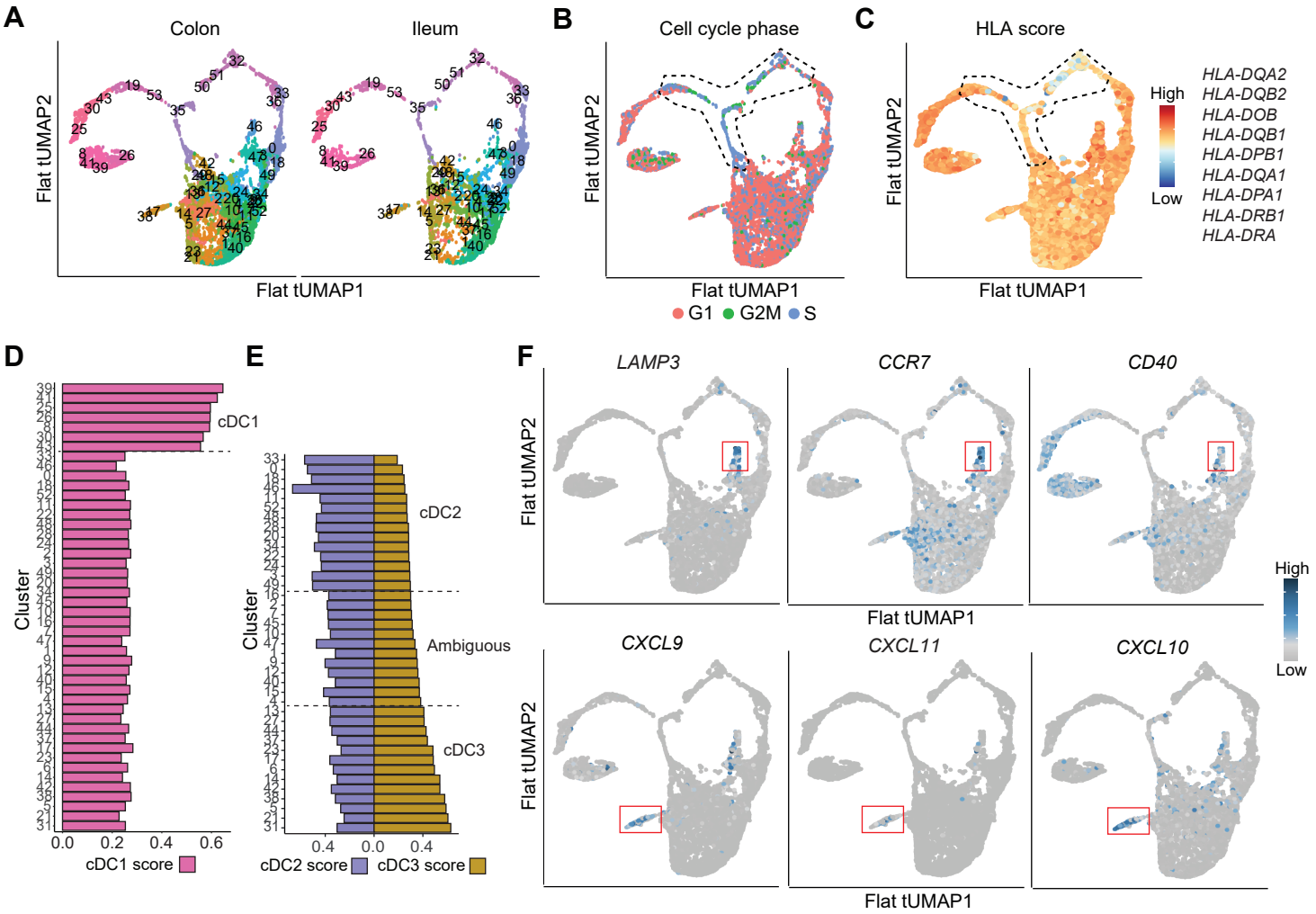

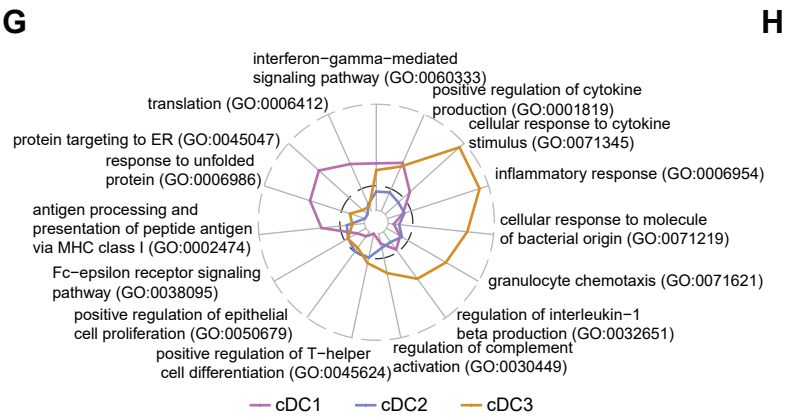

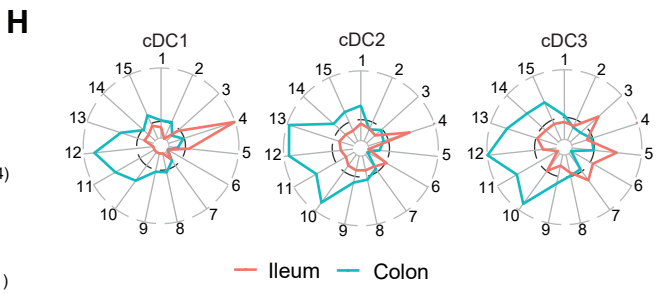

1	(GO:0060333)	interferon−gamma−mediated signaling pathway
2	(GO:0002755)	MyD88−dependent toll−like receptor signaling pathway
3	(GO:0008284)	positive regulation of cell population proliferation
4	(GO:0045047)	protein targeting to ER
5	(GO:0030449)	regulation of complement activation
6	(GO:0030299)	intestinal cholesterol absorption
7	(GO:0001818)	negative regulation of cytokine production
8	(GO:0032655)	regulation of interleukin−12 production
9	(GO:0070498)	interleukin−1−mediated signaling pathway
10	(GO:0043066)	negative regulation of apoptotic process
11	(GO:0080135)	regulation of cellular response to stress
12	(GO:0006986)	response to unfolded protein
13	(GO:0019221)	cytokine−mediated signaling pathway
14	(GO:0051092)	positive regulation of NF−kappaB transcription factor activity
15	(GO:0001819)	positive regulation of cytokine production

Supplementary Figure 3

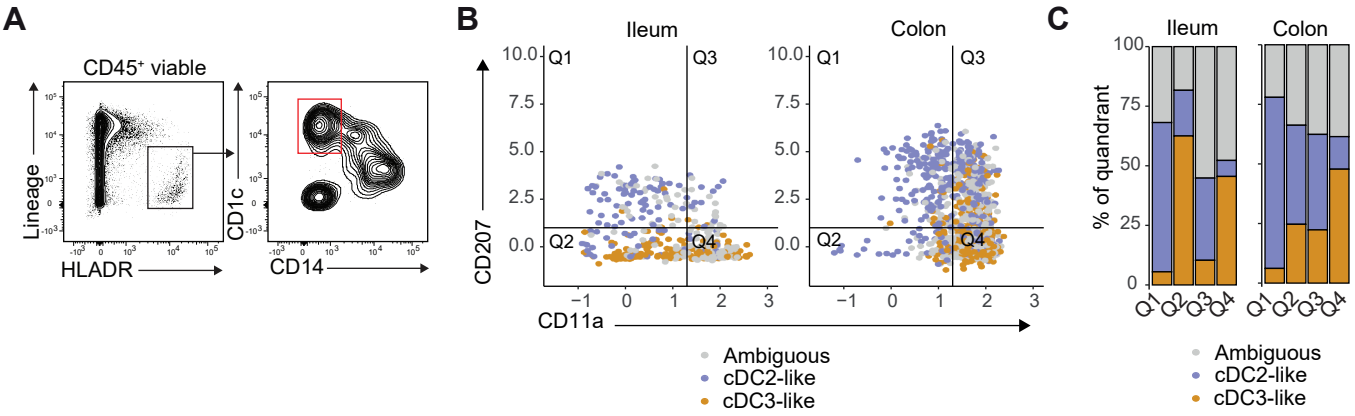

Supplementary Figure 4

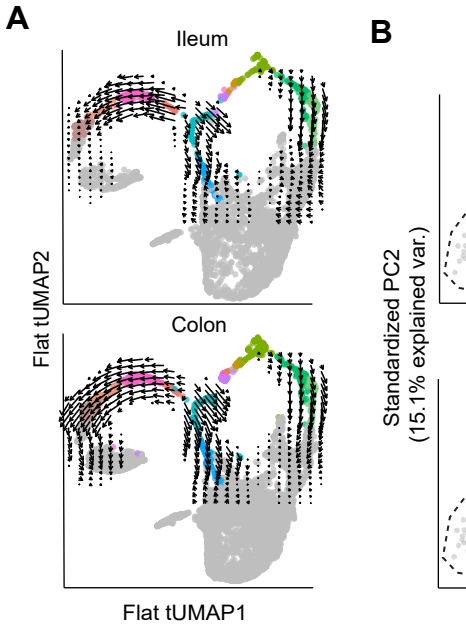

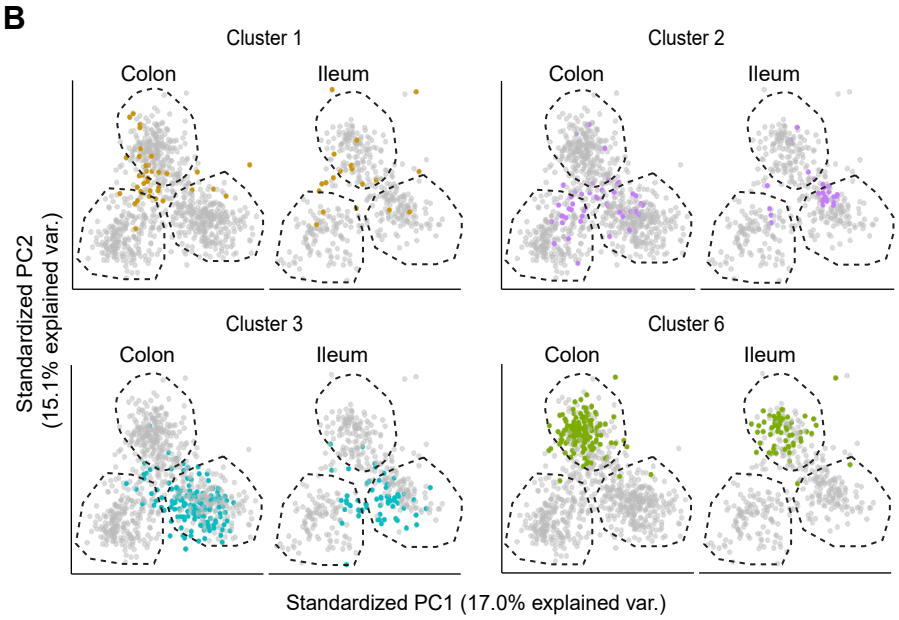

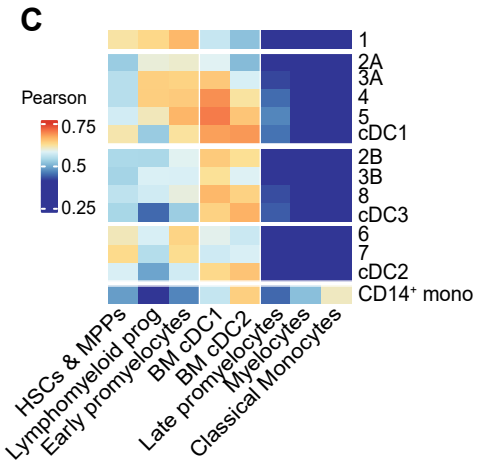

Supplementary Figure 5

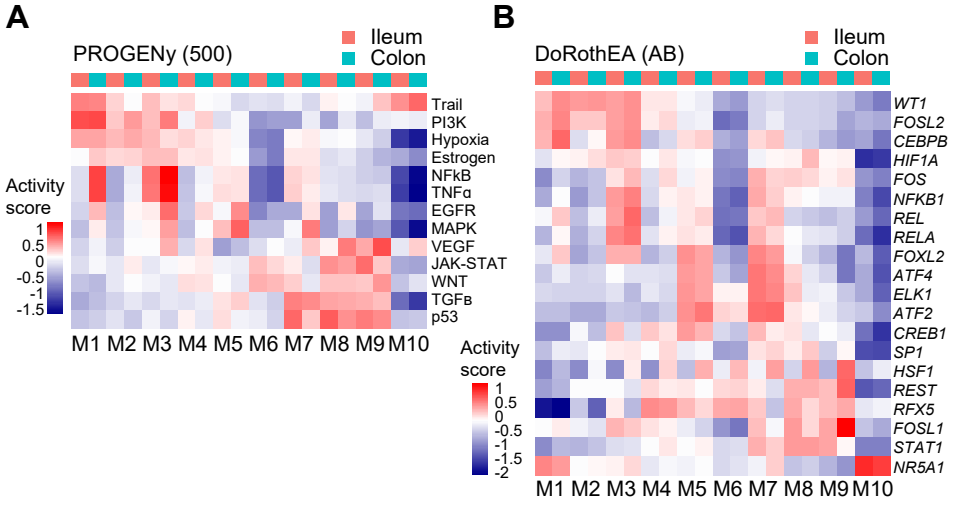

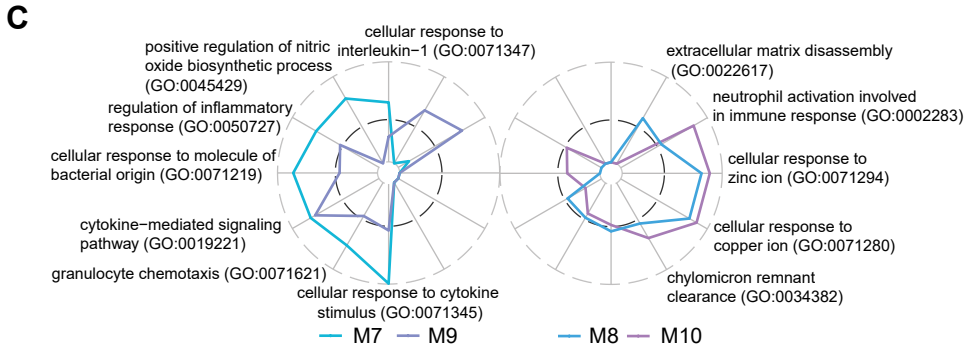

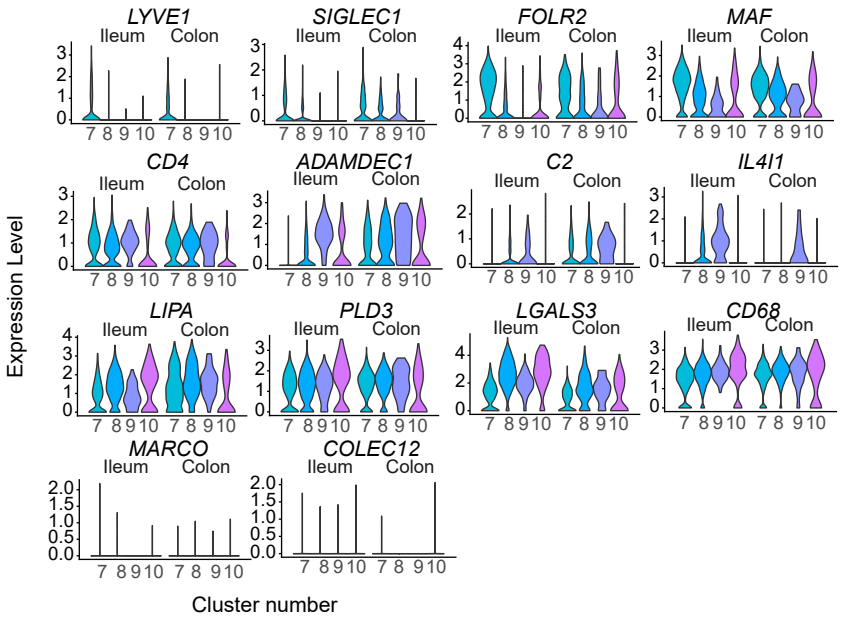

E

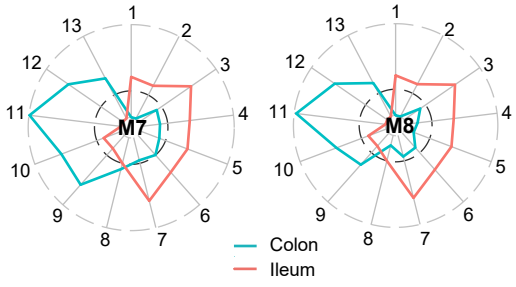

1	(GO:0150146)	cell junction disassembly
2	(GO:0006958)	complement activation, classical pathway
3	(GO:0002478)	antigen processing and presentation of exogenous peptide antigen
4	(GO:0050778)	positive regulation of immune response
5	(GO:0032680)	regulation of tumor necrosis factor production
6	(GO:2000379)	positive regulation of reactive oxygen species metabolic process
7	(GO:0060333)	interferon−gamma−mediated signaling pathway
8	(GO:0071396)	cellular response to lipid
9	(GO:0006898)	receptor−mediated endocytosis
10	(GO:0045047)	protein targeting to ER
11	(GO:0006986)	response to unfolded protein
12	(GO:0080135)	regulation of cellular response to stress
13	(GO:0038096)	Fc−gamma receptor signaling pathway involved in phagocytosis

Supplementary Figure 6

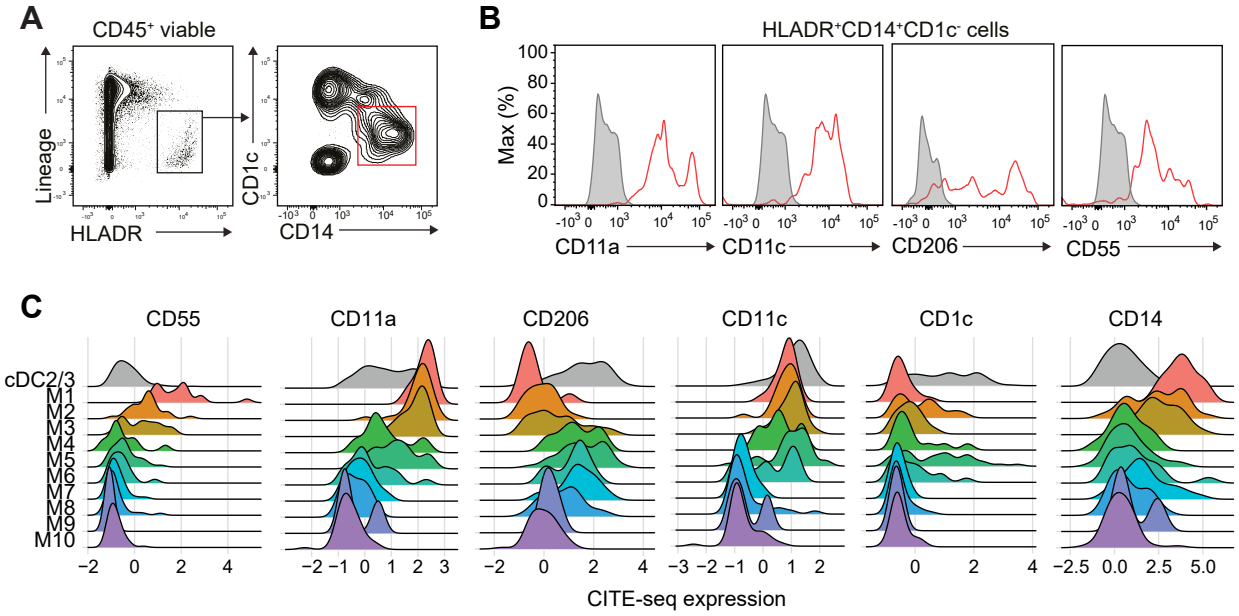

Patient	Age	Sex	Diagnosis	Cancer TNM	Cancer stage	Site of colon resection	Site of SI resection	CITEseq
SC1	66	F	Adenocarcinoma	T1 N0 V0 M0	1	n.d.	Ileum	-
SC2	74	M	Adenocarcinoma	T4a N1a V0 M0	3b	Transverse	Ileum	-
SC3	63	F	Polyp	n.a.	n.a.	Ascending	Ileum	-
SC4	76	F	Adenocarcinoma	T4 N0	2	Transverse	Ileum	Colon+Ileum
SC5	63	F	Polyp	n.a.	n.a.	Ascending	-	Colon
SC6	83	M	Adenocarcinoma	T3 N1 V2 M0	3	Cecum	-	Colon

Table S1 - Characteristics of patient samples used for scRNAseq. n.a = not applicable, n.d. = no data.

Table S2

cluster	gene	avg_logFC	p_val
cDC1	CLEC9A	1.77121966	0
cDC1	IDO1	1.56615761	0
cDC1	CPNE3	1.56209083	0
cDC1	C1orf54	1.50447344	0
cDC1	CADM1	1.3783539	0
cDC1	SNX3	1.26838501	0
cDC1	ID2	1.09695472	0
cDC1	DNASE1L3	1.03392837	0
cDC1	CCND1	0.94740221	0
cDC1	CPVL	0.90499795	0
cDC1	TACSTD2	0.80353558	0
cDC1	SHTN1	0.77907453	0
cDC1	WDFY4	0.74904387	0
cDC1	RAB7B	0.72511212	0
cDC1	PNOC	0.72215078	0
cDC1	HLA-DOB	0.71467434	0
cDC1	XCR1	0.69279714	0
cDC1	KIAA0226L	0.69091174	0
cDC1	ENPP1	0.65754419	0
cDC1	LGALS2	0.62632423	0
cDC1	CAMK2D	0.6257283	0
cDC1	ACTG1	0.61125237	0
cDC1	CLNK	0.59404656	0
cDC1	VCAM1	0.5820313	0
cDC1	TMEM14A	0.57964012	0
cDC1	ASB2	0.5492599	0
cDC1	HLA-B	0.50697587	0
cDC1	C1orf21	0.46030411	0
cDC1	EGLN3	0.40194192	0
cDC1	PLCD1	0.39756319	0
cDC1	FKBP1B	0.39516461	0
cDC1	VAC14	0.37910938	0
cDC1	SLC24A4	0.36508782	0
cDC1	AIM2	0.3648107	0
cDC1	DBN1	0.36318526	0
cDC1	GCSAM	0.36291279	0
cDC1	PLPP1	0.35189124	0
cDC1	CCDC126	0.34981822	0
cDC1	PTK2	0.32055745	0
cDC1	BTLA	0.30137383	0
cDC1	CLCN4	0.2977957	0
cDC1	TSPAN2	0.28215222	0
cDC1	SNX22	0.26229043	0
cDC1	GPR31	0.24675418	0
cDC1	PPY	0.24539174	0
cDC1	PAWR	0.24133892	0
cDC1	FMNL2	0.24044337	0
cDC1	FUCA1	0.54275503	1.38E-303

cDC1	PNRC1	0.37415917	1.87E-300
cDC1	RPLP1	0.34269767	3.73E-298
cDC1	PLPP3	0.22601948	3.21E-292
cDC1	RP11-798K3.3	0.26052021	3.49E-291
cDC1	LGALS1	0.5863341	1.79E-287
cDC1	CKS2	0.80060922	6.17E-281
cDC1	GSTP1	0.47253761	2.08E-280
cDC1	MYL6	0.40737482	3.07E-280
cDC1	MZT2A	0.65429858	2.71E-279
cDC1	FNBP1	0.57733157	1.98E-274
cDC1	PPT1	0.62104036	8.34E-271
cDC1	MIR4435-2HG	0.57962466	9.95E-269
cDC1	RGS10	0.48722647	7.79E-268
cDC1	TSPAN13	0.20046037	7.70E-263
cDC1	PSMB9	0.5263432	2.08E-260
cDC1	KIF16B	0.33738519	2.64E-251
cDC1	HLA-A	0.45186776	6.98E-251
cDC1	PDLIM7	0.27242953	8.08E-249
cDC1	CD59	0.47525804	2.44E-246
cDC1	LAG3	0.2050153	3.30E-239
cDC1	TXN	0.66660661	1.12E-230
cDC1	SLAMF7	0.54597363	8.02E-230
cDC1	UCP2	0.54413173	1.38E-223
cDC1	BATF3	0.50647767	2.54E-223
cDC1	ASAP1	0.47950691	4.99E-222
cDC1	SERPINF2	0.27523995	2.37E-219
cDC1	CKB	0.43878804	3.28E-219
cDC1	TSTD1	0.4640208	7.92E-219
cDC1	TMSB4X	0.46172588	1.87E-218
cDC1	CSRP1	0.37933958	6.28E-216
cDC1	IRF8	0.60483066	6.93E-211
cDC1	GYPC	0.49414723	1.40E-210
cDC1	SUSD3	0.37872262	2.63E-210
cDC1	G3BP2	0.5613288	1.24E-205
cDC1	KLF6	0.83837008	2.67E-205
cDC1	CYB5R3	0.4496696	3.42E-205
cDC1	DEF8	0.268095	6.83E-203
cDC1	RPL8	0.23648854	3.25E-202
cDC1	LIMA1	0.32777794	9.73E-201
cDC1	DCTPP1	0.39900402	3.05E-200
cDC1	FRMD4A	0.21688664	1.21E-197
cDC1	MAP2K6	0.2024215	2.21E-197
cDC1	EHD4	0.38459836	6.98E-193
cDC1	QPRT	0.25656835	8.61E-193
cDC1	RPS21	0.37456119	1.77E-187
cDC1	CDC42EP3	0.55880021	6.15E-187
cDC1	LRRCC1	0.27832569	1.02E-186
cDC1	NAP1L1	0.44868842	3.41E-186
cDC1	APOL3	0.28200373	3.78E-185
cDC1	ADAM19	0.36898673	4.33E-184

cDC1	PARP1	0.40577161	8.98E-181
cDC1	TJP2	0.24545821	3.38E-180
cDC1	ATP6V1H	0.41384757	4.12E-180
cDC1	LSM6	0.41507209	1.57E-177
cDC1	ATP5E	0.28379635	6.05E-176
cDC1	TSPAN33	0.44033906	1.19E-175
cDC1	CD74	0.29916942	1.24E-174
cDC1	SELPLG	0.28961628	2.42E-171
cDC1	LINC00152	0.50092451	2.93E-165
cDC1	ATP1A1	0.47006058	3.22E-165
cDC1	ZFP36L1	0.56328269	8.69E-165
cDC1	CNFN	0.22139585	6.45E-164
cDC1	RAMP1	0.33821978	2.39E-163
cDC1	RAB30	0.20029923	1.70E-162
cDC1	HN1	0.45071853	2.92E-161
cDC1	CDK2AP2	0.4235387	3.84E-161
cDC1	TLR10	0.26603175	1.54E-160
cDC1	EEF1B2	0.36309248	3.62E-160
cDC1	LPP	0.4322844	5.37E-160
cDC1	SLC46A3	0.25954279	1.68E-159
cDC1	CD40	0.38171278	3.06E-159
cDC1	NAAA	0.42348889	1.45E-158
cDC1	RAB11FIP1	0.56873895	4.36E-158
cDC1	DUSP4	0.59123503	2.02E-156
cDC1	RAB29	0.25807406	3.98E-156
cDC1	UPF2	0.43704297	4.05E-156
cDC1	CD226	0.20400354	6.59E-156
cDC1	ANPEP	0.26584799	2.77E-149
cDC1	ZEB1	0.20876783	3.55E-149
cDC1	NDUFC2	0.35392579	1.29E-147
cDC1	NCOA7	0.30109121	2.67E-147
cDC1	TAP1	0.41008254	8.55E-147
cDC1	DAPK2	0.20525188	1.28E-146
cDC1	Sep-11	0.27769303	8.28E-146
cDC1	ENSA	0.36587381	4.64E-144
cDC1	SLC9A9	0.20471264	1.05E-143
cDC1	DSTN	0.37965852	1.46E-143
cDC1	CCSER1	0.21081249	9.16E-143
cDC1	ICAM3	0.32677678	7.53E-141
cDC1	MPEG1	0.42071785	2.78E-139
cDC1	S100B	0.82820931	1.85E-137
cDC1	TAP2	0.31614312	1.49E-135
cDC1	RPS23	0.2448476	8.13E-134
cDC1	PRDX1	0.39729998	1.54E-132
cDC1	REPIN1	0.25688176	4.01E-132
cDC1	LIMD2	0.38065416	5.97E-130
cDC1	BASP1	0.46898747	9.81E-130
cDC1	BCL2L11	0.43903699	2.48E-129
cDC1	PIKFYVE	0.29782276	2.84E-129
cDC1	SFT2D2	0.32548547	1.59E-128

cDC1	C20orf27	0.31687398	5.97E-128
cDC1	LDLRAD4	0.39820552	2.93E-127
cDC1	SERTAD3	0.23822772	2.22E-124
cDC1	HLA-C	0.35328038	3.62E-121
cDC1	GSTM4	0.23410816	1.83E-120
cDC1	ICOSLG	0.25772427	1.11E-119
cDC1	TMEM50B	0.29226297	7.04E-119
cDC1	CEP164	0.22927139	8.31E-119
cDC1	HLA-DPB1	0.22996263	2.76E-118
cDC1	SRSF7	0.52160343	9.56E-118
cDC1	RPS8	0.21979588	3.06E-116
cDC1	FNIP2	0.39841213	1.55E-114
cDC1	DLGAP4	0.21777474	1.41E-113
cDC1	SLC5A3	0.35623243	3.76E-113
cDC1	CCDC186	0.25718456	8.10E-112
cDC1	SRI	0.33010018	1.12E-111
cDC1	NME4	0.24950706	1.94E-111
cDC1	GNG7	0.25713732	2.37E-111
cDC1	OXSR1	0.35637344	3.19E-111
cDC1	CCDC6	0.34956065	3.20E-110
cDC1	TNNI2	0.24226329	1.78E-109
cDC1	LYRM4	0.2513569	2.00E-109
cDC1	RPS20	0.38051544	2.33E-109
cDC1	RGCC	0.51490876	3.26E-109
cDC1	ZYX	0.29677598	1.99E-108
cDC1	PTMS	0.42537366	2.50E-108
cDC1	RNASEH2C	0.40352848	5.92E-108
cDC1	RAB32	0.47719838	1.27E-107
cDC1	CBL	0.21650085	3.46E-107
cDC1	CCR6	0.25228106	6.47E-107
cDC1	AGPAT1	0.22025355	3.86E-106
cDC1	EIF6	0.29393194	2.50E-105
cDC1	HMOX1	0.29108668	6.47E-104
cDC1	TMED3	0.27715482	1.09E-103
cDC1	ACTN1	0.28226377	1.70E-103
cDC1	LY9	0.31495331	3.23E-103
cDC1	ACTB	0.2605768	8.89E-103
cDC1	PTPN22	0.21467183	1.51E-101
cDC1	VMO1	0.42045516	4.73E-101
cDC1	DAPP1	0.32350871	1.65E-100
cDC1	CFL1	0.22276996	7.51E-100
cDC1	OAZ2	0.28000747	4.78E-99
cDC1	COX7C	0.24642598	1.04E-98
cDC1	MRPS6	0.30340051	1.05E-97
cDC1	ROGDI	0.26795459	1.22E-97
cDC1	CKLF	0.3826577	1.50E-97
cDC1	RPL23A	0.24927497	3.58E-97
cDC1	ANXA6	0.27537732	5.21E-97
cDC1	RAB8B	0.31377491	1.20E-96
cDC1	DST	0.29161035	1.49E-96

cDC1	ATP6V0E1	0.27038126	3.17E-93
cDC1	MYCL	0.22697697	4.08E-92
cDC1	SRP14	0.22035809	1.31E-91
cDC1	SMCO4	0.27279047	8.01E-91
cDC1	DUSP10	0.25624431	9.94E-91
cDC1	HSPA8	0.38032024	2.05E-90
cDC1	IFT20	0.27792092	4.09E-90
cDC1	NET1	0.27305308	2.18E-89
cDC1	MZT2B	0.37996252	6.17E-89
cDC1	ELOVL5	0.25059261	1.06E-88
cDC1	FAM129A	0.24968821	8.41E-88
cDC1	MCUR1	0.24839729	1.51E-87
cDC1	HLA-DQB1	0.22073791	6.85E-87
cDC1	SOX4	0.49816704	1.34E-85
cDC1	LSP1	0.26344392	2.68E-85
cDC1	CCPG1	0.20071545	4.63E-85
cDC1	HLA-DPA1	0.22197204	8.44E-85
cDC1	CLIC2	0.24056369	3.21E-83
cDC1	BRD2	0.3131404	5.50E-83
cDC1	CD83	0.3426897	6.29E-83
cDC1	ATP6V1D	0.22197711	1.15E-82
cDC1	TNF	0.32197088	8.41E-82
cDC1	ATG3	0.2752695	2.10E-81
cDC1	PFDN2	0.28429388	5.49E-80
cDC1	RP1-313I6.12	0.24033699	1.92E-79
cDC1	RPS11	0.26564203	4.39E-79
cDC1	INPP5F	0.20501436	4.66E-79
cDC1	WBSCR22	0.24604303	1.29E-78
cDC1	HLA-F	0.26432397	1.38E-78
cDC1	SMS	0.23277699	5.44E-78
cDC1	FLT3	0.2433171	1.08E-77
cDC1	HDAC9	0.22175685	2.67E-77
cDC1	SPNS1	0.22725586	6.80E-77
cDC1	RPS27L	0.24263782	1.28E-76
cDC1	TRMT112	0.2602086	3.35E-76
cDC1	CTTNBP2NL	0.2241378	6.80E-76
cDC1	ABRACL	0.23898982	8.82E-76
cDC1	TPMT	0.2202931	2.71E-75
cDC1	SDHA	0.20893918	2.97E-75
cDC1	STK17A	0.26861438	2.46E-74
cDC1	RPL27A	0.29110069	2.49E-74
cDC1	GINM1	0.20428034	3.37E-74
cDC1	MSL3	0.20887762	5.81E-74
cDC1	LGMN	0.25020618	1.22E-73
cDC1	ERN1	0.35278976	2.43E-71
cDC1	ETV6	0.22626197	1.74E-70
cDC1	C5orf24	0.24254724	2.91E-70
cDC1	RPL37A	0.22786859	4.89E-70
cDC1	C3orf58	0.26085731	1.92E-68
cDC1	DSE	0.26569872	3.17E-68

cDC1	RPS4X	0.21622758	3.18E-68
cDC1	HAVCR2	0.24396058	1.82E-67
cDC1	BIRC3	0.22325729	1.87E-66
cDC1	PPIB	0.2363493	1.26E-65
cDC1	CACYBP	0.39569529	1.28E-65
cDC1	Sep-06	0.25291821	1.60E-65
cDC1	CNN2	0.2434114	2.48E-65
cDC1	RPL31	0.33104345	3.11E-65
cDC1	SOD1	0.25082416	5.04E-65
cDC1	CST7	0.27822414	8.57E-65
cDC1	MAP4	0.20311123	2.59E-64
cDC1	PPP1R14B	0.32627994	2.75E-64
cDC1	CST3	0.38416696	1.54E-62
cDC1	SERPINB6	0.22830685	5.10E-62
cDC1	PRDX2	0.21528893	9.19E-62
cDC1	TWF2	0.21264715	5.15E-61
cDC1	KCNK6	0.21393639	4.09E-59
cDC1	BLOC1S2	0.20103853	4.62E-58
cDC1	SAT1	0.23881146	3.38E-57
cDC1	BACH1	0.26368711	7.27E-57
cDC1	ROMO1	0.21974222	9.51E-57
cDC1	CD48	0.22210699	2.73E-56
cDC1	PTPRE	0.24434947	3.86E-56
cDC1	AMD1	0.23827295	1.02E-55
cDC1	EIF5B	0.21816827	2.04E-55
cDC1	THBD	0.23546541	6.33E-55
cDC1	CAMLG	0.21266122	7.18E-55
cDC1	ODC1	0.21117426	1.01E-53
cDC1	TAPBP	0.2042756	3.14E-52
cDC1	MPC2	0.20258758	6.76E-52
cDC1	RPLP2	0.20138426	3.02E-51
cDC1	RPL13A	0.26832899	3.34E-49
cDC1	CHORDC1	0.287572	4.67E-49
cDC1	LMNA	0.31557629	3.12E-48
cDC1	SGK1	0.3957394	4.03E-46
cDC1	VEGFB	0.20352464	1.34E-45
cDC1	BAG3	0.52008754	4.89E-45
cDC1	BOD1L1	0.20973624	4.57E-44
cDC1	THAP9-AS1	0.218081	4.71E-42
cDC1	DDIT3	0.22254045	7.83E-42
cDC1	MYADM	0.2623305	7.10E-41
cDC1	BTG2	0.30740748	7.16E-41
cDC1	RSRC2	0.21447805	4.14E-40
cDC1	CLK1	0.27872787	4.61E-40
cDC1	CLEC2B	0.23986179	8.59E-38
cDC1	HSPA1B	0.69010048	3.83E-35
cDC1	ZFAND2A	0.45111734	5.74E-35
cDC1	DNAJB1	0.62871514	6.73E-35
cDC1	DNAJA4	0.21116545	1.23E-33
cDC1	DNAJA1	0.34074133	1.25E-31

cDC1	SDSTM1	0.2770312	1.43E-30
cDC1	PFKFB3	0.26546049	3.16E-28
cDC1	FOS	0.586077	4.81E-27
cDC1	PELI1	0.2020569	1.45E-23
cDC1	PPP1R15A	0.23993422	4.97E-20
cDC1	RPS17	0.29266508	2.77E-19
cDC1	HSP90AA1	0.3994365	3.79E-18
cDC1	EGR1	0.22568298	1.99E-17
cDC1	HSPA1A	0.34484926	1.01E-15
cDC1	DUSP2	0.35878599	9.27E-15
cDC1	PMAIP1	0.21548174	1.17E-14
cDC1	HSPB1	0.32592819	1.14E-11
cDC1	HSPD1	0.49353404	1.34E-09
cDC1	RGS1	0.27335953	2.21E-09
cDC3	IL1B	1.52702212	0
cDC3	C5AR1	1.23281133	0
cDC3	EREG	1.17827017	0
cDC3	S100A4	1.16616118	0
cDC3	FCN1	1.10117666	0
cDC3	SOD2	1.02782975	0
cDC3	CXCL2	0.99851486	0
cDC3	NFKBIA	0.90088609	0
cDC3	VSIG4	0.85347284	0
cDC3	CLEC4E	0.83563041	0
cDC3	S100A6	0.83055796	0
cDC3	PLAUR	0.82482213	0
cDC3	CD163	0.79448121	0
cDC3	FCER1G	0.79160961	0
cDC3	EMP3	0.7263603	0
cDC3	TSPO	0.72459094	0
cDC3	HCST	0.70863366	0
cDC3	CTSS	0.70368512	0
cDC3	CSTA	0.69555524	0
cDC3	CFD	0.67283725	0
cDC3	CD14	0.66095443	0
cDC3	CD44	0.65163649	0
cDC3	FCGR2A	0.64794963	0
cDC3	MS4A7	0.63772712	0
cDC3	TYROBP	0.62164638	0
cDC3	CLEC10A	0.60763251	0
cDC3	TNFSF13B	0.60033929	0
cDC3	ITM2B	0.59866657	0
cDC3	TREM1	0.57439128	0
cDC3	C3AR1	0.55118271	0
cDC3	CSF1R	0.5468611	0
cDC3	SERPINA1	0.53251413	0
cDC3	FTH1	0.5073194	0
cDC3	FTL	0.49105262	0
cDC3	SRGN	0.47618711	0
cDC3	LILRB2	0.47557335	0

cDC3	S100A11	0.49581073	0
cDC3	IER3	0.88089957	8.75E-305
cDC3	SLC40A1	0.77704455	4.06E-299
cDC3	LYZ	0.69169736	4.32E-294
cDC3	ZEB2	0.57458545	1.82E-291
cDC3	MAFB	0.62454732	2.80E-289
cDC3	ANXA2	0.55791662	3.19E-287
cDC3	NPC2	0.50547178	1.11E-283
cDC3	YBX3	0.59947296	1.65E-277
cDC3	THBS1	0.95763315	3.72E-277
cDC3	C1QA	1.43315563	5.01E-277
cDC3	SAMSN1	0.57852594	3.09E-274
cDC3	GLUL	0.56372249	2.05E-268
cDC3	PNRC1	0.55283013	3.00E-257
cDC3	TLR2	0.37957869	5.12E-257
cDC3	PSAP	0.45937929	1.60E-253
cDC3	HNMT	0.38926355	2.28E-252
cDC3	TNFAIP3	0.54741233	3.87E-252
cDC3	FCGRT	0.40244717	1.21E-251
cDC3	CTSB	0.50908516	1.04E-249
cDC3	CYBB	0.48357243	3.30E-242
cDC3	AOAH	0.44534196	1.15E-238
cDC3	CD99	0.46532346	5.32E-238
cDC3	ANXA1	0.58306387	8.93E-236
cDC3	CDC42EP2	0.34263354	6.86E-234
cDC3	MARCKS	0.53328113	2.64E-231
cDC3	CXCL3	0.99311592	3.32E-230
cDC3	BTG1	0.46811135	1.81E-228
cDC3	AIF1	0.33437732	2.29E-228
cDC3	S100A9	0.8834333	4.11E-227
cDC3	ELL2	0.40799272	6.74E-225
cDC3	C1QC	1.26121427	1.05E-224
cDC3	IRAK3	0.43435748	3.20E-224
cDC3	LILRB4	0.27449296	1.45E-215
cDC3	EIF1	0.22078315	2.54E-215
cDC3	SAP30	0.6218152	1.15E-214
cDC3	IL1RN	0.81531761	1.45E-210
cDC3	C1QB	1.32807088	2.90E-209
cDC3	SDCBP	0.44744487	5.79E-209
cDC3	RNF130	0.40643024	9.26E-209
cDC3	CD302	0.42272097	2.19E-208
cDC3	NAMPT	0.37378354	3.31E-206
cDC3	CASP1	0.4073271	2.17E-203
cDC3	ZFAND5	0.56754108	2.92E-202
cDC3	MRC1	0.47654023	2.17E-200
cDC3	LGALS3	0.40717472	3.01E-199
cDC3	HBEGF	0.45342104	1.89E-198
cDC3	OLR1	0.37813467	1.65E-197
cDC3	SLC7A7	0.31014861	1.15E-195
cDC3	CLEC12A	0.31228754	2.84E-192

cDC3	CD209	0.21998403	1.87E-190
cDC3	ASAH1	0.43267677	4.23E-189
cDC3	MS4A6A	0.4699494	6.90E-188
cDC3	MTSS1	0.24293733	2.37E-186
cDC3	GPX1	0.29103309	8.45E-184
cDC3	GIMAP4	0.28336695	1.05E-183
cDC3	PID1	0.33352653	2.04E-183
cDC3	ACSL1	0.37132631	1.43E-181
cDC3	APLP2	0.39583901	1.35E-179
cDC3	CD300E	0.25285446	1.08E-175
cDC3	TIMP1	0.47314454	1.14E-172
cDC3	C5AR2	0.35989852	5.35E-171
cDC3	EPB41L3	0.32695335	5.85E-171
cDC3	NINJ1	0.44493108	2.70E-170
cDC3	STX11	0.40508579	2.90E-167
cDC3	CAPG	0.40988758	7.80E-167
cDC3	TFEC	0.2037415	3.21E-164
cDC3	XBP1	0.39274294	6.72E-164
cDC3	KLF2	0.57101351	2.69E-160
cDC3	LAMP1	0.30519336	2.77E-160
cDC3	VCAN	0.24442021	8.16E-159
cDC3	PILRA	0.31683212	7.34E-157
cDC3	S100A10	0.49493124	1.39E-156
cDC3	ANXA5	0.28800484	1.00E-155
cDC3	FPR3	0.26932125	3.04E-153
cDC3	THAP2	0.48720554	1.17E-151
cDC3	PLIN2	0.49126019	5.49E-150
cDC3	IGSF6	0.36655845	4.18E-146
cDC3	MMP19	0.24351608	6.27E-146
cDC3	CD68	0.37578424	1.28E-144
cDC3	FKBP5	0.41043424	1.64E-144
cDC3	NLRP3	0.40834118	4.97E-143
cDC3	ATP13A3	0.32687518	1.95E-142
cDC3	CCRL2	0.31826907	5.90E-142
cDC3	TLR4	0.23216296	2.84E-141
cDC3	STAB1	0.23454504	2.73E-139
cDC3	BLVRB	0.33239108	4.24E-137
cDC3	CD9	0.37141151	4.04E-134
cDC3	NFE2L2	0.31181282	3.30E-133
cDC3	CARD16	0.3215367	1.43E-130
cDC3	FCGR1A	0.23545975	2.25E-130
cDC3	MS4A4A	0.37150253	8.32E-130
cDC3	BNIP3L	0.37161188	1.72E-129
cDC3	HMGB2	0.45742907	5.73E-129
cDC3	LAT2	0.26681767	6.09E-129
cDC3	ICAM1	0.44483652	1.39E-128
cDC3	TNFRSF1B	0.33416171	1.43E-128
cDC3	KYNU	0.31418404	2.01E-128
cDC3	LILRB3	0.24083499	1.28E-127
cDC3	CD63	0.29000321	2.20E-127

cDC3	LDLR	0.27703677	5.24E-127
cDC3	AHNAK	0.32414589	6.44E-127
cDC3	ARRDC3	0.28417633	6.74E-126
cDC3	CAMK1	0.26016544	7.24E-125
cDC3	RILPL2	0.32859969	1.25E-124
cDC3	ELF1	0.34301547	6.97E-124
cDC3	GADD45B	0.33614821	2.10E-121
cDC3	CPM	0.36121099	9.46E-121
cDC3	GLRX	0.3344968	4.63E-120
cDC3	CXCL8	0.92779641	8.93E-120
cDC3	SIRPA	0.22318474	2.06E-119
cDC3	TMEM176B	0.33844543	1.58E-117
cDC3	TKT	0.31796693	1.96E-117
cDC3	ALOX5AP	0.33866477	3.81E-117
cDC3	CTSC	0.44459387	6.25E-117
cDC3	SOCS3	0.34886722	6.96E-117
cDC3	DUSP1	0.24187344	2.00E-116
cDC3	RNF13	0.31316712	2.43E-116
cDC3	MNDA	0.32973043	3.40E-116
cDC3	KCTD12	0.31122764	2.45E-115
cDC3	NCF4	0.30059066	4.67E-114
cDC3	B3GNT5	0.3322778	5.43E-114
cDC3	VEGFA	0.31583595	6.93E-113
cDC3	HSP90B1	0.29705036	6.97E-112
cDC3	LYPD3	0.28869212	2.75E-111
cDC3	GBP2	0.31127195	3.75E-111
cDC3	IL13RA1	0.27744901	6.56E-110
cDC3	FGL2	0.35320053	1.00E-109
cDC3	PLXDC2	0.25692257	1.13E-109
cDC3	C1orf162	0.32254066	1.35E-109
cDC3	FCGR2B	0.3756158	1.08E-107
cDC3	SH3BGRL3	0.28489231	1.54E-107
cDC3	ATP6AP2	0.30733479	4.05E-106
cDC3	CAPN2	0.25454975	1.09E-105
cDC3	ZNF706	0.29809646	3.62E-105
cDC3	CALM2	0.3471639	1.21E-104
cDC3	RAB20	0.30157692	1.60E-104
cDC3	LAPTM5	0.21852894	1.66E-104
cDC3	ISG20	0.35344863	5.30E-104
cDC3	MIR3945HG	0.24087878	1.08E-103
cDC3	FYB	0.32912373	1.78E-103
cDC3	ATP6V1B2	0.28712849	9.49E-102
cDC3	TGFBI	0.2896651	2.33E-101
cDC3	LCP2	0.30375236	4.61E-101
cDC3	ADGRE2	0.21810784	1.53E-100
cDC3	NFKBIZ	0.36622059	7.88E-100
cDC3	PRNP	0.23779122	1.13E-99
cDC3	ARL8B	0.28674776	2.02E-99
cDC3	MXD1	0.27361951	6.67E-99
cDC3	SDS	0.46573753	1.85E-98

cDC3	ITLN2	0.41259097	1.87E-98
cDC3	NUP214	0.26189602	1.23E-97
cDC3	ARL4A	0.30841943	2.59E-97
cDC3	PLA2G7	0.20933142	4.03E-97
cDC3	GSTO1	0.2657378	6.07E-97
cDC3	IRS2	0.28746326	2.89E-96
cDC3	NCF2	0.26167088	3.16E-96
cDC3	CHPT1	0.35701244	7.92E-95
cDC3	PMP22	0.21025224	1.22E-94
cDC3	MT2A	0.9002657	1.86E-94
cDC3	NDUFA12	0.24826217	6.94E-94
cDC3	RIN2	0.2014858	7.14E-93
cDC3	CAST	0.28104474	1.08E-92
cDC3	SPTLC2	0.27388063	1.25E-92
cDC3	ANKRD28	0.27839389	1.68E-92
cDC3	SRGAP1	0.24707304	4.06E-92
cDC3	S100A8	0.2852005	4.10E-91
cDC3	LMNA	0.31127182	5.88E-90
cDC3	IFITM3	0.31966667	6.09E-90
cDC3	PLD3	0.26252685	1.07E-87
cDC3	MPHOSPH6	0.23207417	6.21E-87
cDC3	CH25H	0.51328335	3.42E-85
cDC3	GPCPD1	0.25234276	6.91E-85
cDC3	CEBPB	0.29646067	1.15E-84
cDC3	HES1	0.41953165	2.61E-84
cDC3	ZC3H12A	0.23176136	9.41E-84
cDC3	SEMA6B	0.23133284	1.35E-83
cDC3	SECTM1	0.2005022	1.60E-83
cDC3	CASP4	0.21595969	3.45E-83
cDC3	CCR7	0.35442205	5.98E-83
cDC3	CCL20	0.57600696	1.06E-82
cDC3	CSF3R	0.20861396	3.87E-82
cDC3	RAC1	0.20632397	8.69E-82
cDC3	FOSL2	0.2468831	3.89E-81
cDC3	RHOB	0.29218001	1.61E-80
cDC3	LRPAP1	0.24077585	5.04E-80
cDC3	DUSP6	0.30318396	5.11E-80
cDC3	RAB31	0.25973303	2.46E-78
cDC3	RCSD1	0.20095662	5.59E-78
cDC3	SH3BP5	0.24867071	1.05E-76
cDC3	UBALD2	0.27611659	4.66E-76
cDC3	IL4I1	0.26246541	4.66E-76
cDC3	LACTB	0.23554655	6.37E-76
cDC3	TFRC	0.45968689	5.01E-75
cDC3	LMO2	0.23017594	2.00E-74
cDC3	G0S2	0.54593273	4.58E-74
cDC3	QKI	0.22695836	7.52E-74
cDC3	MGAT1	0.23380006	9.85E-74
cDC3	FGD4	0.20866851	1.09E-73
cDC3	CRTAP	0.20232088	1.73E-73

cDC3	INSR	0.21847507	3.41E-73
cDC3	ZNF267	0.23121466	3.84E-73
cDC3	SLC25A37	0.21437973	1.05E-72
cDC3	TNFAIP2	0.34962589	1.68E-72
cDC3	ABCA1	0.204644	2.38E-72
cDC3	LIPA	0.31801081	3.92E-72
cDC3	JAML	0.2002731	1.89E-70
cDC3	CTSD	0.33744987	3.71E-70
cDC3	VAPA	0.24922182	8.62E-70
cDC3	TWISTNB	0.35374133	1.11E-69
cDC3	ADK	0.23048634	2.09E-69
cDC3	DAB2	0.22413211	2.56E-69
cDC3	ATF5	0.25355643	4.05E-69
cDC3	JUNB	0.23692135	5.01E-69
cDC3	IFITM2	0.2040633	1.35E-68
cDC3	PTGS2	0.38528874	2.29E-68
cDC3	FXYD5	0.21241956	6.97E-68
cDC3	SERP1	0.20368578	1.33E-67
cDC3	THEMIS2	0.20314467	1.85E-67
cDC3	HERPUD1	0.30346659	5.49E-67
cDC3	CXCL10	1.34271755	2.06E-66
cDC3	MAP2K3	0.25504601	2.20E-66
cDC3	FCER1A	0.20427186	5.15E-65
cDC3	FPR1	0.21125863	1.17E-63
cDC3	CD36	0.28388352	2.46E-63
cDC3	TMBIM4	0.22557769	4.17E-63
cDC3	MAFF	0.23879738	1.24E-62
cDC3	CD1C	0.20791253	3.14E-62
cDC3	ARL5B	0.2412769	4.66E-62
cDC3	PABPC4	0.23502396	1.29E-61
cDC3	MIR155HG	0.36296156	2.86E-61
cDC3	PPP1R15B	0.24599455	2.49E-60
cDC3	ATF6	0.2013129	7.28E-60
cDC3	GABARAP	0.22222264	1.13E-59
cDC3	ETS2	0.22095044	1.88E-59
cDC3	VAMP5	0.27495919	2.62E-59
cDC3	PDE4B	0.20028873	2.74E-59
cDC3	BRI3	0.22110608	2.79E-59
cDC3	CEBPD	0.25141451	3.18E-59
cDC3	HSPA5	0.24087473	4.23E-59
cDC3	PRDM1	0.22822367	1.69E-58
cDC3	CD37	0.24138063	2.48E-58
cDC3	PDXK	0.20735133	4.01E-58
cDC3	AHR	0.2274985	6.87E-58
cDC3	CFLAR	0.23535754	8.64E-58
cDC3	PNP	0.22337222	1.27E-56
cDC3	EMILIN2	0.20020323	4.34E-55
cDC3	IL10RA	0.21744301	7.48E-55
cDC3	RASGEF1B	0.24798688	1.60E-54
cDC3	SNX10	0.22274739	2.96E-54

cDC3	TMEM59	0.20521168	6.48E-52
cDC3	HEXB	0.22859701	4.34E-51
cDC3	ABL2	0.20584351	1.20E-50
cDC3	DRAM2	0.20408133	2.23E-50
cDC3	CCL3	0.77495055	2.35E-48
cDC3	KLF4	0.24501902	3.99E-48
cDC3	NCF1	0.26997908	5.31E-46
cDC3	ATP1B3	0.23870119	6.14E-46
cDC3	IRF1	0.22322018	8.92E-46
cDC3	IFNGR2	0.20573582	8.20E-44
cDC3	PTX3	0.20760801	2.58E-42
cDC3	CCL4	0.75878264	4.17E-41
cDC3	EHD1	0.22842187	8.63E-41
cDC3	UBE2D1	0.21408751	3.79E-40
cDC3	CHCHD10	0.20553503	4.52E-40
cDC3	SELK	0.23326334	1.84E-39
cDC3	TNFAIP8	0.29894019	2.12E-37
cDC3	AKIRIN2	0.21087117	3.19E-32
cDC3	AP1S2	0.22544011	3.53E-32
cDC3	GBP1	0.42235617	6.70E-32
cDC3	SEPP1	0.82808831	1.23E-30
cDC3	CRIP1	0.20819451	4.92E-29
cDC3	CCL4L2	0.65821651	4.07E-25
cDC3	CCL3L3	0.52061879	9.04E-25
cDC3	RPS4Y1	0.24271423	3.81E-17
cDC3	PLEK	0.26258008	3.67E-11
cDC2	CD207	1.27717977	0
cDC2	PLAC8	0.79175964	0
cDC2	DUSP5	0.69273492	3.99E-306
cDC2	RAPGEF4	0.34925069	3.82E-285
cDC2	SLC38A1	0.5102326	9.58E-284
cDC2	DSG2	0.33943918	1.91E-273
cDC2	IRF4	0.52340209	1.11E-241
cDC2	PKIB	0.65370217	2.35E-241
cDC2	CIB1	0.39710403	1.05E-209
cDC2	CDH17	0.41374966	1.25E-205
cDC2	CD1E	0.624732	5.95E-200
cDC2	PPP1R14A	0.43723635	2.85E-193
cDC2	PPA1	0.39748691	6.79E-169
cDC2	SPINT2	0.35440307	2.69E-156
cDC2	FCER1A	0.46751296	7.31E-148
cDC2	AREG	0.44537034	5.58E-140
cDC2	JAML	0.31834441	5.30E-137
cDC2	ENTPD1	0.44605343	1.24E-135
cDC2	GPR65	0.44588198	3.06E-134
cDC2	HIC1	0.34911905	8.80E-133
cDC2	FAM110A	0.37455031	4.11E-130
cDC2	YPEL5	0.34216031	3.17E-129
cDC2	PSTPIP2	0.31996326	4.60E-129
cDC2	GABARAPL2	0.32465666	1.38E-124

cDC2	CD1D	0.23784017	3.18E-120
cDC2	LST1	0.27251792	9.51E-120
cDC2	PAK1	0.30603398	2.43E-118
cDC2	CD86	0.34099891	5.09E-117
cDC2	TRABD2A	0.230542	7.36E-117
cDC2	FCMR	0.20902725	5.98E-115
cDC2	LYST	0.23143435	1.26E-109
cDC2	PLD4	0.29066901	4.43E-107
cDC2	CLN8	0.32695244	1.08E-104
cDC2	ITM2C	0.26521043	3.23E-104
cDC2	SPATS2L	0.29930048	1.72E-102
cDC2	PALLD	0.29401507	2.39E-102
cDC2	LTB	0.40620171	4.36E-102
cDC2	MBOAT7	0.25639765	3.56E-99
cDC2	GNB5	0.22487041	1.52E-98
cDC2	PLSCR1	0.26524643	3.05E-98
cDC2	BCL7A	0.22897764	2.30E-97
cDC2	TMEM14C	0.25211339	1.43E-94
cDC2	CST7	0.31619377	2.37E-94
cDC2	GPRIN3	0.32163645	1.22E-92
cDC2	STK4	0.31178243	4.58E-92
cDC2	CD1C	0.35830073	2.34E-91
cDC2	TBC1D9	0.26851467	3.41E-88
cDC2	TSHZ1	0.23764232	3.03E-87
cDC2	SPIB	0.25351696	6.19E-87
cDC2	SMAP2	0.25974074	1.05E-86
cDC2	LITAF	0.28864811	1.58E-86
cDC2	PRELID1	0.26510617	1.84E-86
cDC2	RALA	0.33160139	7.83E-86
cDC2	IL2RG	0.24982056	8.12E-86
cDC2	PRMT9	0.31413146	2.95E-84
cDC2	PAPD5	0.28779636	3.90E-84
cDC2	CFP	0.27812856	1.20E-83
cDC2	CLEC4A	0.24951961	1.24E-82
cDC2	IL18	0.26535541	1.71E-82
cDC2	INSIG1	0.38835362	2.27E-82
cDC2	HIF1A	0.27039292	1.29E-81
cDC2	SNAP29	0.22292142	5.64E-81
cDC2	GDI2	0.21349968	1.17E-80
cDC2	EXOC3	0.22130283	2.61E-80
cDC2	LSP1	0.2276415	3.66E-78
cDC2	SMCO4	0.26117397	2.92E-76
cDC2	ACAA1	0.25839753	8.91E-75
cDC2	ARF6	0.27035025	5.83E-74
cDC2	RP5-1171I10.5	0.28142676	1.47E-73
cDC2	C11orf31	0.23334282	6.17E-73
cDC2	ADAM8	0.22070881	1.22E-72
cDC2	STK17B	0.2843323	3.12E-71
cDC2	RGS2	0.25835739	3.61E-70
cDC2	MALT1	0.30469855	4.21E-70

cDC2	NET1	0.28598163	1.51E-68
cDC2	PRR13	0.23915554	2.10E-67
cDC2	PIP4K2A	0.20602249	2.11E-66
cDC2	HMGN1	0.21643266	8.58E-66
cDC2	MAP3K8	0.27556434	1.24E-65
cDC2	NR4A3	0.27104997	5.01E-65
cDC2	HLA-DQB2	0.22858617	1.44E-63
cDC2	FAM118A	0.25663414	1.93E-62
cDC2	ARL4C	0.28898812	3.16E-61
cDC2	RGS1	0.20685547	1.23E-59
cDC2	SNAI1	0.22009815	7.29E-59
cDC2	CCL22	0.39321354	1.35E-58
cDC2	ZC3HAV1	0.31595585	1.82E-58
cDC2	FDFT1	0.22975436	2.02E-57
cDC2	FAM89B	0.21752455	9.45E-57
cDC2	SEC14L1	0.24160557	9.60E-57
cDC2	PDE4A	0.24268772	1.03E-56
cDC2	ELMO1	0.21541197	2.94E-55
cDC2	LAMP3	0.21951974	3.65E-54
cDC2	HECTD1	0.28113365	6.03E-54
cDC2	COTL1	0.21981231	6.90E-54
cDC2	GAPT	0.20560825	2.19E-53
cDC2	CD52	0.20180684	2.42E-53
cDC2	RASSF5	0.21081694	1.35E-52
cDC2	RP11-347P5.1	0.23182069	3.29E-52
cDC2	CTSH	0.20242656	6.51E-52
cDC2	ARHGAP5	0.25682721	3.10E-50
cDC2	MMP12	0.42838296	3.72E-50
cDC2	RNASE6	0.2449045	9.54E-47
cDC2	DDX24	0.20273262	8.02E-46
cDC2	SYTL3	0.20520468	8.03E-46
cDC2	CELF2	0.20169857	1.03E-39
cDC2	CEBPB	0.20129299	1.08E-39
cDC2	CEBPZ	0.22338235	4.97E-39
cDC2	AIM1	0.20658266	8.09E-37
cDC2	IFI30	0.22592078	5.57E-36
cDC2	YWHAH	0.24977315	2.28E-35
cDC2	NRARP	0.20417074	3.86E-35
cDC2	IDI1	0.21107334	2.41E-34
cDC2	FAM107B	0.21083836	6.32E-31
cDC2	TUBA1A	0.20785013	2.89E-30
cDC2	RUNX3	0.23102859	9.98E-29
cDC2	RANBP2	0.21458378	1.72E-27
cDC2	GADD45A	0.30502937	1.28E-25
cDC2	KCNK6	0.21212561	2.04E-23

Table S3

cDC1

Ileum DEGs	avg_logFC	adj. p-value	Colon DEGs	avg_logFC	adj. p-value
RNASE6	0.699953	6.24E-51	HSPA1A	-2.4656001	5.27E-107
RPS17	0.572912	3.76E-26	HSPA1B	-1.6855916	8.02E-79
RPS20	0.435677	6.22E-27	HSPD1	-1.5425108	2.44E-65
XIST	0.423595	6.01E-24	HSP90AB1	-0.9575958	2.26E-59
MT-ND1	0.417815	1.35E-29	HSPE1	-1.1487947	2.15E-57
RPL13A	0.405945	1.68E-24	HSP90AA1	-1.3307031	6.56E-56
RPL31	0.402658	2.59E-26	MARCKSL1	-0.6543432	2.22E-52
LINC00152	0.396268	2.13E-26	DNAJB1	-1.3675298	2.47E-51
XCR1	0.363549	1.24E-24	BAG3	-1.1250307	3.50E-43
MT-ND2	0.361882	6.14E-22	HSPH1	-1.0301936	1.20E-41
C1orf54	0.354598	1.78E-36	RPL13	-0.4597356	1.10E-38
AIF1	0.345476	9.93E-42	DNAJA1	-0.6866342	7.55E-35
AC090498.1	0.345331	0.0001965	PPP1R15A	-0.6107766	8.01E-33
HIPK2	0.332219	8.40E-24	CACYBP	-0.591286	2.33E-31
RPL27A	0.328222	3.63E-20	CDC42EP3	-0.5457458	8.79E-29
PNOC	0.310208	2.47E-05	RPS4Y1	-0.3680037	6.68E-28
CKLF	0.302118	4.37E-17	S100A10	-0.4361229	1.43E-26
NAP1L1	0.297364	5.31E-25	TSPO	-0.2735462	3.25E-26
C1QA	0.286141	1.53E-10	HSPA6	-1.7547927	5.12E-26
RPL38	0.283794	1.26E-30	EIF4A3	-0.5694685	5.14E-26
CDH17	0.280609	2.29E-17	SH3BGRL3	-0.2865177	2.31E-25
RPL37A	0.269093	1.04E-29	HSPA8	-0.4253183	3.21E-25
FDFT1	0.268906	1.56E-11	ZFAND2A	-0.9370867	3.74E-25
TYROBP	0.267425	4.98E-07	CHORDC1	-0.4598921	6.43E-25
RPS27	0.26431	3.42E-32	TCP1	-0.3500559	9.68E-25
CCR6	0.260848	5.23E-16	IGHA1	-0.5775122	2.07E-24
RPL23A	0.253122	8.96E-24	PFN1	-0.3342327	1.88E-23
CSF2RA	0.250238	1.04E-11	JUND	-0.493049	3.58E-23
RPLP2	0.249823	1.14E-14	GADD45B	-0.708583	1.54E-22
FCER1G	0.247191	1.35E-08	RPS2	-0.365461	1.94E-22
RPS11	0.244391	3.67E-17	DDX3Y	-0.2867972	3.51E-22
MPEG1	0.244345	1.31E-15	RAB32	-0.361217	4.03E-22
RPL23	0.243677	2.49E-15	LMNA	-0.5176417	5.17E-22
MIR4435-2HG	0.239422	3.06E-11	LYZ	-0.3039646	2.54E-21
ARHGDIB	0.236891	3.28E-16	FKBP4	-0.3743937	5.56E-21
NPC2	0.234786	3.09E-16	DNAJA4	-0.4099558	1.29E-20
VMO1	0.234742	1.28E-09	ATP5D	-0.3045288	2.51E-20
MS4A6A	0.23359	0.0032821	DNAJB6	-0.4840682	3.31E-20
CXCR4	0.229935	7.62E-07	TNFAIP8	-0.4323021	2.23E-19
NBEAL1	0.224716	2.25E-09	PTGES3	-0.3704377	8.93E-19
CLNK	0.223456	4.91E-05	GNA15	-0.3606215	4.01E-18
RPS29	0.217545	1.71E-33	NFKBIA	-0.4962741	1.05E-17
RPL27	0.217085	5.33E-16	YBX1	-0.2724152	1.91E-17
C10orf54	0.216339	4.35E-05	CTSZ	-0.3117685	3.13E-17
RGS1	0.216325	1.58E-11	COX5A	-0.2744236	6.99E-17
RP11-1143G9.4	0.214844	1.40E-07	SQSTM1	-0.4571231	1.95E-16

RPS21	0.213657	2.29E-23	CCT4	-0.2755941	2.19E-16
ANAPC16	0.212687	1.70E-12	EMP3	-0.3447057	1.09E-15
NLRP3	0.211673	1.97E-05	UBC	-0.3333398	4.62E-15
GMFG	0.211255	6.15E-11	MZT2B	-0.2841662	7.43E-15
C1QB	0.21078	9.38E-05	HSPB1	-1.1696499	8.93E-15
ATPIF1	0.208338	3.72E-10	PPP1R14B	-0.2994856	1.77E-14
HLA-DRB5	0.206636	1.47E-07	IER5	-0.8319901	2.01E-14
RBPJ	0.206198	5.93E-08	GTF3A	-0.2631864	2.62E-14
RPS4X	0.203491	6.58E-22	H2AFX	-0.2699513	2.63E-14
LST1	0.203137	6.09E-10	ARL6IP4	-0.2435121	2.91E-14
TUBA1A	0.203097	1.69E-08	AHSA1	-0.2885327	3.46E-14
RPL7	0.203079	2.23E-14	H2AFZ	-0.3523065	4.45E-14
C6orf48	0.201366	1.10E-05	UBE2S	-0.3198426	8.22E-14
C1QC	0.201274	5.20E-07	NME4	-0.2267113	1.15E-13
			ATP1B1	-0.4365583	1.41E-13
			HNRNPU	-0.3026656	1.43E-13
			IRF1	-0.3944046	5.03E-13
			HLA-DQA2	-1.0917673	8.08E-13
			CCDC85B	-0.3056501	9.27E-13
			GPBP1	-0.2690991	1.54E-12
			TSPAN33	-0.2903964	2.69E-12
			C19orf43	-0.2170941	5.02E-12
			TYMP	-0.2805578	6.44E-12
			MAP2K2	-0.226395	1.00E-11
			GABARAP	-0.206698	1.58E-11
			SLC5A3	-0.3387212	1.64E-11
			DEDD2	-0.245238	1.71E-11
			MZT2A	-0.2344661	1.72E-11
			GADD45GIP1	-0.200648	1.85E-11
			PNRC1	-0.2925806	2.01E-11
			MXD1	-0.3304527	2.09E-11
			ARL6IP5	-0.299728	2.92E-11
			DEK	-0.2477285	3.19E-11
			SNX3	-0.2359324	3.85E-11
			SOD2	-0.3680574	4.20E-11
			BASP1	-0.248707	4.29E-11
			RUNX3	-0.3165882	4.39E-11
			MRPL18	-0.3159489	4.73E-11
			CCR7	-0.2094362	7.59E-11
			KPNA4	-0.2225477	1.33E-10
			PRDX1	-0.2716996	1.39E-10
			MAP1LC3B	-0.2567634	2.79E-10
			C1QBP	-0.2039858	2.82E-10
			MAP2K3	-0.2681831	2.89E-10
			PGLS	-0.2289698	4.36E-10
			CCT4	-0.2361129	5.65E-10
			NUDC	-0.2649	6.25E-10
			CLTA	-0.2017864	6.78E-10
			TXN	-0.4192061	7.33E-10
			SLC25A3	-0.228084	9.24E-10

PTP4A2	-0.2962479	1.06E-09
FSCN1	-0.2297665	1.23E-09
CDV3	-0.2435802	2.11E-09
INPP5F	-0.2024106	2.47E-09
DUSP2	-0.4024741	3.17E-09
SERPINH1	-0.2055484	3.60E-09
MIF	-0.2099325	4.00E-09
PTMS	-0.2439178	4.08E-09
S100B	-0.5922955	7.96E-09
JUN	-0.884917	8.04E-09
RGCC	-0.3181228	9.14E-09
FLNA	-0.2225739	1.31E-08
RAB21	-0.2297175	1.61E-08
GNAS	-0.2465077	1.70E-08
IRF8	-0.2296429	2.40E-08
CD83	-0.2666498	4.88E-08
SLC3A2	-0.2395973	5.30E-08
SOCS3	-0.2269454	7.21E-08
ZNF267	-0.2240714	8.63E-08
BCL2A1	-0.2783706	1.13E-07
LGALS3	-0.3397468	1.17E-07
FTH1	-0.2802996	1.65E-07
TOP1	-0.2363575	2.57E-07
RP1-313I6.1	-0.2193347	3.22E-07
CSRNP1	-0.2065657	1.10E-06
PPIF	-0.3681435	1.34E-06
NINJ1	-0.2890793	1.42E-06
VIM	-0.2483026	1.50E-06
STMN1	-0.2273416	1.79E-06
JUNB	-0.285428	2.55E-06
ERN1	-0.2539568	5.38E-06
IER2	-0.4336007	5.64E-06
EGR1	-0.2531833	6.67E-06
MBP	-0.2193632	7.56E-06
IGHA2	-0.2006997	1.03E-05
IER3	-0.3743481	1.06E-05
PHLDA1	-0.2384406	1.10E-05
PIM3	-0.2312074	1.42E-05
CXCL9	-0.4273522	2.90E-05
ARL5B	-0.2574697	4.65E-05
HMOX1	-0.2607332	8.46E-05
JCHAIN	-0.4655107	0.0001459
LAP3	-0.2206524	0.0001499
IGLC2	-1.1033641	0.000152
MAFF	-0.2204495	0.0001959
PHLDA2	-0.3253814	0.000228
KLF6	-0.2657549	0.0002977
H1FX	-0.2343952	0.0003148
BTG1	-0.2625637	0.0005258
CYBA	-0.2154659	0.0005815

LTB	-0.3190892	0.0009243
ARL4C	-0.310349	0.0010908
TSPYL2	-0.25755	0.0012981
TANK	-0.2032896	0.0022215
UBB	-0.2276287	0.0022375
ATF3	-0.3947232	0.0023623
CD44	-0.2037996	0.002757
S100A4	-0.221257	0.0151517
EIF4E	-0.2253224	0.0162119
BAZ1A	-0.2006952	0.0167013
GADD45A	-0.2511612	0.0189875
NABP1	-0.2260553	0.0311235
TWISTNB	-0.3571673	0.0495264

cDC2

Ileum DEGs	avg_logFC	adj. p-value	Colon DEGs	avg_logFC	adj. p-value
AC090498.1	0.68955172	2.42E-58	HSPA1A	-2.626801	3.49E-294
CD207	0.64768246	9.82E-113	HSP90AA1	-1.413662	1.13E-193
FCER1A	0.54435185	4.39E-76	HSPA1B	-1.374895	1.10E-193
RNASE6	0.48008775	1.20E-89	DNAJB1	-1.285	3.90E-130
STK17B	0.46312264	1.67E-104	HSPA6	-1.269233	1.62E-62
GAPT	0.45434909	1.34E-89	HLA-DQA2	-1.253211	6.49E-90
PALLD	0.43869737	1.19E-83	HSPD1	-1.064861	1.20E-122
INSIG1	0.43514759	4.16E-59	IL1B	-1.04615	2.21E-63
RP11-347P5.1	0.42681847	6.61E-83	HSPH1	-0.997992	2.11E-103
ENTPD1	0.41856433	3.26E-59	G0S2	-0.970776	8.33E-50
NET1	0.41054738	5.32E-57	S100A4	-0.954051	1.09E-153
CDH17	0.40707246	4.06E-73	HSP90AB1	-0.916208	9.81E-193
LAIR1	0.39650622	3.03E-79	HSPB1	-0.906212	7.02E-31
HERPUD1	0.39573715	2.39E-76	CXCL8	-0.885966	3.39E-20
IRF4	0.39500409	9.05E-44	HSPE1	-0.875042	8.20E-110
AREG	0.39106455	3.07E-62	NFKBIA	-0.871095	1.29E-82
FDFT1	0.38597634	1.73E-72	IER3	-0.830732	2.01E-89
IDI1	0.38472679	7.67E-56	EMP3	-0.809518	1.18E-130
RAPGEF4	0.38325661	1.24E-99	LYZ	-0.762924	2.36E-71
CD1E	0.38061085	2.22E-30	GADD45B	-0.747366	2.54E-98
CEBPB	0.37143038	1.11E-51	LMNA	-0.715887	1.05E-85
SEPP1	0.36317903	8.57E-52	LGALS3	-0.704976	2.87E-92
RGS1	0.35310833	3.75E-64	C15orf48	-0.694436	3.72E-34
MS4A6A	0.35032549	1.71E-53	S100A10	-0.693323	7.46E-112
KCNK6	0.34877806	2.48E-38	CD83	-0.687136	4.93E-98
ARF6	0.34561874	9.05E-56	SOD2	-0.683403	1.86E-76
XIST	0.3397252	1.34E-35	BAG3	-0.681595	1.18E-78
CELF2	0.33962009	2.03E-55	DNAJA1	-0.662581	1.00E-105
HIPK2	0.33905887	9.81E-64	TIMP1	-0.63586	1.13E-67
RIPK2	0.33607196	6.36E-41	TXN	-0.632033	2.32E-24
CPVL	0.33232734	5.52E-63	ID2	-0.609452	4.45E-38
PLAC8	0.33054071	6.99E-36	SQSTM1	-0.584015	2.44E-78
PKIB	0.32800135	6.98E-31	ANXA2	-0.557275	2.57E-86
JAML	0.32688685	8.54E-72	TNFAIP2	-0.551379	7.32E-42
RPL31	0.32636198	3.71E-54	PPIF	-0.549459	1.39E-56
ANAPC16	0.32571241	3.04E-61	MARCKSL1	-0.524542	2.28E-92
SMCO4	0.32306207	4.14E-54	PHLDA2	-0.524158	3.53E-59
EVI2B	0.31863512	1.11E-50	TSPO	-0.52313	8.86E-115
IFNGR1	0.31469719	5.75E-52	CCR7	-0.521533	7.35E-79
NBEAL1	0.30891124	5.82E-19	PPP1R15A	-0.521322	2.56E-69
RPS17	0.29917506	4.38E-31	AHNAK	-0.511879	5.21E-55
LDLR	0.29795014	3.29E-69	PRDX1	-0.501987	3.37E-79
ARL5A	0.28535397	8.35E-33	KLF2	-0.49859	2.75E-28
LEPROTL1	0.28478784	5.09E-44	JUN	-0.492534	6.72E-11
NPC2	0.28026385	8.17E-35	EIF4A3	-0.47828	1.20E-34
RGS2	0.27181807	2.16E-31	RPS4Y1	-0.471849	5.56E-44

SIK1	0.27065704	5.07E-36	FREM3	-0.467613	0.000914
SGK1	0.26859976	2.08E-36	DDX3Y	-0.464237	1.79E-72
MRC1	0.26655712	4.94E-20	MARCKS	-0.463916	2.78E-29
CCR6	0.26449276	3.89E-34	IL4I1	-0.454227	5.35E-73
LST1	0.26427844	4.64E-66	TWISTNB	-0.451397	6.00E-32
ADAM28	0.25949887	5.01E-30	PLEK	-0.444248	9.27E-34
PLD4	0.25670094	2.03E-25	BIRC3	-0.440649	9.89E-38
RPS27	0.25554108	2.15E-92	CD44	-0.440196	2.54E-47
MAP3K8	0.25400161	8.92E-25	PIM3	-0.439975	2.69E-46
CPM	0.25374653	2.50E-29	IGHA1	-0.437217	2.07E-24
HLA-DRB1	0.25242183	1.01E-45	S100A6	-0.433864	1.68E-40
ZFP36L2	0.25017003	4.62E-24	ZFAND2A	-0.422804	2.57E-12
PRR13	0.24987407	2.56E-36	RAB11FIP1	-0.421883	8.20E-52
CYSLTR1	0.24950368	3.88E-46	NINJ1	-0.420595	9.61E-45
CD36	0.2491835	7.35E-37	YBX3	-0.419877	1.36E-34
CLEC11A	0.24789557	2.51E-33	CXCL2	-0.418477	7.53E-07
TMEM97	0.24663482	1.03E-36	ATF5	-0.410433	7.95E-37
CYTIP	0.24486886	1.75E-32	VIM	-0.394065	1.37E-40
RNF7	0.24475273	2.57E-35	IER5	-0.391182	1.04E-14
COMMD5	0.24420288	5.03E-28	RGCC	-0.38457	6.99E-12
AKNA	0.24193475	3.67E-24	ALOX5AP	-0.38053	1.45E-17
ATPIF1	0.24178737	2.54E-34	PNRC1	-0.380147	5.07E-36
RPL13A	0.2414642	3.44E-37	MNDA	-0.379685	5.00E-42
SAMSN1	0.24072348	2.56E-25	GNA15	-0.377826	3.86E-58
GLIPR1	0.23929222	4.69E-33	GPR157	-0.372832	1.28E-38
POR	0.23902934	2.60E-31	CAPG	-0.367966	2.79E-52
UCP2	0.23800785	9.72E-20	TNFAIP8	-0.36372	2.90E-25
HMGN2	0.23783855	1.18E-29	ICAM1	-0.360857	3.07E-20
SRGAP2B	0.23745735	3.51E-27	CRIP1	-0.359241	6.44E-33
GPRIN3	0.23721667	2.93E-17	MAP2K3	-0.359012	4.70E-53
CLEC4A	0.23688353	1.48E-31	CFLAR	-0.35823	1.01E-39
ARHGAP5	0.23685434	1.47E-20	IRF1	-0.357892	2.40E-38
TMEM14C	0.23683996	2.24E-38	ARL5B	-0.35587	7.80E-33
RPS29	0.23593301	3.73E-100	KLF6	-0.354255	5.56E-10
SMAP2	0.23538615	4.09E-32	CST3	-0.350406	2.22E-44
PTMS	0.23397951	8.01E-20	HSPA8	-0.350111	9.04E-41
GCLC	0.23189296	9.94E-38	FLNA	-0.346355	2.71E-52
ERP29	0.23165803	3.00E-37	IRF8	-0.345594	1.32E-28
ARHGDIB	0.23115149	2.05E-35	GSN	-0.342364	1.10E-34
RPL7	0.2305682	2.39E-44	NFKB1	-0.331852	3.02E-29
C10orf54	0.22978457	1.29E-29	ALDH2	-0.330291	1.14E-34
PELI1	0.22966346	6.20E-17	TUBB4B	-0.328283	9.44E-40
NAP1L1	0.22917969	1.07E-45	ARL4C	-0.327747	4.01E-31
RNF149	0.22903054	7.28E-21	MIR155HG	-0.324814	5.58E-35
VAMP2	0.22753919	1.39E-27	CTSZ	-0.314813	6.63E-42
GPSM3	0.22361717	9.28E-29	SERPINB1	-0.314564	3.05E-23
TMSB4X	0.22337996	3.26E-40	ARL4A	-0.312812	4.91E-27
CXCR4	0.22290248	3.33E-28	MS4A7	-0.306814	5.28E-27
RPL23A	0.22225476	3.37E-75	SLAMF7	-0.304068	3.07E-21
SARAF	0.22026868	8.99E-29	ZNF267	-0.303033	4.50E-33

MAL2A	0.21952902	9.53E-16	FTH1	-0.302402	1.91E-20
RPS20	0.21865233	2.76E-35	BLVRB	-0.301969	8.09E-37
PPP1R14A	0.21853697	2.41E-20	CD9	-0.301795	2.69E-27
RP5-1171I10.5	0.21665937	3.59E-21	GPX4	-0.299143	1.04E-43
SLC2A3	0.21521237	3.52E-22	CCND2	-0.296471	4.89E-22
TBXAS1	0.21395601	7.65E-26	REL	-0.295937	2.02E-19
THBS1	0.21307647	2.15E-18	MAFF	-0.294466	4.38E-23
CD1D	0.21190095	1.01E-23	SERPINA1	-0.293432	4.95E-57
RPL27A	0.2115128	5.78E-37	THAP2	-0.292785	2.34E-27
SPINT2	0.21082794	3.33E-25	JUND	-0.288705	1.46E-27
DYNLT1	0.21022782	5.75E-27	MRPL18	-0.287927	5.61E-19
TMA7	0.20994728	4.67E-39	CDKN1A	-0.287127	3.38E-24
GSTM4	0.20839157	3.13E-38	IL1RN	-0.285883	2.98E-33
C1orf56	0.20832168	0.00144353	LGALS1	-0.283932	2.57E-38
LAMP5	0.20677546	3.84E-55	ZFP36L1	-0.27873	1.74E-12
RNF144B	0.20616101	5.09E-21	ICAM3	-0.27832	5.10E-42
TCTN3	0.20444181	6.60E-07	PHACTR1	-0.274957	2.65E-15
GNB5	0.20387439	1.29E-27	LACTB	-0.271919	3.08E-34
DSG2	0.20369748	1.36E-35	CD99	-0.271016	1.23E-27
TSC22D3	0.20166519	5.83E-29	ZC3H12A	-0.270197	4.04E-42
CD69	0.20108731	2.83E-24	SPAG9	-0.26972	8.70E-22
			BHLHE40	-0.267462	7.52E-26
			TYMP	-0.265832	6.32E-27
			S100A11	-0.265475	8.89E-35
			HCST	-0.265332	2.40E-23
			IL10RA	-0.264984	1.03E-27
			DNAJA4	-0.264514	7.89E-36
			DENND4A	-0.264477	2.72E-14
			CD40	-0.263152	3.30E-13
			TUBA1C	-0.261587	1.74E-21
			RUNX3	-0.261222	4.34E-17
			H2AFZ	-0.260898	4.24E-19
			TNFRSF1B	-0.258939	2.24E-20
			FSCN1	-0.258097	1.34E-22
			IL1R2	-0.255557	0.000536
			TANK	-0.255463	4.37E-19
			TRAF1	-0.255425	6.76E-43
			DNAJB6	-0.25393	6.77E-15
			CTSH	-0.253247	4.18E-27
			ANXA1	-0.252478	0.000181
			NFAT5	-0.252091	1.27E-23
			ATP5D	-0.251518	8.68E-32
			RPL13	-0.251116	7.63E-76
			PTGES3	-0.250855	1.76E-21
			PNP	-0.249298	1.75E-32
			DUSP2	-0.246107	1.14E-07
			MXD1	-0.244656	8.84E-15
			RRAD	-0.244261	9.75E-15
			HES4	-0.238985	1.50E-11
			GBP1	-0.238584	0.018081

NFE2L2	-0.23748	4.22E-19
RASSF4	-0.236908	3.47E-23
GPR35	-0.236011	4.21E-44
TNFSF13B	-0.235777	2.43E-19
CREB5	-0.23558	2.72E-29
NEAT1	-0.233329	2.94E-26
ISG20	-0.232155	4.03E-12
MGAT1	-0.231699	2.45E-21
FTH1	-0.23131	6.11E-27
PPP1R15B	-0.230045	2.44E-11
CCRL2	-0.229906	5.64E-32
KLF10	-0.228613	8.31E-25
ARFGAP3	-0.22767	3.33E-22
TUBB	-0.226092	2.70E-11
PLAUR	-0.223684	9.05E-05
HLA-B	-0.221992	8.62E-28
CDC42EP3	-0.220025	2.58E-31
HMOX1	-0.218954	1.49E-27
AES	-0.218236	6.65E-18
ARL8B	-0.216331	1.71E-16
RAB9A	-0.215056	4.50E-14
FCGR2A	-0.214914	6.93E-09
GABARAP	-0.21327	1.93E-23
CACYBP	-0.21258	1.56E-06
TPRA1	-0.212548	5.38E-21
KDM6B	-0.211967	1.06E-12
KCNQ1OT1	-0.211551	1.11E-07
APOE	-0.210716	7.02E-18
PLK3	-0.209247	1.67E-18
AHSA1	-0.20764	3.70E-18
AHR	-0.207312	8.58E-09
BAZ1A	-0.206929	1.52E-15
RALA	-0.205805	5.98E-05
MAP4K4	-0.205778	1.24E-20
USP12	-0.205689	7.27E-22
SEMA6B	-0.204733	5.59E-17
CALR	-0.203834	1.93E-11
ANKRD37	-0.202612	2.50E-07
VAMP5	-0.202096	1.07E-14
CSTB	-0.201971	4.21E-10
DNTTIP2	-0.201745	2.20E-15
CAST	-0.201502	1.42E-17
CST7	-0.200943	0.000193

cDC3

Ileum DEGs	avg_logFC	adj. p-value	Colon DEGs	avg_logFC	adj. p-value
SEPP1	0.869608825	2.78E-46	HSPA1A	-2.66262	4.15E-233
C1QC	0.816656542	3.66E-74	HSP90AA1	-1.29789	1.52E-162
C1QA	0.803818228	8.09E-81	HSPA1B	-1.23126	5.46E-139
THBS1	0.711103901	2.75E-60	HLA-DQA2	-1.12548	7.11E-38
VSIG4	0.585361752	2.04E-93	HSPD1	-1.07415	2.74E-90
TFRC	0.577898206	2.36E-53	DNAJB1	-1.07331	3.86E-90
AC090498.1	0.532021322	3.30E-25	IL1RN	-0.93429	3.12E-53
TMEM176B	0.5133235	2.24E-87	IL1B	-0.90288	2.48E-32
NPC2	0.503775426	3.01E-133	HSPH1	-0.89126	2.89E-66
C1QB	0.500756046	3.93E-43	G0S2	-0.88112	3.14E-50
CTSC	0.490385487	2.56E-62	HSPA6	-0.88054	7.91E-34
C5AR1	0.46104254	1.47E-36	CCR7	-0.85452	9.74E-78
SLC40A1	0.455029919	5.83E-52	HSPE1	-0.84353	8.89E-82
AREG	0.422149791	5.95E-45	HSP90AB1	-0.77394	1.43E-132
CTSS	0.416617641	2.59E-98	HSPB1	-0.75706	1.50E-05
RGS1	0.412625862	7.06E-70	S100A9	-0.73807	1.91E-39
CD163	0.390681833	7.16E-49	S100A10	-0.72688	2.86E-127
HERPUD1	0.388333638	4.08E-51	IGKC	-0.68942	6.78E-09
CFD	0.385524488	1.04E-08	DNAJA1	-0.68486	9.41E-102
SDS	0.366809829	1.18E-27	CXCL8	-0.67889	2.58E-19
ACP5	0.361081127	4.04E-36	VIM	-0.61654	1.60E-92
CPM	0.353408434	6.82E-47	IER3	-0.61535	1.64E-46
SMIM3	0.35245098	4.30E-37	LMNA	-0.6043	1.23E-82
IFNGR1	0.344148488	4.16E-44	EMP3	-0.59319	2.64E-107
XIST	0.337134724	1.01E-34	NFKBIA	-0.58704	5.42E-27
JAML	0.330221064	1.60E-65	MIR155HG	-0.58407	2.91E-39
SAMSN1	0.327589651	2.80E-41	BAG3	-0.58086	7.51E-53
LAIR1	0.326931253	5.76E-50	BCL2A1	-0.57642	3.09E-31
AKR1B1	0.325836663	9.35E-40	PLEK	-0.56936	8.59E-49
CD36	0.324647136	3.50E-36	JUN	-0.56929	3.03E-26
TMEM176A	0.324277752	1.64E-60	TSPO	-0.56547	1.93E-86
ZFP36L2	0.323948787	6.52E-39	C15orf48	-0.56295	5.67E-33
PALLD	0.321127642	1.79E-54	PPP1R15A	-0.56147	5.41E-55
FAM105A	0.313097319	1.35E-36	FCN1	-0.56058	5.58E-31
RGS2	0.312433143	2.39E-37	S100A4	-0.55945	1.08E-90
HN1	0.311450022	5.39E-36	IL4I1	-0.52714	4.44E-60
MT-ND2	0.306296925	1.55E-54	IL1R2	-0.52541	2.76E-49
DNASE1L3	0.303405946	5.05E-21	S100A6	-0.52519	5.98E-74
FTL	0.303256475	3.83E-62	KLF2	-0.51273	3.28E-14
CXCR4	0.30275466	1.00E-36	PHLDA2	-0.50766	7.04E-45
ZFAND5	0.299722357	7.21E-24	DDX3Y	-0.50163	9.46E-58
SGK1	0.29570434	1.57E-36	CD83	-0.49766	3.91E-59
TSC22D1	0.289998271	1.86E-14	SOD2	-0.48685	7.24E-52
CD81	0.287932173	6.07E-13	RPS4Y1	-0.48374	1.20E-35
AXL	0.283683293	4.55E-25	TNFAIP8	-0.48336	8.31E-36
C3AR1	0.283171324	5.08E-29	ARL4C	-0.47157	1.38E-67

CD207	0.282903603	6.41E-18	GPNMB	-0.46477	1.21E-32
TSC22D3	0.282497354	2.32E-30	MAP2K3	-0.45434	3.77E-54
RPS17	0.281456607	1.83E-14	MARCKSL1	-0.45058	5.06E-47
PELI1	0.278409381	8.08E-27	PPIF	-0.44853	5.45E-51
HBEGF	0.274294563	1.62E-14	JUND	-0.44333	7.17E-60
HLA-DRB1	0.27246477	1.03E-42	CD52	-0.44211	3.70E-31
PSAP	0.271894663	5.49E-46	GADD45B	-0.43541	2.13E-34
ZNF331	0.271787673	1.94E-16	ZFAND2A	-0.42924	3.45E-05
MT-ND1	0.267599229	4.58E-27	TIMP1	-0.4288	2.68E-22
INSIG1	0.267234037	7.77E-12	IGLC2	-0.42718	3.96E-06
GCLC	0.266700776	2.54E-45	TNFAIP2	-0.42483	7.71E-21
NBEAL1	0.264750333	1.15E-15	TWISTNB	-0.42245	1.37E-11
ENTPD1	0.264644798	3.00E-23	ATF5	-0.42188	4.11E-38
LIPA	0.261770975	4.01E-08	CD55	-0.41356	1.83E-44
RP11-1143G9.4	0.261195907	4.25E-13	SH3BGRL3	-0.4123	2.43E-89
TMSB4X	0.258987978	5.84E-53	SQSTM1	-0.40677	7.68E-38
CD68	0.253039966	2.47E-26	EIF4A3	-0.39261	1.62E-22
CD1E	0.252015298	6.94E-07	RHOF	-0.38527	2.07E-48
PLBD1	0.251624386	1.26E-24	PNP	-0.3807	5.29E-52
RPL31	0.251295613	1.16E-19	CFLAR	-0.37999	4.58E-45
CPVL	0.250461286	9.12E-28	CD99	-0.37262	1.01E-46
STK17B	0.249529957	6.71E-27	RAB11FIP1	-0.37033	8.53E-38
VIMP	0.249474724	4.09E-17	ANXA2	-0.36859	6.68E-56
CD209	0.247797535	7.81E-43	MARCKS	-0.35829	7.67E-19
GPR65	0.247266112	7.04E-19	HSPA8	-0.35706	2.44E-33
CLEC7A	0.247232631	1.68E-25	EZR	-0.35656	3.01E-36
NCF1	0.245065586	6.73E-21	FCGR2B	-0.3439	1.58E-41
IRS2	0.244140371	2.41E-28	CD44	-0.34012	3.35E-28
CHMP1B	0.243141024	4.98E-20	LRRFIP1	-0.33629	6.14E-33
LDLR	0.241750088	7.49E-32	RUNX3	-0.33563	7.59E-24
HEXB	0.24083124	1.95E-19	PHACTR1	-0.33422	1.58E-29
CD74	0.240319306	7.63E-68	LGALS3	-0.33228	3.66E-28
PLD4	0.239228427	8.00E-17	NFKB1	-0.3261	1.59E-33
CYTIP	0.239101373	3.52E-24	CRIP1	-0.32419	1.17E-22
ITM2B	0.238843947	1.90E-26	DNAJB6	-0.32355	1.57E-28
GAPT	0.237319587	2.02E-23	TRAF1	-0.32212	1.66E-32
FGL2	0.236515297	8.07E-28	SERPINA1	-0.32033	2.24E-37
ZC3HAV1	0.235603465	6.20E-11	CD1C	-0.31928	5.40E-33
ZFP36	0.234768554	1.71E-29	SERPINB1	-0.31523	2.60E-27
TYROBP	0.232036811	1.15E-65	CAPG	-0.31513	6.00E-30
CLEC11A	0.23199437	2.84E-19	LINC00936	-0.31504	1.76E-12
FOS	0.230942966	1.86E-29	PIM3	-0.31421	1.17E-17
RNASE6	0.230683343	5.74E-24	GNA15	-0.3086	7.76E-31
TMEM59	0.230488471	4.77E-23	NEAT1	-0.30212	5.29E-32
HMGN2	0.230329925	6.20E-22	CCND2	-0.3017	1.07E-28
IGF1	0.226669878	2.49E-20	REV3L	-0.3003	8.89E-22
C5AR2	0.223336683	5.44E-16	FTH1	-0.29845	1.23E-44
CD1D	0.22237089	1.83E-20	EHD1	-0.29803	7.58E-15
DYNLT1	0.221318541	2.96E-26	RPL13	-0.29631	1.29E-76
PTMS	0.220617384	3.42E-16	LGALS1	-0.29409	3.44E-32

CTSB	0.220203663	5.39E-25	KLF6	-0.29282	4.28E-09
ATP1B3	0.220899709	4.85E-19	AHNAK	-0.29271	1.88E-19
LGALS3BP	0.21960171	8.94E-41	MRPL18	-0.28765	3.10E-20
CTSD	0.218646986	1.24E-06	ID2	-0.28686	5.50E-09
VAMP8	0.217515721	6.83E-35	CD40	-0.28552	6.61E-06
MPEG1	0.215739183	3.69E-14	ANXA1	-0.28546	8.02E-16
HMGB2	0.214817286	1.79E-17	GSN	-0.28319	3.88E-30
NAP1L1	0.212574271	2.59E-23	PNRC1	-0.28278	4.43E-20
ADAM28	0.212420826	2.13E-18	NINJ1	-0.28163	7.95E-16
MS4A6A	0.211738938	6.63E-15	GAPDH	-0.28031	1.94E-42
AIF1	0.211500895	4.74E-49	FCGR2A	-0.27984	3.17E-22
PPT1	0.210428864	3.58E-15	CFP	-0.27895	1.75E-22
GRN	0.208048243	4.55E-25	TNFRSF1B	-0.27418	9.49E-19
FUCA1	0.207053993	5.45E-21	NFAT5	-0.27204	3.15E-20
PLAC8	0.204978816	0.005701633	METRNL	-0.27154	3.75E-19
CSF1R	0.204395514	3.01E-12	PLAUR	-0.27042	0.000538
CH25H	0.202859174	1.32E-11	MAFF	-0.26644	1.35E-15
SLC7A7	0.20257888	1.92E-20	CAPN2	-0.26471	6.27E-39
ITM2C	0.202378919	1.10E-18	AP1S2	-0.25919	6.93E-19
RGS10	0.202143011	1.48E-23	SPAG9	-0.25823	3.19E-23
SH3PXD2B	0.201720414	7.51E-32	VASP	-0.25727	2.92E-19
FCGRT	0.201256657	1.88E-28	ATP1B1	-0.25301	2.32E-16
JUNB	0.201003133	2.17E-10	CDKN1A	-0.25271	2.88E-15
HIPK2	0.200297534	6.30E-26	MALT1	-0.25259	2.87E-14
			CDC42EP3	-0.25163	4.53E-21
			CCRL2	-0.24912	3.31E-19
			MAP4K4	-0.24841	1.35E-17
			ARL5B	-0.24832	1.06E-14
			USP12	-0.24672	3.03E-22
			CSTB	-0.24527	2.33E-22
			FLNA	-0.2439	1.01E-20
			BAZ1A	-0.24277	4.92E-14
			BLVRB	-0.2416	5.60E-22
			CD300E	-0.24043	1.32E-23
			IRF1	-0.23862	9.33E-16
			RAPGEF1	-0.23821	4.52E-17
			PRDX1	-0.23792	5.39E-14
			JCHAIN	-0.23668	0.000288
			PLAU	-0.23095	1.23E-15
			RALA	-0.23012	3.49E-08
			ICAM3	-0.2299	3.17E-25
			AES	-0.22919	1.05E-21
			TPRA1	-0.22756	5.68E-17
			DENND4A	-0.22714	5.66E-14
			GPR157	-0.22658	5.17E-14
			MYO1G	-0.22621	3.63E-26
			CD37	-0.2258	9.94E-17
			DNTTIP2	-0.22575	2.88E-13
			CACYBP	-0.22512	5.15E-11
			S100A8	-0.22491	6.36E-12

MYADM	-0.22328	9.91E-10
TUBB4B	-0.22247	1.72E-17
CALM1	-0.22163	4.51E-17
IL10RA	-0.22013	5.81E-15
KDM6B	-0.22007	1.32E-15
PPP1R14B	-0.21807	1.48E-18
LACTB	-0.21789	2.58E-16
DUSP2	-0.21716	4.92E-07
EFHD2	-0.21419	5.24E-18
ARL8B	-0.21247	6.34E-13
STIP1	-0.21213	4.80E-21
CTSZ	-0.21142	7.96E-15
CAST	-0.21121	1.77E-16
ICAM1	-0.21029	0.03484
PLK3	-0.21004	4.13E-12
CD9	-0.20856	0.004541
PNPLA8	-0.20804	3.73E-14
PPP1R15B	-0.20788	3.05E-05
CHORDC1	-0.20753	6.10E-18
ZFY	-0.20737	6.35E-33
C1orf162	-0.20713	1.05E-22
ZC3H12A	-0.20684	2.82E-15
MBP	-0.20476	5.41E-14
CITED4	-0.20347	5.39E-13
MNDA	-0.20274	4.13E-15
ACTG1	-0.20257	2.54E-25
CD48	-0.2013	2.66E-11
RPL18	-0.20096	1.30E-44

Table S4

cluster	gene	avg_logFC	p_val
M7	FOSB	1.009063	4.23E-276
M7	TNFAIP3	0.971054	5.07E-259
M7	MRC1	0.85316	1.41E-232
M7	KLF4	0.845135	3.19E-213
M7	NR4A2	0.852964	1.50E-207
M7	DUSP1	0.747596	2.21E-193
M7	FOS	0.93288	2.97E-172
M7	CD83	0.620904	3.84E-170
M7	FOLR2	0.888235	9.32E-169
M7	KLF6	0.715811	2.92E-156
M7	CD163	0.612903	2.92E-148
M7	PNRC1	0.508571	2.85E-144
M7	ZFP36	0.522818	6.07E-132
M7	NEAT1	0.681366	9.53E-132
M7	SLC40A1	0.505537	1.53E-131
M7	ZFAND5	0.596218	2.78E-131
M7	EGR1	1.06785	1.02E-130
M7	F13A1	1.099542	7.28E-129
M7	TSC22D3	0.535036	5.21E-125
M7	CCL3	0.902018	2.06E-123
M7	JUNB	0.517427	2.25E-122
M7	KLF2	0.80861	2.63E-121
M7	MAF	0.540628	3.15E-118
M7	NFKBIZ	0.581204	7.87E-112
M7	CCNL1	0.526068	1.80E-111
M7	HES1	0.698375	4.54E-111
M7	JUND	0.510955	1.06E-110
M7	JUN	0.816444	1.31E-110
M7	ICAM1	0.588734	2.77E-110
M7	MAFF	0.590731	6.69E-108
M7	KDM6B	0.566587	2.33E-103
M7	IER3	0.712718	2.96E-103
M7	STAB1	0.622278	1.38E-99
M7	IER2	0.674185	5.07E-99
M7	LYVE1	0.692658	1.53E-97
M7	ATF3	0.667888	2.40E-97
M7	CCL4	0.856588	4.37E-96
M7	HSPA5	0.518535	1.78E-94
M7	CXCL2	0.780531	3.09E-94
M7	LTC4S	0.589625	7.54E-94
M7	ELL2	0.553941	1.25E-84
M7	CXCL8	0.590623	3.14E-81
M7	PDK4	0.657982	2.34E-79
M7	BTG2	0.579485	1.26E-78
M7	CCL4L2	0.755012	4.10E-76
M7	CXCR4	0.538895	2.11E-75
M7	IL1B	0.599742	2.99E-72
M7	PTGS2	0.634458	6.29E-72

M7	MTARC1	0.508809	4.69E-69
M7	TRA2B	0.546561	1.69E-65
M7	NR4A1	0.506879	2.39E-64
M7	NLRP3	0.538157	2.68E-59
M7	DUSP6	0.518986	4.77E-57
M7	CCL3L3	0.813307	4.25E-52
M7	HSPA1B	0.533624	1.97E-50
M7	CXCL3	0.578672	8.07E-49
M7	PRDM1	0.501032	1.10E-46
M7	RNASE1	0.611347	6.06E-40
M7	THBS1	0.553799	7.57E-31
M7	IGLC3	0.523912	0.000629
M8	ACP5	0.790933	1.36E-174
M8	LGALS3	1.005682	1.08E-170
M8	CD9	0.692784	4.52E-132
M8	SDS	0.704316	2.94E-130
M8	LYZ	0.593559	4.88E-125
M8	FABP5	0.638491	9.66E-85
M8	GPNMB	0.580736	1.62E-82
M8	MMP12	0.51479	1.69E-78
M8	TIMP1	0.500267	3.27E-74
M8	APOC1	0.508046	1.47E-33
M8	MT2A	0.566905	2.70E-25
M8	MT1G	0.523668	1.14E-23
M8	MT1X	0.608234	7.40E-20
M9	IL22RA2	1.170857	9.76E-226
M9	NRG1	0.70072	3.41E-167
M9	PLA2G2D	0.841636	3.28E-120
M9	IL2RG	0.839857	5.79E-91
M9	MMP12	2.122317	6.28E-88
M9	TNFRSF9	0.567362	1.63E-77
M9	IL7R	0.801193	1.60E-67
M9	MMP9	1.932434	1.50E-62
M9	ENPP2	1.191284	1.12E-60
M9	LGALS2	1.323239	1.59E-58
M9	IL4I1	0.830911	4.47E-55
M9	PTGDS	2.020959	2.84E-54
M9	HLA-DQB2	0.734882	7.48E-50
M9	ATOX1	1.152716	1.54E-49
M9	CST7	0.74162	4.94E-47
M9	TMEM176	0.851909	2.78E-46
M9	CTSH	0.895847	5.36E-44
M9	TMEM176	0.780614	7.90E-44
M9	LYZ	1.106362	2.33E-43
M9	IL1RN	0.893798	2.83E-43
M9	GSTP1	0.694707	2.41E-42
M9	S100B	1.054142	8.93E-42
M9	SERPINA1	0.655293	5.70E-41
M9	ADAMDEC	0.783831	7.92E-39
M9	ARHGDIB	0.662509	1.07E-38

M9	ANXA1	0.719718	4.43E-37
M9	BASP1	0.77034	1.21E-36
M9	ENO1	0.634591	1.61E-35
M9	CAPG	1.020336	2.83E-35
M9	GSN	0.745927	5.91E-34
M9	PLA2G7	0.651554	8.98E-33
M9	PRELID1	0.69906	1.45E-30
M9	PPA1	0.790676	1.92E-30
M9	ALOX5AP	1.278542	4.85E-29
M9	ITGB2	0.53707	1.37E-25
M9	CSTA	0.585328	2.20E-25
M9	SERPINF1	0.659014	2.55E-25
M9	SYNGR2	0.573878	5.68E-25
M9	PRDX1	0.509078	7.01E-23
M9	RALA	0.506197	2.22E-22
M9	EFHD2	0.544071	5.66E-22
M9	C15orf48	0.66877	1.98E-20
M9	TYMP	0.552502	2.85E-20
M9	COTL1	0.512371	9.51E-20
M9	MYDGF	0.528733	3.76E-19
M9	PFN1	0.555179	2.85E-18
M9	CXCL9	1.167317	7.34E-14
M9	FUCA1	0.566332	2.17E-12
M9	IL18	0.542143	7.13E-12
M9	G0S2	0.528025	3.84E-08
M10	FTL	0.717363	2.45E-92
M10	OAZ1	0.509002	1.12E-66
M10	GAPDH	0.679266	2.96E-63
M10	RPL7A	0.543585	1.31E-62
M10	YBX1	0.583305	6.37E-53
M10	S100A11	0.619082	3.37E-45
M10	GNAS	0.570088	4.66E-41
M10	GSTP1	0.557185	5.09E-41
M10	BRI3	0.569526	2.18E-33
M10	APOE	1.210938	2.01E-27
M10	FUCA1	0.980098	2.51E-26
M10	LGALS3	0.695002	2.45E-21
M10	PRDX1	0.598175	1.85E-19
M10	NUPR1	0.720171	3.18E-19
M10	CSTB	0.734237	3.53E-19
M10	CTSD	0.665014	1.90E-16
M10	APOC1	0.843922	2.43E-14
M10	ATP6V0D2	0.595397	8.64E-10
M10	PLA2G7	0.675315	7.28E-09
M10	VEGFB	0.571188	3.68E-07
M10	MT1G	1.007437	7.43E-07
M10	CRYAB	0.776308	8.32E-07
M10	RAB42	0.538144	7.49E-06
M10	MT1X	0.744601	2.01E-05
M10	MT1E	0.557885	0.00012

M1G	M1ZA	0.619267	0.000723

Table S5

Ileum DEGs	avg_logFC	adj. p-value	Colon DEGs	avg_logFC	adj. p-value
ADAMDEC1	0.996761	1.45E-126	RNASE1	-1.93465	4.38E-142
DNASE1L3	0.901433	2.34E-146	HSPA1A	-1.60061	1.38E-169
JAML	0.759474	1.38E-126	HSPA6	-1.47618	4.26E-25
CXCL1	0.720775	1.34E-40	HSPA1B	-1.41809	6.45E-138
LGALS2	0.659704	4.64E-71	HSP90AA1	-1.25347	2.01E-147
C11orf96	0.630179	1.24E-36	F13A1	-1.21704	4.18E-89
CCDC186	0.629328	4.07E-56	HLA-DQA2	-1.20187	5.48E-54
C5AR2	0.608943	6.00E-42	HSPH1	-1.19345	3.85E-86
GCLC	0.595748	2.86E-62	DNAJB1	-1.17886	1.07E-101
LIPA	0.577865	2.28E-18	S100A4	-1.17192	3.21E-117
C1QC	0.571755	9.43E-87	BAG3	-1.05034	4.83E-46
CCL18	0.562822	6.44E-18	HSPD1	-1.01277	7.50E-57
AC090498.1	0.558439	1.86E-26	HSPB1	-0.98473	4.41E-11
CD74	0.536484	3.46E-124	HSP90AB1	-0.89437	4.39E-118
FAM21A	0.514193	2.76E-20	DNAJA1	-0.81016	1.09E-85
HLA-DQA1	0.502852	7.40E-61	DDX3Y	-0.78398	1.10E-43
ITGB7	0.501784	6.77E-74	ALOX5AP	-0.75779	2.71E-47
LGALS3BP	0.501581	1.53E-61	ZFAND2A	-0.75132	7.44E-20
CTSC	0.499622	1.86E-74	IGHA1	-0.70837	2.41E-46
TMSB4X	0.498796	9.82E-78	APOE	-0.69966	9.29E-15
B2M	0.48109	1.36E-73	HSPE1	-0.69765	1.37E-50
CLEC10A	0.479676	5.81E-68	S100A6	-0.69731	1.39E-36
CXCL12	0.47937	1.11E-55	FCGR3A	-0.66533	5.15E-42
TXN	0.476254	6.95E-40	IGKC	-0.65731	6.29E-50
C1orf54	0.470133	3.37E-38	S100A9	-0.63287	1.48E-34
ACP5	0.467697	9.30E-58	LTC4S	-0.63136	2.72E-52
RNASET2	0.467211	2.26E-66	KLF2	-0.61363	7.34E-30
THBS1	0.467069	4.26E-24	RHOB	-0.61359	2.00E-17
NET1	0.452648	4.67E-55	DNAJA4	-0.61243	4.77E-37
HLA-DRB1	0.450787	8.03E-92	EGR1	-0.59126	1.90E-23
AKIRIN2	0.449223	3.21E-33	TSPO	-0.57828	7.25E-72
SEPP1	0.448535	2.86E-84	C1orf162	-0.56849	8.49E-55
FABP6	0.434882	1.67E-57	STAB1	-0.54203	1.14E-30
CXCL3	0.43126	2.43E-27	IL1B	-0.53819	3.66E-21
TSC22D1	0.425073	1.07E-22	FCGR2B	-0.5367	8.71E-41
ITM2C	0.415703	4.99E-40	CD14	-0.53	3.12E-32
IL6	0.412459	1.30E-28	IGLC2	-0.52513	1.11E-17
LPAR6	0.410369	2.99E-37	PNP	-0.52028	3.67E-39
FAM105A	0.403027	5.44E-38	IER3	-0.50923	1.75E-25
CYTIP	0.388709	7.76E-35	GSN	-0.49684	8.58E-39
LYZ	0.388098	8.18E-48	GYPC	-0.49588	2.63E-29
NPC2	0.385387	3.46E-45	HSPA8	-0.49154	1.00E-32
VSIG4	0.381495	8.02E-35	FOSB	-0.4867	5.70E-42
CRIP1	0.381179	4.80E-25	C5AR1	-0.47528	5.16E-27
EPB41L2	0.377263	2.40E-31	EMP3	-0.46846	2.66E-26
PLBD1	0.374731	1.92E-41	IER5	-0.4564	2.74E-06
VIMP	0.37214	2.16E-29	EIF4A3	-0.45525	2.94E-10

RGS1	0.370771	2.12E-40	CCL4	-0.45225	9.86E-10
HLA-DRA	0.36253	7.02E-61	TWISTNB	-0.45027	6.94E-06
HLA-DMB	0.353856	9.92E-46	SOD2	-0.44181	4.85E-41
MS4A6A	0.353354	2.77E-55	JUND	-0.4405	1.56E-49
IL2RA	0.351498	1.68E-30	CAPG	-0.43497	1.60E-17
TMEM176B	0.350029	1.35E-36	LGALS3	-0.42962	3.40E-15
HLA-DMA	0.345094	2.23E-60	HCST	-0.42847	1.60E-25
CYBA	0.338707	5.98E-39	RPL22L1	-0.42755	6.26E-18
CPVL	0.333835	1.76E-15	UBE2S	-0.42603	2.75E-11
MPEG1	0.331011	1.79E-31	JUN	-0.42388	5.04E-08
SULT1A1	0.330961	2.61E-34	MEF2C	-0.41862	5.62E-22
VCAM1	0.329567	1.01E-36	PPIF	-0.41023	4.67E-13
GADD45A	0.328237	4.88E-22	FCGR2A	-0.40784	4.06E-33
DYNLT1	0.325289	2.15E-27	DNAJB4	-0.40517	3.13E-14
NBEAL1	0.321567	6.23E-21	S100A10	-0.40429	7.63E-14
HEXB	0.321385	1.05E-18	HSPA5	-0.40373	3.94E-27
LAPTM4A	0.320691	4.95E-24	PMAIP1	-0.39629	2.56E-11
MGST2	0.31491	1.92E-19	RPS12	-0.38147	1.29E-59
DNAJB9	0.314441	1.95E-20	TXNIP	-0.37922	3.69E-14
ADORA3	0.313034	1.08E-27	ZFP36L1	-0.37789	9.29E-09
TMEM59	0.309929	1.06E-17	PLAUR	-0.3773	0.0048616
SMIM3	0.309011	4.89E-24	CD9	-0.37499	3.43E-21
METTL7A	0.304936	4.63E-33	NEAT1	-0.37402	5.80E-26
CPM	0.299788	1.41E-16	CD55	-0.37175	2.26E-08
SULF2	0.298379	1.21E-38	METRNL	-0.36557	4.51E-14
C1QA	0.297475	1.52E-55	MRPL18	-0.36497	8.64E-15
LAG3	0.296617	3.84E-38	SLC1A3	-0.36246	1.28E-19
CXCL2	0.294812	7.65E-21	KDM6B	-0.36201	1.93E-19
CTSS	0.293869	8.34E-45	CHORDC1	-0.35637	3.77E-13
SIAH2	0.29359	3.37E-25	CYBB	-0.35401	1.50E-20
CLEC11A	0.291552	1.85E-11	DNAJB6	-0.35039	2.15E-18
PALLD	0.290639	3.52E-44	UBB	-0.34706	2.54E-19
C1QB	0.288841	4.19E-48	OGFRL1	-0.34082	6.88E-16
HLA-E	0.288002	7.10E-41	IRF1	-0.33913	9.81E-12
TBXAS1	0.287543	1.09E-21	HBEGF	-0.33912	5.30E-07
PPDPF	0.287154	5.82E-18	NR4A2	-0.33746	4.87E-11
EPHX1	0.286587	5.50E-39	MT-ND5	-0.33017	4.62E-32
EPSTI1	0.285867	7.30E-21	KLF4	-0.32999	1.99E-09
AXL	0.28338	4.38E-13	MRC1	-0.32776	2.22E-18
GSTP1	0.28269	5.61E-30	TUBB4B	-0.32479	1.05E-07
N4BP2L1	0.280338	3.43E-23	MIDN	-0.32467	1.36E-06
CXCL16	0.279765	7.76E-20	OLR1	-0.32137	1.13E-07
SERPINF1	0.278132	3.59E-19	HSP90B1	-0.31403	1.02E-15
SFT2D1	0.275704	2.44E-14	SRSF7	-0.31226	2.65E-09
LINC00996	0.275255	2.97E-22	BLVRB	-0.30899	1.33E-10
CD69	0.274252	5.54E-14	MAP1LC3B	-0.30859	5.61E-09
CLEC7A	0.274212	1.83E-18	MTSS1	-0.30839	5.72E-13
CD1D	0.274149	1.85E-23	PPP1R15A	-0.3071	1.01E-08
C3AR1	0.273197	1.00E-17	ITGAM	-0.29966	1.73E-25
GRN	0.271659	2.03E-23	BASP1	-0.28967	7.39E-09

FYB	0.269867	9.98E-12	KIAA1143	-0.28828	1.60E-08
SARAF	0.267181	2.77E-25	JCHAIN	-0.28742	4.30E-17
NAAA	0.266719	8.91E-20	FXYD5	-0.286	4.53E-11
TNFSF9	0.26564	4.14E-12	AHNAK	-0.28415	3.09E-09
CHPT1	0.265433	6.18E-14	NR4A1	-0.28343	7.30E-10
PTGER2	0.264681	4.49E-27	GAS6	-0.28302	4.55E-16
RAB9A	0.263163	6.60E-23	NFKB1	-0.28285	5.76E-05
CD36	0.262334	6.81E-19	RPS7	-0.28201	3.29E-29
PPT1	0.260507	6.09E-10	THBD	-0.27848	8.80E-08
TMBIM4	0.257373	2.63E-13	FOLR2	-0.27808	8.01E-06
GPR34	0.256107	1.19E-09	RPS4Y1	-0.2753	7.81E-09
TYROBP	0.25463	2.32E-44	SERTAD1	-0.27104	1.70E-06
GPR183	0.251087	4.69E-21	HIF1A	-0.27088	2.46E-05
RPL7	0.250021	1.28E-17	SQSTM1	-0.26875	0.00267
CSF2RA	0.249276	1.87E-18	KLF10	-0.26823	0.0228293
HLA-DPB1	0.249073	1.25E-45	CALM1	-0.26803	1.80E-12
CHMP1B	0.248752	1.39E-18	RBMS1	-0.26663	7.75E-07
ZDHHC4	0.248574	1.71E-22	EGFL7	-0.26575	2.42E-18
HMGN3	0.246346	7.29E-12	ITGAX	-0.26366	2.39E-10
SAMSN1	0.245696	1.17E-06	YBX3	-0.26182	5.42E-09
CTSZ	0.243072	9.75E-11	SERPINA1	-0.26154	3.37E-21
IFNGR1	0.243004	8.14E-13	CD37	-0.25892	4.19E-10
DSTN	0.242837	2.99E-15	SLC5A3	-0.25624	8.21E-11
SNX2	0.242679	6.83E-15	BCAT1	-0.25494	9.30E-14
SLAMF7	0.24215	3.61E-16	NAMPT	-0.25479	8.62E-13
CXCR4	0.242025	4.25E-17	RPL30	-0.25395	1.23E-21
PELI1	0.23993	5.23E-11	RPL13	-0.25339	1.36E-33
MYL12A	0.238664	3.95E-07	SRSF3	-0.25316	4.70E-12
ASAH1	0.238266	9.21E-17	C3	-0.25036	2.38E-13
FAM110A	0.238214	3.63E-18	FTH1	-0.24956	3.58E-18
IFNGR2	0.238028	4.98E-17	RPL24	-0.24955	8.93E-26
SERPING1	0.236098	4.34E-21	SFPQ	-0.24948	8.77E-11
SASH1	0.234545	9.30E-13	RPL18	-0.24905	2.87E-31
LRPAP1	0.232396	1.90E-15	RPS24	-0.24898	3.69E-35
CAT	0.232326	1.79E-17	EEF1B2	-0.24864	4.87E-17
GUSB	0.23177	1.72E-17	SEMA4A	-0.24765	0.0015357
LILRB5	0.229894	4.75E-16	TPT1	-0.24473	2.86E-24
FNBP1	0.228937	1.34E-11	RPL28	-0.24429	9.31E-35
DST	0.228668	1.33E-15	SNX6	-0.24401	6.08E-06
SH3PXD2B	0.227767	4.14E-22	BTG1	-0.2431	2.04E-05
OAZ2	0.2276	2.07E-18	SH3BGRL3	-0.24222	6.44E-08
RHOH	0.227392	8.50E-24	TNFRSF1B	-0.23949	1.43E-06
SLC31A2	0.225736	4.89E-13	LMNA	-0.23842	7.06E-05
XIST	0.225199	5.25E-09	CLTC	-0.236	0.000748
CDKN1C	0.224702	5.11E-18	FSCN1	-0.23527	2.58E-13
P2RY13	0.22434	8.19E-13	PSTPIP2	-0.23476	7.26E-07
NDUFA12	0.223611	7.99E-11	VPS13C	-0.23278	0.0020609
VAMP8	0.222942	1.50E-18	MAF	-0.23242	2.92E-07
RDX	0.222668	1.58E-14	MAFF	-0.23206	0.0282349
IGF1	0.221777	8.90E-12	CCL2	-0.23036	1.81E-05

ARL6IP5	0.219871	1.28E-08	TECR1A	-0.2249	2.89E-08
GDI2	0.219824	1.18E-10	CALR	-0.2273	3.80E-09
GSTM3	0.219348	1.26E-22	CYFIP1	-0.22666	9.44E-05
SRSF9	0.219155	4.93E-09	RPL7A	-0.22653	2.70E-14
SUMO2	0.218929	3.51E-14	SLC25A3	-0.22465	0.0015303
RPL31	0.218679	2.59E-11	ATF3	-0.22457	1.91E-05
FAM26F	0.218175	1.01E-16	YWHAZ	-0.22341	0.0001264
GMFG	0.217211	9.69E-12	GNAQ	-0.22309	0.0187358
LEPROTL1	0.216947	8.42E-14	LAMP1	-0.22231	4.03E-07
ANXA5	0.216057	1.06E-12	DAB2	-0.22217	0.0038852
PRR13	0.215808	1.35E-13	TPM3	-0.22134	1.39E-06
SYNGR2	0.215437	1.97E-15	ACSL1	-0.21967	0.014275
NFKBID	0.214747	6.78E-05	VIM	-0.21748	0.0115412
AKAP9	0.213547	1.81E-08	AES	-0.21622	0.0024993
UQCR11	0.212609	1.19E-12	AMD1	-0.21612	0.0319001
ATP6V0E1	0.211737	1.53E-14	ADAP2	-0.21588	0.0005048
ADI1	0.211368	1.16E-14	ZFAS1	-0.21358	3.05E-06
TMA7	0.210457	1.35E-14	DHRS7	-0.20866	0.00127
C2	0.207501	1.30E-14	PID1	-0.20785	1.08E-06
RNASE6	0.207353	2.17E-11	FKBP4	-0.20678	0.0073282
SLC25A6	0.207068	6.05E-09	CYTL1	-0.20479	7.06E-11
HLA-DQB1	0.207046	3.21E-20	CD83	-0.20429	5.39E-10
SPINT2	0.206912	1.41E-11	PPP1R14B	-0.20374	0.0014172
BIRC3	0.206869	9.63E-08	EPS8	-0.20325	2.12E-05
CD53	0.206195	7.82E-12	RPS23	-0.20306	1.24E-22
TMEM176A	0.20566	7.70E-14	MT-ND1	-0.20239	4.63E-13
HNMT	0.204447	2.68E-08			
TMEM37	0.204105	1.56E-19			
RALB	0.204058	1.86E-14			
CD68	0.20361	1.14E-11			
HLA-DPA1	0.20264	1.26E-32			
PTMS	0.202373	5.41E-09			
WBSCR27	0.202198	4.57E-18			
C1orf56	0.201795	2.53E-07			
MPC1	0.201137	1.27E-08			
FOXO3	0.200594	5.84E-07			
CCNDBP1	0.200364	1.11E-18			
RPL13A	0.200072	7.38E-14			

Ileum DEGs	avg_logFC	adj. p-value	Colon DEGs	avg_logFC	adj. p-value
SEPP1	0.804048	1.32E-63	HSPA1A	-1.86305	1.38E-106
CXCL1	0.774727	9.01E-31	HSPA6	-1.6796	1.96E-32
ADAMDEC1	0.703654	6.38E-45	HLA-DQA2	-1.50396	2.96E-54
C11orf96	0.668562	5.77E-16	HSPA1B	-1.49631	1.13E-91
THBS1	0.661768	6.55E-33	S100A4	-1.45598	1.92E-158
JAML	0.653356	6.34E-73	APOE	-1.42209	5.93E-34
GPR34	0.597441	6.32E-40	DNAJB1	-1.40084	1.28E-71
TSC22D1	0.559713	1.63E-22	RNASE1	-1.35544	6.57E-41
VSIG4	0.544301	5.31E-52	HSP90AA1	-1.30736	7.61E-93
CXCL3	0.531465	4.49E-19	IGKC	-1.1164	1.85E-19
LGALS3BP	0.513535	1.64E-41	HSPD1	-1.1129	1.66E-64
CPM	0.512301	3.24E-47	HSPB1	-1.09222	2.07E-16
C5AR2	0.498139	3.93E-17	BAG3	-1.03949	1.70E-48
MS4A6A	0.497769	4.85E-59	S100A6	-0.98662	1.05E-95
RGS1	0.479312	8.68E-42	HSPH1	-0.96748	2.57E-41
C1QC	0.479277	1.63E-44	LGALS3	-0.90848	1.16E-61
AC090498.1	0.467606	1.39E-13	G0S2	-0.90666	2.53E-16
GCLC	0.464751	2.05E-30	HSP90AB1	-0.90117	4.92E-88
CTSC	0.454981	1.18E-47	HSPE1	-0.84965	7.21E-62
RNASET2	0.452785	1.48E-38	DNAJA1	-0.76185	1.98E-45
ITM2C	0.452392	8.76E-29	APOC1	-0.75239	8.78E-16
CD74	0.441354	8.35E-68	ZFAND2A	-0.74468	2.06E-21
C1QA	0.427073	7.47E-60	S100A10	-0.74107	4.48E-79
CXCL12	0.423492	9.82E-31	ALOX5AP	-0.73456	5.01E-41
FABP6	0.414357	4.09E-44	S100A9	-0.70092	3.44E-38
FAM105A	0.40691	8.10E-26	TSPO	-0.68726	2.80E-97
CD209	0.402958	4.50E-33	IGHA1	-0.65492	2.77E-22
NPC2	0.397562	6.32E-50	FCGR2B	-0.63652	1.33E-53
LIPA	0.396187	4.80E-06	CAPG	-0.62762	4.30E-51
LILRB5	0.391527	4.56E-19	JUN	-0.61238	0.0027475
ADORA3	0.390251	4.64E-23	LGALS1	-0.61161	3.36E-77
EVI2B	0.384595	9.18E-31	IER5	-0.58965	4.77E-09
LAG3	0.383745	1.39E-20	VIM	-0.58934	1.43E-51
CXCL2	0.383154	6.82E-19	CD9	-0.56487	1.37E-50
CCDC186	0.37339	1.01E-17	EMP3	-0.53186	1.08E-40
SMAP2	0.366526	2.89E-28	CTSD	-0.52757	1.26E-12
EPB41L2	0.364408	1.99E-18	BASP1	-0.52574	1.53E-24
TMSB4X	0.364143	1.70E-33	PRDX1	-0.51689	2.95E-41
HERPUD1	0.363789	3.58E-35	CTSH	-0.51019	2.07E-39
TBXAS1	0.355325	5.44E-30	F13A1	-0.50496	1.97E-22
TMEM59	0.354627	3.32E-19	HSPA8	-0.47748	1.75E-34
CLEC11A	0.354454	6.33E-12	RHOB	-0.4764	1.20E-06
IL2RA	0.350729	1.25E-18	CSTB	-0.47605	1.26E-24
C1orf54	0.349097	7.66E-16	IL4I1	-0.47573	4.94E-26
FCGRT	0.348741	6.62E-33	SH3BGRL3	-0.47465	8.86E-49
TYROBP	0.346604	1.15E-63	IL1B	-0.47414	0.0099606
AKIRIN2	0.34475	2.25E-09	TWISTNB	-0.47149	4.97E-13

B2M	0.342696	4.43E-35	DDX31	-0.46651	2.27E-31
GMFG	0.340281	6.96E-35	C10orf162	-0.45876	7.49E-37
SIAH2	0.339153	1.11E-21	DNAJA4	-0.45426	2.03E-21
LAPTM4A	0.334958	1.84E-21	C15orf48	-0.45218	2.38E-06
NET1	0.333808	2.04E-20	TXNIP	-0.43776	3.86E-07
GSTM3	0.327709	3.58E-23	IER3	-0.42588	2.18E-06
METTL7A	0.320768	1.83E-21	TYMP	-0.4207	1.89E-31
CAT	0.312877	6.12E-18	EIF4A3	-0.42009	5.98E-09
LPAR6	0.309444	1.06E-15	LSP1	-0.41091	1.54E-22
INSIG1	0.309335	1.39E-05	FCGR3A	-0.41024	2.74E-14
QPRT	0.309119	1.07E-20	GSN	-0.41	1.60E-30
JUNB	0.308968	3.91E-20	GAPDH	-0.38937	4.30E-35
CXCR4	0.307923	4.17E-11	PLA2G7	-0.38837	1.11E-08
NBEAL1	0.306507	7.29E-13	JCHAIN	-0.386	0.0180776
DNAJB9	0.306042	1.83E-07	PNP	-0.38325	1.28E-28
SARAF	0.305426	3.05E-26	HCST	-0.37282	1.19E-28
PLBD1	0.305365	7.37E-19	CALM1	-0.37261	2.70E-30
RNASE6	0.303621	4.06E-20	HSPA5	-0.36862	3.45E-11
MGST2	0.299303	5.18E-18	ANXA2	-0.35691	2.02E-28
TMEM176B	0.298733	7.17E-18	LDHA	-0.35508	2.27E-10
RNF144B	0.29858	1.43E-13	PLEK	-0.3479	1.89E-09
C1QB	0.296088	3.17E-28	ACTG1	-0.3478	3.93E-34
C3AR1	0.294071	7.64E-17	CHORDC1	-0.3448	1.60E-17
MRC1	0.294001	2.67E-11	FLNA	-0.34389	8.48E-28
PALLD	0.293774	9.97E-26	TUBB4B	-0.33444	2.97E-15
PRDM1	0.291377	3.87E-06	MARCKSL1	-0.32608	5.96E-08
CXCL16	0.290857	2.59E-19	S100A11	-0.32597	4.04E-25
CD163	0.290372	9.21E-20	HMOX1	-0.3252	9.89E-11
C2	0.290065	1.37E-13	UBE2S	-0.32485	3.06E-12
SULT1A1	0.288549	1.93E-11	JUND	-0.32338	6.64E-15
LINC00996	0.285842	5.41E-19	PPP1R14B	-0.31994	2.87E-21
MS4A4A	0.285395	3.50E-05	CALR	-0.31826	3.98E-18
IL6	0.283577	6.56E-10	ANXA1	-0.31712	3.79E-09
CD302	0.281776	3.39E-18	PPIF	-0.31595	4.66E-11
GPR183	0.281354	2.37E-21	RPL22L1	-0.31359	1.59E-11
RPL7	0.281194	8.96E-19	LAMP1	-0.31117	1.37E-17
LST1	0.281056	1.19E-21	CCND2	-0.3106	2.08E-33
PELI1	0.277413	1.23E-12	SQSTM1	-0.30571	7.36E-11
NAAA	0.277198	2.01E-13	CD44	-0.30443	6.20E-09
TMBIM4	0.276614	1.61E-11	PPP1R15A	-0.30179	0.0002676
SLC31A2	0.276539	9.71E-15	IL1RN	-0.3009	1.06E-08
CTSS	0.275942	4.45E-38	FCGR2A	-0.29864	2.62E-10
RPL31	0.272464	6.69E-15	LMNA	-0.29685	6.57E-07
SERPINF1	0.271478	1.83E-06	SERPINA1	-0.29614	8.10E-21
CSF1R	0.2712	2.83E-15	CFD	-0.29548	4.10E-07
RBPJ	0.270485	6.88E-13	TUBA1C	-0.29381	2.13E-13
ZFAND5	0.267319	2.20E-14	CD40	-0.29285	7.58E-08
AXL	0.266535	1.85E-13	ATF5	-0.29145	4.39E-10
HLA-E	0.265426	4.31E-27	SOD2	-0.28983	1.00E-07
CLEC10A	0.263535	5.20E-14	NAGK	-0.28942	2.69E-13

HLA-DRB1	0.259611	1.12E-30	CD48	-0.28796	1.94E-13
CD163L1	0.257151	1.74E-09	ENO1	-0.28696	5.72E-16
LGALS2	0.256783	8.36E-09	MNDA	-0.28675	3.57E-13
NCF4	0.255072	1.29E-11	ZFAS1	-0.28616	1.26E-14
IRS2	0.252215	5.24E-10	RPS4Y1	-0.286	1.10E-10
CD69	0.251977	0.0122226	EFHD2	-0.284	1.03E-14
NCOA4	0.250833	4.83E-13	SLC16A3	-0.27757	6.08E-11
CHPT1	0.249442	1.54E-07	CD55	-0.27745	1.56E-08
C1orf56	0.249182	0.000974	MRPL18	-0.27638	1.42E-09
HLA-DRA	0.24671	2.97E-28	C5AR1	-0.27604	8.01E-06
STK17B	0.245539	1.17E-11	YWHAH	-0.27464	5.19E-07
LDLR	0.245176	7.44E-14	H2AFZ	-0.27431	1.57E-05
FNBP1	0.23994	6.20E-10	LRRFIP1	-0.27424	8.86E-09
EIF4A2	0.239887	9.02E-14	ITGAX	-0.27279	3.15E-14
AKAP9	0.239831	9.80E-07	CDKN1A	-0.27249	1.02E-06
CYBA	0.239791	9.28E-17	RPS7	-0.27225	6.10E-26
CHMP1B	0.239452	3.78E-09	PMP22	-0.26766	7.92E-11
AIF1	0.238367	2.40E-22	SERTAD1	-0.26549	1.85E-09
P2RY13	0.238228	7.99E-07	GBP1	-0.26458	0.012776
DCK	0.237663	1.72E-11	DNAJB4	-0.26424	2.16E-05
C10orf54	0.236664	2.94E-13	PSMA7	-0.2615	7.82E-21
SERPING1	0.235996	2.80E-11	RPS12	-0.25571	1.02E-21
DRAM2	0.235967	1.04E-10	CACYBP	-0.25462	2.45E-07
CPVL	0.235144	0.0006781	METRNL	-0.25218	2.37E-06
DUT	0.234962	1.82E-09	ADM	-0.25174	0.0001737
SNX9	0.234201	1.27E-07	GNAI2	-0.25099	8.47E-13
CREM	0.233768	1.22E-11	IGLC2	-0.25072	6.79E-06
HSD17B11	0.232857	5.59E-13	IER5L	-0.25061	0.0003219
KLF9	0.232762	1.18E-07	NME1	-0.24867	1.88E-15
CD36	0.230668	3.22E-11	RPL7A	-0.24803	2.71E-18
CSF2RA	0.230448	5.26E-10	DNTTIP2	-0.24784	4.43E-10
SLCO2B1	0.230402	1.08E-12	SAMHD1	-0.24694	1.48E-07
SGPL1	0.230212	5.27E-09	SSR3	-0.24625	1.00E-12
IFNGR1	0.229115	5.24E-11	DNAJB6	-0.24559	0.0029308
RPL13A	0.228663	3.73E-22	EIF5A	-0.24503	1.19E-10
XIST	0.22859	4.14E-08	RPL18	-0.24338	1.82E-28
GADD45A	0.228543	1.16E-05	RPL28	-0.24328	2.68E-29
RPL21	0.228455	4.31E-20	HSP90B1	-0.23994	0.0007864
ZNF331	0.227928	4.01E-07	AHNAK	-0.23924	3.32E-07
ATP1B3	0.227894	9.51E-11	FKBP4	-0.23874	2.92E-06
RALB	0.227781	2.95E-13	SEC61B	-0.23758	5.47E-15
GCA	0.226777	8.98E-10	TNFAIP8	-0.23737	0.0024666
TCF7L2	0.226577	4.53E-09	CHCHD2	-0.23708	5.26E-17
WBSCR27	0.225231	1.09E-15	FXYD5	-0.23667	1.12E-12
IGF1	0.225184	8.59E-05	RALA	-0.23139	7.15E-05
ZFP36	0.22494	1.99E-14	OGFRL1	-0.23073	2.65E-06
NRP1	0.223972	2.21E-09	CD52	-0.23054	4.69E-09
OLFML2B	0.222603	1.04E-22	CD99	-0.23005	2.06E-08
SASH1	0.221871	2.13E-05	GNG5	-0.22987	3.12E-10
SESN1	0.22145	4.72E-11	RPL24	-0.22914	1.46E-22

PGD2	0.220183	5.21E-16	HIST1H4C	-0.22841	4.29E-08
CREBRF	0.220074	6.59E-05	ATP1B1	-0.22796	1.52E-06
FYB	0.219523	1.63E-08	CTSB	-0.22787	2.51E-05
SMIM3	0.219283	1.06E-05	RHOC	-0.22756	9.62E-17
ITGB7	0.219143	6.94E-07	CKLF	-0.2271	3.08E-05
SH3PXD2B	0.218938	1.32E-09	ATOX1	-0.22492	0.0002248
CEBPB	0.218893	3.17E-08	RPL13	-0.22459	1.42E-19
TGIF1	0.218867	1.70E-08	ACP5	-0.22444	0.0046771
TFRC	0.21865	0.0003609	TCEB1	-0.22395	1.57E-09
ANXA5	0.218174	8.87E-14	HNRNPAB	-0.22219	3.17E-08
HEXA	0.217595	3.57E-10	CCT4	-0.22207	1.50E-11
ME1	0.217372	1.07E-10	TXN	-0.22191	0.0170626
DNPH1	0.216984	5.15E-06	UBB	-0.21808	0.0021119
RGS2	0.21675	3.08E-09	NDUFC2	-0.2142	6.79E-09
CDKN1C	0.216589	6.53E-07	GYPC	-0.21399	1.31E-08
RGS18	0.216341	1.10E-09	PPIB	-0.2118	1.28E-07
IDH1	0.216083	4.82E-07	COX4I1	-0.21173	4.44E-17
SFT2D1	0.214157	2.16E-06	SNAI1	-0.21114	0.0038082
GATM	0.214086	1.08E-05	RPL8	-0.21024	3.18E-25
H1FX	0.210647	0.0030097	SOD1	-0.20859	2.41E-06
HES1	0.210025	3.34E-07	STIP1	-0.20708	7.23E-08
FOXO3	0.209097	1.85E-07	BLVRB	-0.20637	0.004762
MAT2B	0.208461	1.21E-06	SDSL	-0.20626	2.03E-05
CYTIP	0.208347	5.07E-06	TUBB	-0.20624	1.71E-05
EVL	0.207917	5.01E-08	TPM4	-0.20618	2.76E-05
TPP1	0.207224	7.72E-10	MT-ND5	-0.20605	4.49E-08
HLA-DQA1	0.206384	1.20E-05	CD37	-0.20604	3.59E-12
GSTM4	0.205717	6.03E-08	ATP5G3	-0.20603	3.80E-10
PYCARD	0.205165	2.21E-07	SLAMF7	-0.20601	0.0411307
TNFAIP3	0.203833	0.0025986	HIF1A	-0.20597	0.0028359
FES	0.202133	4.77E-08	SLC25A3	-0.20547	3.26E-08
WLS	0.201442	9.57E-14	SFPQ	-0.20425	6.72E-06
ALDH9A1	0.200825	3.65E-09	GADD45GIP1	-0.20407	2.09E-08
EPHX1	0.200603	2.22E-16	RAB11FIP1	-0.20364	0.0027564
HCK	0.200198	1.77E-05	EEF1B2	-0.20336	6.69E-09
			ALDOA	-0.20312	0.000504
			GSTO1	-0.20279	2.31E-06
			CYB561A3	-0.20269	0.0016909
			PSMB6	-0.20245	6.81E-05
			GNA15	-0.20085	1.08E-06

Ileum DEGs	avg_logFC	adj. p-value	Colon DEGs	avg_logFC	adj. p-value
VSIG4	0.912084	0.0021631	HSPA1A	-1.8675	3.59E-06
MRC1	0.82344	0.0261213	DNAJB1	-1.25767	0.0027274
LILRB5	0.612959	0.0005295	HSPA1B	-1.23605	0.0025651
CPM	0.526976	0.0005793	ALOX5AP	-1.2062	0.0065258
TYROBP	0.335817	0.0251729	MMP9	-1.07254	0.0038624
			HSPH1	-1.00004	0.0182016
			CAPG	-0.93086	0.000829
			HSPD1	-0.90223	0.0132324
			HSPE1	-0.78245	0.0125559
			CTSH	-0.62801	0.0124939
			GSN	-0.62619	0.0462378
			PPM1N	-0.60866	0.0283811

Ileum DEGs	avg_logFC	adj. p-value	Colon DEGs	avg_logFC	adj. p-value
CXCR4	1.364101	1.16E-12	APOE	-1.91748	7.15E-24
CCL4L2	1.21756	1.01E-09	HLA-DQA2	-1.75881	1.57E-12
RGS1	1.082339	5.72E-11	S100A4	-1.57335	8.74E-30
AREG	1.082295	9.94E-05	RPS4Y1	-1.49608	4.66E-20
MALAT1	1.081388	0.000101462	LGALS3	-1.35654	7.47E-20
CCL3L3	1.075992	8.98E-07	APOC1	-1.32836	6.16E-13
ZFAND5	1.073519	1.29E-08	S100A9	-1.23975	3.35E-09
ZFP36	1.058909	1.21E-07	S100A6	-1.1496	8.52E-12
FOS	0.960156	1.93E-07	MMP12	-1.082	0.0058456
GPR183	0.924235	1.06E-09	LGALS1	-1.07428	2.09E-24
JUNB	0.920226	4.65E-10	FUCA1	-1.02144	1.07E-08
HERPUD1	0.913016	4.43E-15	RNASE1	-0.98904	7.36E-08
KLF4	0.901195	1.79E-06	CTSD	-0.94499	3.64E-08
THBS1	0.873745	1.50E-05	TSPO	-0.93512	2.26E-11
SMAP2	0.842677	0.002752991	PRDX1	-0.91139	2.37E-13
TNFAIP3	0.837199	0.002772452	PLA2G7	-0.88408	1.84E-06
CEBPD	0.828651	1.01E-09	CSTB	-0.85671	8.02E-07
TSC22D3	0.815955	1.04E-08	S100A10	-0.80776	1.70E-09
CXCL2	0.815281	0.000303029	CTSB	-0.76922	0.000234
NFKBIA	0.780736	0.000106096	CD52	-0.75972	2.69E-06
FABP6	0.762313	4.87E-06	CD9	-0.7301	4.22E-05
STK17B	0.758021	0.019080236	CAPG	-0.71357	1.06E-06
CEBPB	0.738453	1.69E-06	BAG3	-0.70693	0.001682
DUSP1	0.727604	0.000195931	LYZ	-0.70416	1.43E-10
CXCL3	0.663772	0.00356095	ALOX5AP	-0.6693	0.0020388
MRC1	0.65217	0.016183174	GPNMB	-0.64969	0.0021004
MCL1	0.621611	0.001184653	PSAP	-0.64087	1.59E-05
SRGN	0.611554	0.00018572	GSN	-0.60462	0.0138756
SEPP1	0.597976	2.71E-11	LSP1	-0.60438	4.93E-05
CPM	0.581787	0.007883268	CTSH	-0.60066	0.0021917
BTG1	0.566345	0.002973751	ATOX1	-0.58371	0.01346
CXCL12	0.537693	0.041732602	TYMP	-0.58016	1.35E-05
VCAM1	0.511234	0.001800766	FABP5	-0.5786	0.0133932
MS4A6A	0.504789	3.83E-06	HSP90AA1	-0.56937	0.0151734
TAGLN2	0.481398	0.028723905	EMP3	-0.53202	0.0007805
UBC	0.470287	0.000422337	GAPDH	-0.53129	5.04E-10
RNASET2	0.414562	0.009133782	FTL	-0.50288	2.33E-11
RPS29	0.365477	1.64E-06	ANXA2	-0.49188	0.0017267
RPS4X	0.294923	0.001265063	ABRACL	-0.4859	0.0054349
CST3	0.275784	0.000828014	DBI	-0.47639	0.0188397
			S100A11	-0.4705	4.54E-06
			SH3BGRL3	-0.46494	0.0001013
			FCGR2B	-0.4649	0.0366712
			RHOA	-0.45469	0.0006678
			COTL1	-0.42974	0.0133686
			PARK7	-0.42786	0.0360932
			ACTB	-0.402	3.03E-08

YCEB2	-0.39595	0.0230942
MYL12A	-0.38364	0.006941
VIM	-0.37058	0.0002355
MYL6	-0.35176	0.0074443
ACTG1	-0.34998	6.72E-05
OAZ1	-0.29553	0.0023666
SERF2	-0.28703	0.0069673

Table S6

Patient	Diagnosis	Site	Severity	Vedolizumab
1	CD	Colon	Active- mild	YES
1	CD	Colon	Quiescent	YES
1	CD	Ileum	Quiescent	YES
2	CD	Colon	Active- mod	
2	CD	Colon	Quiescent	
2	CD	Ileum	Active- mild	
3	CD	Colon	Active- mild	
3	CD	Colon	Quiescent	
4	CD	Colon	Active- mild	
4	CD	Colon	Active- mild	
4	CD	Colon	Active- mod	
5	IBDU (CD)	Colon	Active- mild	
5	IBDU (CD)	Colon	Quiescent	
6	CD	Colon	Active-mod	
7	IBDU (CD)	Colon	Active- mild	
7	IBDU (CD)	Colon	Quiescent	
8	UC	Colon	Active- mod	
8	UC	Colon	Quiescent	
9	UC	Colon	Active- mod	YES
9	UC	Colon	Quiescent	YES
9	UC	Ileum	Quiescent	YES
10	CD	Colon	Quiescent	
10	CD	Ileum	Active- mild	
11	IBDU (UC)	Colon	Quiescent	
11	IBDU (UC)	Ileum	Quiescent	
12	UC	Colon	Quiescent	
13	UC	Colon	Active- mod	
13	UC	Colon	Quiescent	
14	Healthy	Colon	Healthy	
14	Healthy	Ileum	Healthy	
15	Healthy	Colon	Healthy	
16	Healthy	Colon	Healthy	
16	Healthy	Ileum	Healthy	
17	Healthy	Colon	Healthy	
17	Healthy	Ileum	Healthy	
18	UC	Colon	Active- mild	
18	UC	Ileum	Active-mild	
19	CD	Colon	Quiescent	
20	CD	Colon	Active- mild	
20	CD	Ileum	Active- mod	
21	UC pan	Colon	Active- mod	YES
21	UC pan	Ileum	Quiescent	YES
22	UC pan	Colon	Quiescent	
22	UC pan	Ileum	Quiescent	
23	Healthy	Colon	Healthy	
23	Healthy	Ileum	Healthy	
24	Healthy	Colon	Healthy	
25	CD	Ileum	Quiescent	

25	CD	Ileum	Quiescent	
26	UC	Colon	Quiescent	YES
26	UC	Colon	Quiescent	YES
26	UC	Rectum	Active- mild	YES

Table S7

Experiment	Label	Target	Clone
Flow cytometry	BUV737	CD38	HB-7
	BUV393	CD45	HI30
	BV786	CD1c	F10/21A3
	BV711	CD141	1A4
	BV650	CD163	
	BV605	CD103	B-Ly7
	BV480	CD1a	
	BV421	CD14	MϕP9
	BB700	CD123	7G3
	BB515	CYTOX	F10/21A3
	PE/Cy7	CD55	JS11
	PE/Cy5	CD206	15-2
	PE/CF594	CD3	UCHT1
	PE/CF594	CD19	HIB19
	PE	CD5	UCHT2
	APCFire750	CD11a	TS2/4
	AF700	HLADR	G46-6
	APC	CD207	10E2
FACS	BUV393	CD45	HI30
	BV650	HLADR	G46-6
	7-AAD	via	via
	PE/CF594	CD19	HIB19
	AF647	CD3	UCHT1
CITEseq	Totalseq-A	CD1c	L161
	Totalseq-A	CD14	M5E2
	Totalseq-A	CD11a	TS2/4
	Totalseq-A	CD55	JS11
	Totalseq-A	CD5	UCHT2
	Totalseq-A	CD206	15-2
	Totalseq-A	CD209	9E9A8
	Totalseq-A	CD11c	S-HCL-3